The Dissertation Committee for Ashwini Gopal certifies that this is the approved version of the following dissertation:

Multicolor Colloidal Quantum Dot Based Inorganic Light Emitting Diode on Silicon: Design, Fabrication and Biomedical Applications

Committee:

Xiaojing Zhang, Supervisor

Dean P. Neikirk, Co-Supervisor

Ananth Dodabalapur

Edward T. Yu

Michael F. Becker

Seth R. Bank

Multicolor Colloidal Quantum Dot Based Inorganic Light Emitting Diode on Silicon: Design, Fabrication and Biomedical Applications

by

Ashwini Gopal, B.E., M.S.E.,

Dissertation

Presented to the Faculty of the Graduate School of

The University of Texas at Austin

in Partial Fulfillment

of the Requirements

for the Degree of

Doctor of Philosophy

The University of Texas at Austin

December 2010

Dedication

For Appa, Amma and Priyanka

Acknowledgements

Wow this journey in my life was fantastic!

Here goes my series of thank yous! I would first like to thank my advisor, Prof. John Zhang, for his advice, guidance and training that helped me get to this point in my graduate career. He provided the vision, constant encouragement and expertise that made this dissertation possible. I cannot thank him enough for the influence he has had on me.

I would also like to thank my committee members, Dr. Ananth Dodabalapur, Dr. Dean Neikirk, Dr. Seth Bank, Dr Michael Becker and Dr. Edward Yu for making this thesis a reality. Thank you!

Special thanks to my collaborators Dr. Muaro Ferrari, Dr. Grady Rylander, Dr. James Tunnell, Dr. Andrew Dunn, Dr. Peter Gascoyne, Dr. Paul Ho and Dr. Christine Schmidt who have helped broaden my horizons. If it were not for them I would not have been exposed to the different research topics besides my thesis.

The students at the BioMEMs lab have been incredible and made graduate school life exciting and interesting. I would like to thank them for their feedback of my research, attending my practice talks; proofreading my abstracts and papers and indulging in technical and non-technical discussions that kept me entertained and provoked my thinking. I would like to make a special mention of our research associate, Dr. Kaz Hoshino, for without him this dissertation would not have been possible. He has been a

great mentor and friend during my 5 years of Ph.D. I would also like to thank Yu-Yen Huang (Eric), Tushar Sharma, Zhiguo Wang, Elaine Ng, Ellen Blinka and Kathryn Loeffler for a great time in the lab and on Thursday nights. I would like to thank my co-workers in the, past and present, Jean Fakhoury, Andrew Horton, Sunmin Kim, Travis Turner, Yuyan Wang, Ye Hu, Karthik Kumar and Gabe Dagani who have made working in the lab an enjoyable experience.

My social life outside the lab was a rich source of sustenance during grad school. I owe it to my best friends at Austin, especially Reeja Jayan, Aji Anirudhan, Chinmayi Krishnappa, Hari Nair, Ramya Duddukuri, Jubin Jose, Aneesh Reddy, Priyamvada Jadaun and Yagnya Deepika. You guys have helped me survive more than you know it.

How can I forget, my first two years of graduate school, when I started in the fall of 2005, there were a few people I really got close to and I would like to thank them for my growth. I owe it all to Narasimhan Rajaram, Ashwin Parthasarathy, Sarath Deverajan and Kartik Agaram. Thanks for being there. I would also like to thank my ex-roommates Vacha Dave, Priyaveena Puvanakrishnan and Madhavi Krishnan for their cooking without whom I would have gone hungry on many occasions.

Finally there are three people in my entire life that made it happen. Thanks to Amma, Appa and Pinky who have been through my ups and downs during grad school. Having extended hours of skype chat almost every day, laughing and fighting over numerous topics, helped me grow as a person. Thanks for the infinite patience, help, advice, and encouragement and support you provided. I couldn't have done it without

you. Special thanks to Kartik Sundareswaran for supporting me during my last stages of the Ph.D. and managing a long distance relationship just after marriage.

Writing the acknowledgement section has been surprisingly a valuable opportunity to thank everyone for everything I learned over the years. I am really grateful to all of you.

Multicolor Colloidal Quantum Dot Based Inorganic Light Emitting Diode on Silicon: Design, Fabrication and Biomedical Applications

Publication No._____

Ashwini Gopal, Ph.D.

The University of Texas at Austin, 2010

Supervisor: Xiaojing Zhang

Co-Supervisor: Dean P. Neikirk

Controlled patterning of light emitting diodes on semiconductors enables a vast variety of applications such as structured illumination, large-area flexible displays, integrated optoelectronic systems and micro-total analysis systems for real time biomedical screening. We have demonstrated a series of techniques of creating quantum-based (QD) patterned inorganic light emitting devices at room temperature on silicon (Si) substrate. In particular:

(I) A combination of QDs self-assembly and microcontact printing techniques were developed to form the light emission monolayer. We expand the self-assembly method with the traditional Langmuir-Schaeffer technique to rapidly deposit monolayers of core: shell quantum dots on flat substrates. A uniform film of QDs self-assembled on

water was transferred using hydrophobic polydimethylsiloxane stamps with various nano/micro-scale patterns, and was subsequently stamped. A metal oxide electron transport layer was co-sputtered onto the QDs. The structure was completed by an e-beam evaporating thin metal cathode. Multicolor light emission was observed on application of voltage across the device.

(II) We also demonstrate the photolithographic patterning capability of a metal cathode for top emitting QDLEDs on Si substrates. Lithographic patterning technique enables site-controlled patterning and controlled feature size of the electrode with greater accuracy. The stability of inorganic silicon materials and metal oxide based diode structure offers excellent advantages to the device, with no significant damage observed during the patterning and etching steps. Efficient electrical excitation of QDs was demonstrated by both the methods described above.

The technique was translated to create localized QD-based light sources for two applications: (1) Three-dimensional scanning probe tip structures for near field imaging. Combined topographic and optical images were acquired using this new class of "self-illuminating" probe in commercial NSOM. The emission wavelength can be tuned through quantum-size effect of QDs. (2) Multispectral excitation sources integrated with microfluidic channels for tumor cell analyses. We were able to detect the variation of sub-cellular features, such as the nucleus-to-cytoplasm ratio, to quantify the absorption at different wavelength upon the near-field illumination of individual tumor cells towards the determination of cancer developmental stage.

Table of Contents

Acknowledgements ..... **v**

List of Tables ..... **xiii**

List of Figures ..... **xiv**

CHAPTER 1: BACKGROUND AND SIGNIFICANCE **23**

1.1 Motivation 23

1.1.1 Near Field Scanning Optical Microscopy 26

1.1.2 On Chip Spectrometer for Point of Care 28

1.2 Dissertation Roadmap 32

CHAPTER 2: DESIGN OF QUANTUM DOT BASED LIGHT EMITTING DIODES **33**

2.1 Introduction 33

2.2 Review Of Light Emitting Diodes 33

2.2.1 Inorganic Light Emitting Diodes on Silicon 33

2.2.2 Organic Light Emitting Diodes on Silicon 36

2.3 Colloidal Quantum Dot based Light Emitting Diodes 38

2.3.1 Quantum Dots 38

2.3.2 Quantum Dot Patterning Methods 42

2.4 Structure and Energy Band Diagram 45

2.4.1 Structure Design 45

2.4.2 Band Diagram 46

2.5 Summary 48

CHAPTER 3: DEVICE FABRICATION **50**

3.1 Introduction 50

3.2 Device Fabrication 51

3.2.1. Silicon Substrate Preparation 53

3.2.2. Re-suspension of Quantum Dots 54

3.2.3. Sputtering Conditions 54
3.2.4. E-Beam Evaporation Conditions 54
3.3 Thin Film Formation 55
3.3.1. Radius of Curvature of Water Level 56
3.3.1 Theory of Thin Film Formation 57
3.3.2 Solvent Optimization 59
3.3.3 Water Surface Curvature 60
3.3.4 Evaporation Rate 60
3.4 Micro contact printing 61
3.4.1. Transfer of Particles 61
3.5 Sputtered Thin Films 64
3.6 Metal Cathode Films 65
3.7 Summary 65

CHAPTER 4: PROCESS CHARACTERIZATION 67
4.1 Introduction 67
4.2 Nanoparticle Characterization 67
4.2.1 Transmission Electron Microscopy 69
4.2.2 Atomic Force Microscopy 70
4.2.3. Absorption Measurement 74
4.2.3 Scanning Electron Microscopy 76
4.3 Nanoparticle Thin Film: Optimization and Working 77
4.4 Metal oxide optimization 79
4.5 Meal oxide film characteristics 81
4.5.1 X-Ray Diffraction 81
4.5.2 Atomic Force Microscopy 83
4.6 Summary 84

CHAPTER 5: QDLED CHARACTERIZATION 86
5.1 Introduction 86
5.2 Electroluminescent Characteristics 86
5.3 Diode Characteristics 88

5.3.1 Silver/Gold Cathode 88
5.3.2 Aluminum Cathode 93
5.4 Operation Characteristics 96
5.5 Post Processing of Diode 97
5.5.1 Fabrication Process 99
5.5.2 Electroluminescence Characteristics 101
5.6 Nano-partterning to Define Light Source 104
5.7 Summary 111

CHAPTER 6: APPLICATION OF QD-LED 113
6.1 Introduction 113
6.2 Nano-LEDs for NSOM Application 113
6.3 Micro-contact Printing of QDs onto Silicon Probe Tips 116
6.4 Multicolor Light Emitting Sources on Silicon Probes 118
6.5 On Chip Integrated Spectrometer 123
6.6 QD-LEDs Integrated with Biosamples 125
6.6.1 Cancer Samples 126
6.6.2 Excitation of Cells 128
6.7 Summary 134

CHAPTER 7: CONCLUSIONS AND FUTURE WORK 136

References 140

Vita 150

List of Tables

Table 4.1: Estimated concentration of quantum dots required to create thin monolayers.....69

Table 4.2: Bandgap energy of the Quantum dot particles.....75

Table 4.3: Metal/Metal oxide characteristics (a) Roughness (b) Film Thickness.84

Table 5.1: Observed luminance of the device with different cathodes.....96

List of Figures

Figure 1.1: Schematic of a typical QD-LED structure [HTL: Hole transporting layer, ETL: Electron Transporting Layer]. 25

Figure 1.2: Schematic of near field scanning optical microscope scanning a surface. 26

Figure 1.3: Schematic of integrated bio-imaging system. 31

Figure 2.1: Synthesized Colloidal quantum dots made of the same material CdSe: ZnS [60]. 38

Figure 2.2: Absorption (vs.) Fluorescence of quantum dot with different emission wavelength [60]. 39

Figure 2.3: Core: Shell CdSe: ZnS configuration with outer TOPO or ligand layer [60]. 40

Figure 2.4: Band diagram comparison of bulk semiconductor CdSe vs. colloidal nanocrystal CdSe. 41

Figure 2.5: Schematics of silicon-based quantum dot light emitting diode design.46

Figure 2.6: Schematic of the band diagram of the diode. 46

Figure 2.7: Device function on application of voltage to the device. 47

Figure 2.8: Band diagram of the device in forward bias. 48

Figure 3.1: Schematic of silicon-based quantum dot light emitting diode. 51

Figure 3.2: Fabrication process for quantum dot light emitting diode (a) <100> p type wafer with 1 nm silicon dioxide grown on surface. (b) Self-assembled quantum dot film was transferred onto a PDMS micropattern. (c) Transfer of quantum dot pattern onto silicon substrate. (d) Sputtering of 40 nm of ZnO: SnO_2 onto the quantum dot substrate. (e) E-beam evaporation of metal. 53

Figure 3.3: Experimental setup for monolayer formation. (a) Schematic of experimental setup indicating the teflon ring with inner diameter of 2 cm and outer diameter of 5 cm was placed in the center, pinning down the water and creating a slightly convex water shape in the middle. The hydrophobic colloidal suspension was slowly poured on top of this surface. (b) Picture of the actual setup with quantum dots excited by an ultraviolet light emitting diode (UV LED) source in the bottom. Emission wavelength of the particles is 606 nm.....56

Figure 3.4: Self-Assembly Mechanism. (A) The solvent evaporates, thinning the layer of colloidal suspension throughout the water surface. (B) Menisci of solvent forms between the exposed nanoparticles and capillary immersion forces pack them together. (C) The contact line grows outward radially due to further evaporation and convective force that draws additional nanoparticles from the suspension to the edge of the growing film. (D) The meniscus slope angle increases, which cause multilayers of nanoparticles to form near the edge ($\beta>\alpha$). 59

Figure 3.5: Microcontact printing of Quantum dots onto substrate.....61

Figure 3.6: Principle of quantum dot film self-assembly and micro-contact printing. These steps illustrate total film self-assembly and microcontact printing process: 1. Convex water surface is created; 2. Colloidal suspension is poured; 3. Film is self-assembled; 4. Hydrophobic PDMS stamp is lowered, picking up the film; 5. PDMS stamp is lowered onto flat substrate; 6. Film is stamped onto the flat substrate. 62

Figure 3.7: QDs on PDMS substrate (a) Before micro-contact printing and (b) After microcontact printing. 63

Figure 3.8: Photoluminescence of patterned quantum dots (a-d) PDMS stamps with 100 μm-diameter cylinders were used to stamp uniform, self-assembled films with quantum dots of emission wavelengths (from left) 620 nm, 600 nm, 580 nm and 560 nm (Scale: 50 μm). (e) Fluorescence image of Bevo with emission wavelength 600 nm and particle size 9.0 nm (Scale:50 μm).....63

Figure 3.9: Optical transmittance spectrum of top inorganic layers indicated. Solid line: ZnO: SnO_2 (40 nm), Dashed line Au (5 nm)/Ag (12nm)/ ZnO: SnO_2 (40 nm).....64

Figure 4.1: TEM images of stamped particles (9.0 nm average diameter) deposited using the microcontact printing technique (the arrows indicate the close-in view into the rectangular window). 70

Figure 4.2: Numerical image processing flow to correlate thickness of stamped film to its photoluminescence. Samples of stamped quantum dot films using 100 μm diameter PDMS stamps were used to correlate the thickness of film to its fluorescence intensity, or photoluminescence. (a) Section analysis on the film edges was performed to measure thickness of the stamped film. (b) The fluorescence optical micrograph was processed by MATLAB® by first averaging RBG values per pixel to yield fluorescence intensity, then averaging the fluorescence intensity values inside each region of the film.This value was plotted with the corresponding film thickness. 72

Figure 4.3: Patterned particles with 576 nm emission wavelength: (a) Fluorescence image. (b) AFM image indicating the height of deposition 33 nm. (c) Thickness of film measured by the AFM was plotted versus processed fluorescence intensity values. Using the plotted graph, thickness distribution of the quantum dot layer can be easily estimated from the fluorescence image without time taking AFM measurement. Positive linear correlations were seen in the films with all emission wavelengths tested. 74

Figure 4.4: Absorption spectrum of the particles with emission wavelength (620 nm, 600 nm, 580 nm and 560 nm) 75

Figure 4.5: SEM images of stamped quantum dots. (a) Image of a single 100 μm diameter stamped pattern (b) Circular array pattern. The SEM images show that the quantum dot crystals are not very monodisperse or spherical, but that they can still form a closely packed and uniform monolayer. 76

Figure 4.6: Photo/Electroluminescence from an identical circular pattern (circle diameter: 100 μm). (a) Photoluminescence image. (b) Electroluminescence observed from thinner portion of quantum dot layer. (c) Intensity plot of photoluminescence to estimate local thickness distribution. 79

Figure 4.7: Simultaneous emission from ZnO and CdSe: ZnS nanoparticles. Photoluminescence observed from particles with emission wavelength of 598 nm. Electroluminescence identical to ZnO: SnO_2 (yellowish-white) emission was simultaneously observed along with particle emission (Orange) on application of voltage. (Embedded image: CdSe: ZnS and ZnO: SnO_2 emission (Scale bar: 100 μm). 80

Figure 4.8: EDX data indicating 40% Zn and 25% Sn in ZnO: SnO_2 mixture (Inset: TEM image of 40 nm deposited film. Scale: 30 nm).....81

Figure 4.9: XRD of ZnO sputtered onto silicon substrate. 82

Figure 4.10: XRD image indicating the amorphous nature of the ZnO: SnO_2 mixture deposited over an area of 1 inch x 1 inch. 83

Figure 4.11: AFM of sputtered thin film (a) ZnO (b) ZnO: SnO_2 (c) Al/ZnO: SnO_2. 84

Figure 5.1: Photoluminescence and electroluminescence from patterned silicon substrate with the average diameters of (a, b) 9.8 nm and (c, d) 7.8 nm. (Circle pattern: diameter-100 μm). 87

Figure 5.2: Band diagram of the quantum dot based light emitting diode on silicon working under forward bias conditions. 88

Figure 5.3: Basic characteristics of three different color (red, orange and yellow) LEDs. (a1, b1, c1): Current versus voltage. (a2, b2, c2): Luminance versus current characteristics. (a3, b3, c3): Photoluminescence and electroluminescence with different operating conditions. The inset images show electroluminescence for the QD-LED under operation.92

Figure 5.4: Intensity characteristics of four different color (red, orange, yellow, green) LEDs. (a, b, c, d): Photoluminescence and electroluminescence with different operating conditions.....94

Figure 5.5: Electroluminescence observed from patterned quantum dots on silicon substrates. (Top row) Patterned light emission observed from circles of diameter 100μm with emission wavelength 620 nm, 580 nm and 560 nm. (Bottom row) Nano-patterned electroluminescence with smallest feature size 500 nm x 500 nm and emission wavelength 600 nm and 560 nm. Light emission was also observed from Bevo pattern.....95

Figure 5.6: Variation of electroluminescence intensity versus time for light emitting diode with different metal cathode. 97

Figure 5.7: Fabrication process of QD-LED. (a) Microcontact printing of monolayer's of quantum dots onto SiO_2/p-Si substrate. (b) Transfer of particles. (c) Sputter deposition of ZnO: SnO_2 (10 nm) and e-beam evaporation of Al (15 nm).(d) Spin coating of AZ 5209A. (d) Pattern, develop and reactive ion etching of the device. (f) Completed inorganic light emitting diode.....100

Figure 5.8: Optical transmission of the various films deposited. 101

Figure 5.9: Patterned top aluminum electrode. (a) Electroluminescence observed for patterned top electrodes with feature size 20 μm; (b) Schematic of patterned nanoparticles and Top Aluminum electrode. 101

Figure 5.10: Patterned electrode emission from two colors. (a) Photoluminescence from 620 nm and 580 nm patterned quantum dots. (b) Electroluminescence observed from particles with emission wavelength 620 nm at a voltage of V = 12 V.(c) Electroluminescence observed from particles with emission wavelength 580 nm at 15 V. 102

Figure 5.11: Electroluminescence and Photoluminescence (PL) observed from particle size of (a) 9.0 nm and (b) 7.8 nm. 103

Figure 5.12: Current density versus voltage characteristics of a 2 mm^2 area inorganic light-emitting device. Inset: Electroluminescence intensity variation with current flowing through the device (Emission wavelength of the diode 600 nm). The completed device consists of 15 nm thick Al/10 nm thick ZnO: SnO_2 top of 25 nm thick CdSe: ZnS nanoparticles /SiO_2/p-Si.104

Figure 5.13: AFM of the master mold for nano-stamps 106

Figure 5.14: Electroluminescence observed for different emission wavelength. (Scale: 25 μm).....106

Figure 5.15: (Left) Electroluminescence of particles with emission wavelength 560 nm. (Right) Dotted lines give the exact area where AFM was performed. 107

Figure 5.16:AFM versus electroluminescence for nanopatterned light emitting diodes observed from particle size of (a) 9.0 nm and (b) 7.8 nm.....108

Figure 5.17: (Left) Schematic of patterned aluminum electrode and measured values of PL, EL and AFM at the yellow lines indicated in the images on the right. (Right) Patterned top metal cathode (a) Photoluminescence (b) Electroluminescence and (c) Atomic force microscopy of etched aluminum electrode with 5μm feature size. Arrows in the bottom indicate aluminum step and the arrows on top indicate the quantum dot step. (The profile measurement on the left figure was measured at the orange bar indicated.) 110

Figure 6.1: Translation of LED on flat substrate to 3D probe structure on silicon substrates.....116

Figure 6.2: Quantum dot stamping on the probe tip. (a) Bright field image of the silicon probe. (b) Photoluminescence image of the probe stamped with QDs. (c) Photoluminescence "void" pattern of the PDMS stamp after the film is picked up by the probe. (d) AFM image of the void pattern. (e) Electroluminescence from the probe tip. (f) Illustration showing the stamping process (g) AFM profile of the QD void pattern showing the film thickness. The embedded picture shows the scan line, taken from the tip part of the AFM image (d)[6]. 118

Figure 6.3: Chemically wet etched silicon probe tips.....119

Figure 6.4: Schematic of LED created on silicon probe tips. 120

Figure 6.5: Electroluminescence (EL) from QD-LED probe tip. Emission wavelengths peak ranged from 580 nm to 620 nm. Scale bars = 50 μm. 120

Figure 6.6: Characteristics of the on-probe QD-LEDs. (a) EL spectra measured from QD-LEDs at probe tips. (b) Typical current-voltage (I-V).....121

Figure 6.7: Nano-LED mounted on an NSOM setup. 122

Figure 6.8: Schematic of integrated bio-imaging system. 125

Figure 6.9: Cultured and stained. (Left) MDA 235. (Right) PC 3 cells on glass slides. 127

Figure 6.10: HEMA 3 stains. (a) Absorption measurement. (b) Transmission measurement. 128

Figure 6.11: Excitation of MDA 435 using multicolor colloidal quantum dot based LED. (a) Transmission observed from the MDA 435. (b) Electroluminescence from QD-LED observed. 129

Figure 6.12: (a) Electroluminescence spectrum of individual excitation sources. (b) QD-LED with emission wavelength 580 nm. (c) 560 nm (d-f) MDA 435 cancer cells excited by QD-LED. 130

Figure 6.13: QD-LED excitation of (a,c) MDA 435 (b) MDA 231 (d) PC3 131

Figure 6.14: Measured transmission of the dye along with the electroluminescence from QD-LED (a) 620 nm and (b) 580 nm. 131

Figure 6.15: Excitation of the exact same region using two excitation sources. (a) PC 3 cells. (b) MDA 435 cells (Scale 100 μm) [Orange line indicates intensity variation]. 132

Figure 6.16: Intensity variation in a single cell excited by two-excitation source (a) 580 nm (b) 606 nm (MDA 435 cells). 133

Figure 6.17: Intensity variation in a single PC 3 cell excited by (a) QD-LED on silicon and (b) Commercial LED. 134

Figure 7.1: Towards translation research. 138

CHAPTER 1: BACKGROUND AND SIGNIFICANCE

1.1 MOTIVATION

Silicon based light sources represents a new path towards integrated, compact and mass manufacturable microsystems for advanced computing, networking and sensing [1-3]. Silicon light emitting diodes (LEDs) have been demonstrated in the visible spectrum, using porous silicon [1] and, most recently, multi-color emission from silicon nanowire [2]. Silicon optical emitters are in particular one of the key components in future nanophotonics-based micro-total analysis systems for sensing and imaging with molecular resolution [4, 5]. Recently, we have demonstrated silicon scanning probes with monolithically integrated nanometer scale light emitting diodes at a probe tip, and successfully acquired near-field optical images [6-10].

Silicon-based light emitting diodes have also been developed on bulk substrates using ion implantation at high doses with subsequent high-temperature annealing [11]. However, silicon, being an indirect band gap material, makes it fundamentally a poor light emitter [12]. Silicon light emitting diodes in the visible spectrum have been demonstrated using porous silicon [1], silicon/silicon dioxide superlattice [13] and embedding silicon nanoparticles in silicon dioxide [14]. Each of these techniques has shortcomings that make silicon not suitable as a light emitter. Silicon by itself is not an efficient light-emitting source. There are certain advantages of silicon that make it really attractive for light emitting diode applications. Silicon can be fabricated into desired shapes and configurations using lithography and etching techniques. These make it

desirable for various micro-electro-mechanical systems (MEMS) based integrated application systems. Silicon being complementary metal oxide semiconductor (CMOS) compatible makes it attractive for numerous on-chip integrated photonic systems applications. Making use of existing technologies, we use silicon as a base or fundamental structure for charge injection in the LEDs that we developed. Instead of using silicon as the light-emitting layer we use semiconductor colloidal quantum dots as a light emitter in our device.

Colloidal quantum dots have recently been used as lumophores in light emitting devices on glass or indium tin oxide (ITO) [15-17], largely due to their unique tunable luminescence properties. The emission wavelength of the particle is controlled by the size of the nanoparticles of the same material. Nanoparticle or quantum dot based light emitting structures with integrated organic layers have shown improved external quantum efficiencies [18]. Advantages such as narrow bandwidth and high luminescence quantum yield make them suitable for LED applications [19, 20].

Typical colloidal quantum dot based light emitting diodes have a sandwich structure. The quantum dots are present between a hole transporting layer (HTL) and an electron-transporting layer (ETL) in the device. On application of voltage excitons are formed near the quantum dot region whereby light emission is observed from the nanoparticles (Figure 1.1). Despite their high quantum efficiencies observed in the diodes**,** these organic based light emitting structures are susceptible to atmospheric conditions, moisture, thermal and electrochemical degradation [16, 21]. It is hence desirable to have inorganic transport layers for robust LED structures. Early work on inorganic LEDs had quantum dots sandwiched between either silver and Indium Tin Oxide (ITO) [22] or NiO and ZnO:SnO_2[23]. These LEDs have been developed on ITO

substrates, which are not efficient in injecting holes to polymer layers, and an additional hole transporting layers is typically required [24, 25].

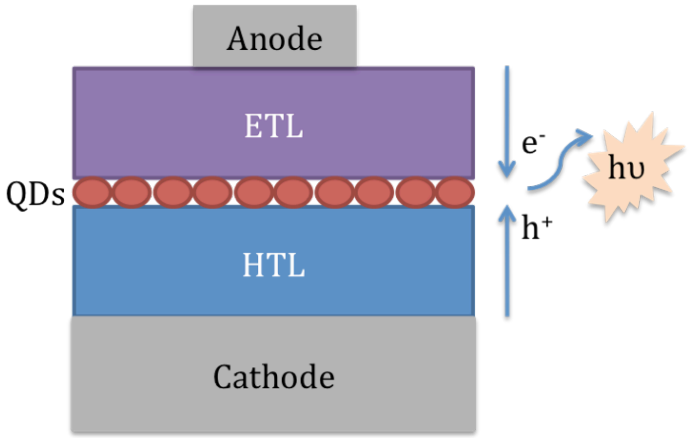

Figure 1.1: Schematic of a typical QD-LED structure [HTL: Hole transporting layer, ETL: Electron Transporting Layer].

In our device we have used colloidal quantum dots (QDs) as the light emitter in an inorganic light-emitting device with silicon as the hole transporting layer. The light emitting sources are patterned onto the substrate via micro-contact printing. The emission areas (quantum dot area) are patterned by two methods: (a) micro-contact printing and (b) post processing of top electrode to define emission area. Both methods have advantages for various applications. Micro-contact printing of the active area enables the creation of patterned light sources defined by the size of the patterning polymer. Post processing enables the creation of multicolor light sources on a single substrate, which can be excited in close proximity for imaging biological specimens.

The ease of fabrication and processing of colloidal quantum dots on silicon, through microcontact printing and further integration with metal oxides, opens up the possibilities for creating nanophotonic microsystems with mass reproducibility and

enables robust and tunable imaging, sensing and display applications. Here we describe two possible applications that have been investigated with the diodes created: (a) Nano-light emitting diodes for near-field scanning optical microscopy and (b) Multispectral light sources for point of care detection devices.

1.1.1 Near Field Scanning Optical Microscopy

Near field scanning optical microscopy (NSOM) is a microscopic technique for investigating nanostructures that breaks the far field resolution limit [26]. An NSOM can be operated with an aperture and a non-aperture mode. Apertured tips have many issues associated with the tips such as heating, artifacts, contrast, sensitivity, topology and interference amongst others. Conventional NSOM has a resolution that is directly related to the size of the light through the probe used. Typical size of the aperture of probe is 50 nm to 150 nm in diameter. NSOM have typically been used for a number of applications such as molecular feature characterization of organic interfaces [27], polymers [28] and optical recording for data storage devices [29].

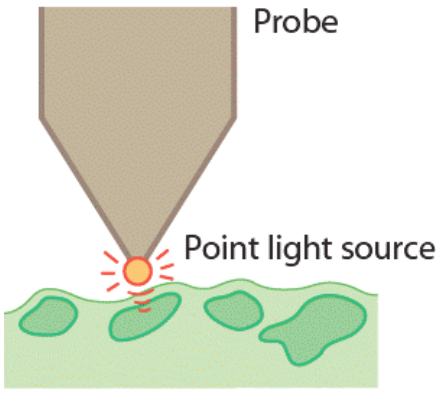

Figure 1.2: Schematic of near field scanning optical microscope scanning a surface.

Conventional NSOM is a powerful tool for exploring nanoscale features in thin films (Figure 1.2). The major drawback with this system is the manual assembly process of the probe with an illuminating fiber that reduces its capability for large-scale applications. Also, the requirement of an external light source for each probe increases the complexity. A number of techniques for miniaturizing the NSOM probes have been developed using MEMS [4]. Light absorbing gold particles [30] and fluorescent beads [31] have been attached to the scanning tips to improve the resolution of the NSOM tips. The resolutions of these have been determined by the amount of light coupled to the tip. An external laser source is required for excitation that makes the system bulky and complicated.

Creation of 'apertureless' small light sources will directly lead to resolution improvement. Secondly, the light source is built in on the tip, and a compact system can be made without any external light sources. Vertical-cavity surface-emitting lasers [32] on the NSOM probes were reported to integrate a light source, but the light emitting areas were larger than several micrometers and the probes still required a metal coating with an aperture to obtain the diffraction's limited resolution. Integration of organic light emitting diodes (OLEDs) on the scanning probe has also been reported recently, and the size of the light emitting diode was approximately 10 μm x 10 μm [33]. This light source would be too large to work in near field applications.

We believe that creating a small light emitting diode with inorganic semiconductor quantum dots as the light emitter would improve the resolution of the near field imaging system. The resolution of the system is mainly defined by the size and position of the light emitting diode. Resolution that we could achieve theoretically would be that of a single QD molecule (size: 5 nm - 10 nm). Another advantage of using the QD-based light source is that multicolor emission can be observed by varying the QDs

incorporated into the system. Inorganic LEDs tend to improve the lifetime and the stability of the system. These near field imaging systems have potential applications in nano-drug distribution measurement in biomaterials [34].

In order to create an inorganic light emitting diode we initially fabricated QD-LEDs on flat silicon test substrates [19]. The emission wavelength was tailored by a choice of quantum dots used. The creation of the light emitting diodes on the flat silicon substrate was then translated to silicon probes that were fabricated using conventional silicon fabrication techniques [8]. Our experiments and efforts reveal that multicolor colloidal quantum dot based light emitting diodes fabrication process is compatible with traditional CMOS processing in the semiconductor industry thus would enable integration with near field imaging system while significantly reducing fabrication costs.

1.1.2 On Chip Spectrometer for Point of Care

Site-controlled patterning of light emitting diodes has importance in a number of applications such as MEMS and multicolor excitation sources in micro-total analysis systems (μ-TAS). Combination of filter cubes or laser sources are typically used for standard fluorescence microscopes, which are not suitable for easy-to-use on-site reduced cost diagnostic tools.

We have developed QD-LEDs that are planar and easy to integrate to on-chip systems compared to commercial systems. The light emitting area in these diodes can be defined by a combination of (a) micro-contact printing and (b) post processing the cathode of the device. These diodes were then post processed to define the cathode, thereby defining multicolor sources on a single substrate. Multicolor LEDs on a single

substrate offer a unique capability to excite cells with individual excitation sources in a single substrate for on-chip multicolor imaging.

Integration of LEDs for biomedical applications has been demonstrated previously by incorporating OLEDs [31, 35, 36]. Integrated OLEDs are placed on the rear side of the glass substrate and a microfluidic channel made out of polydimethylsiloxane (PDMS) on the front side. The emission wavelength of the OLED is 520 nm and has a relatively wide peak of 70 nm. Visual inspection of excitation of fluorescent dye Rhodamine B was demonstrated [37].

Polyfluorene-based OLEDs fabricated on a separate glass substrate were placed in close proximity to a glass chip as an excitation source. The emission peak was centered at 488 nm and could be operated with only 3.7 V. The dyes fluorescein and carboxyfluorescein were separated and detected at detection limits as low as 1 μM [38]. OLEDs with a 0.3 mm-thick interference filter combined with a 400 μm pinhole were used to achieve effective excitation at the appropriate wavelength [35]. Detection of the emission light was achieved by an optical fiber coupled to a PMT, giving a detection limit of 3 μM for the Alexa 532 fluorescent dye.

The current drawbacks of OLEDs are low irradiance and light purity. The OLEDs typically require an additional excitation filter that would enable excitation from a narrow bandwidth light source. The full width half maximum (FWHM) emission of OLEDs is typically broad. These devices have to be secured in special enclosures to make sure there is no contact with oxygen or moisture since the devices are susceptible to damage under different circumstances.

Integration of silicon photodiode on the microchip has been demonstrated by [39]. They used a blue LED, cadmium sulfide (CdS) optical filter and a silicone photodiode. The optical chip used for detection in the microfluidic channel was placed in close proximity to achieve a compact system [39]. The advantage of this system was that the integrated microfluidic system was disposable while the optics part could be reused.

An alternate method of integrating a light-emitting silicon avalanche diode, which consisted of a single-mode planar waveguide, a Si photodetector and a microfluidic channel cast in PDMS, has been presented [40]. The device was tested with the biotin–streptavidin-binding assay giving detection limits of 3.8 and 13 pM for the gold nanoparticle-labeled streptavidin concentration for continuous and stopped–flow assays, respectively.

An integrated excitation source with a lab-on-a-chip would have impact in many areas including: (1) diagnostics, (2) environmental and (3) biomedical research by reducing costs for expensive projects such as genomics or proteomics measurements.

Our experiments were carried out using site-controlled QD-LEDs patterns to excited MDA 435 and PC-3 cancer cells (Figure 1.3). MDA 435 cell line was derived from a female patient with breast cancer and has been used as a model for critical studies in early cancer diagnosis [41]. PC 3 is a prostate cancer cell line that is derived from advanced bone metastasized prostate cancer [42]. The technology to create diodes is potentially capable of patterning colloidal quantum dots with well-defined geometry and size. The full width half maximum of the emission wavelength is narrow on the order of 15-20 nm. This gives good control on the emission wavelength and light purity for spectroscopic measurement in the visible wavelength. These diodes have a capability of multicolor excitation on as single chip. Each individual excitation can be easily

controlled due to the patterning capability of the top electrode. The measured nucleus-to-cytoplasm ratio of the cancer cells indicates the developmental stage of the cancer cells**.** This technology opens up exciting opportunities for on-chip fluorescence based tumor cell identification for early cancer detection.

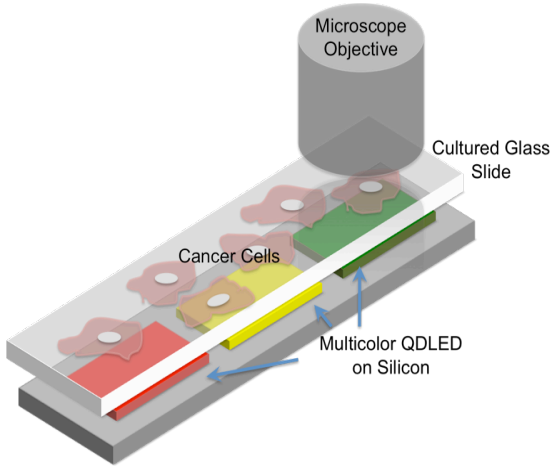

Figure 1.3: Schematic of integrated bio-imaging system.

This dissertation presents three specific intellectual contributions. First, we have developed a simple process of creating multicolor light emitting diodes on silicon. The light emitting area is patterned by a combination of modified Langmuir Schaefer and micro-contact printing of the quantum dots onto the silicon substrate. Taking the advantage of color tunability of colloidal quantum dots and integrating it with silicon would help create a CMOS compatible LED. These LEDs were created using a combination of inorganic materials such as metal, metal oxides and quantum dots on silicon. These light-emitting diodes have demonstrated extended lifetimes and post-processing capability.

Second, we demonstrated the translation of the nano-light emitting diodes from flat substrate to silicon probe tips to create apertureless near field scanning optical microscopy systems. Near-field Scanning Optical Microscopy measures sub-wavelength

optical properties as well as nano-scale topographic properties. A near-field optical scanning probe equipped with a nanoscale light emitting diode (Nano-LED) would help improve the resolution of the imaging system.

Third, we demonstrated the use of multicolor emissions from the light emitting devices that can be incorporated as a part of point of care devices. It is possible to accurately define multicolor light sources on a single substrate, which open up the possibilities for creating microsystems for imaging multiple cancer cell lines. Integration of QD-LED with cancer cells or microfluidic systems can be integrated into a single chip to create a spectroscopic measurement system that would act like a biosensor.

1.2 DISSERTATION ROADMAP

The motivations for the dissertation and the choice of approach are introduced in Chapter 1. An overview of silicon-based and colloidal quantum dot based light emitting diodes technologies that can be combined and used in the development of multicolor light sources on a single substrate is discussed in Chapter 2. Chapter 3 describes the design and fabrication of the light emitting diodes on silicon using quantum dots as the light emitters. Chapter 4 presents the thin film characteristics of the device that is required for the ideal device performance. The electroluminescence and diode characteristics of the devices are described in Chapter 5. In Chapter 5 we also describe the creation of nano-light emitting diodes by two methods: (a) micro-contact printing and (b) post processing. Chapter 6 describes the application of light emitting diodes as a near field-imaging source and as multispectral light sources for point of care. Finally, Chapter 7 summarizes the dissertation and presents future research directions.

CHAPTER 2: DESIGN OF QUANTUM DOT BASED LIGHT EMITTING DIODES

2.1 INTRODUCTION

Light emitting diodes (LEDs) emit light by passing current through an emissive layer [43]. These light-emitting devices can be classified into two types: (a) inorganic based light emitting diodes and (b) organic based light emitting diodes. LEDs have vast applications in traffic signals, full color displays for televisions, cell phones, flashlights, etc. [43]. LEDs typically have good viewing angles and better power consumption because of their lack of additional filters.

We start with the discussion of inorganic based light emitting diodes on silicon, followed by organic light emitting diodes on silicon. We continue the discussion by introducing colloidal quantum dot based light emitting diodes and implementation into one of these systems to create inorganic colloidal quantum dot based light emitting diodes on silicon.

2.2 REVIEW OF LIGHT EMITTING DIODES

2.2.1 Inorganic Light Emitting Diodes on Silicon

Silicon is an indirect band gap material. The radiative band-to-band transitions are rare. These materials have radiative recombination lifetime on the order of milliseconds. As a consequence, nonradiative recombination at the defects is dominant. This leads to very low efficiencies, especially at room temperature. A number of different methods

have been used to investigate emission from silicon. These can be classified into (a) Bulk silicon light emitting diodes, (b) rare earth doped nanocrystalline silicon, (c) SOI based LEDs and (d) porous silicon based LEDs.

(a) Bulk Silicon Based Light Emitting Diodes

Bulk silicon based light emitting diodes are typically fabricated using ion implantation followed by a thermal process. These diodes have high efficiency that is caused by the carrier confinement due to the local potential barriers introduced by a stress free field around the dislocation loops. However, these LEDs in bulk Si have the disadvantage of low switching speed, limited by the long radiative recombination lifetime and lack of spatial confinement of generated light, which makes it difficult to use it as a source for optical on-chip interconnects [44-46].

(b) Rare Earth Doped Silicon Diodes

Rare earth elements such as Erbium, Gadolinium and Ytterbium (Er, Gd, Yb) are typically doped into silicon LEDs. These diodes can emit in the violet (316 nm), visible (850 nm) and infrared (1500 nm) region. The working principle for the generation of photons is the excitation of rare earth atoms by hot electrons. Erbium doped silicon diodes have seen vast applications in telecommunication wavelengths. The emission from these diodes has a broad spectrum of emission wherein the color purity is not good. These diodes have a drawback of poor stability and poor operation speeds [47].

(c) SOI Based LEDs

LEDs fabricated on silicon on insulator (SOI) have advantages over bulk silicon, such as better optical switching speeds, lower power consumption and better coupling of light into waveguides. These diodes have, however, lower output efficiency compared to bulk silicon LEDs [7]. Low radiation occurs due to the non-radiative recombination process that occurs at the interface.

(d) Porous Silicon Based LED

Electroluminescent devices using porous silicon was observed during anodic oxidation that is using a liquid contact [48]. LEDs reported later emitted red light at the junction between gold and n-type porous silicon substrate [49]. These LEDs emitted light with the same intensity in both forward and reverse bias at high voltages and operated with low threshold efficiency. The main disadvantage of these systems is that there is the long carrier lifetime that restricts the modulation rate of the device.

Silicon by itself is not an efficient light emitting device source, but the advantage of silicon is that it can be fabricated to desired shapes and configurations making it desirable over a number of MEMS based applications. Also, the CMOS compatibility of silicon makes it attractive for numerous on-chip integrated systems. Taking the advantages of silicon we use it as a base structure for charge injection in the light emitting diodes that we create.

2.2.2 Organic Light Emitting Diodes on Silicon

Since it is very difficult to gain good light emission from silicon directly because of its indirect band gap nature, one alternate way to overcome this obstacle is to combine an organic light-emitting diode (OLED) with a silicon wafer [50]. Organic light emitting diodes are devices in which the electroluminescent layer is a film of organic compounds that emit light when current pass through the device. The organic semiconductor material is typically formed between two electrodes.

Compared to inorganic light emitting diodes, organic light emitting diodes are cheap to produce. OLEDs are now available in cell phones, television, digital cameras, etc. [51]. OLEDs have the advantage of good color, brightness, contrast, power efficiency and fast response time. They also possess problems such as instability and lower carrier mobilites in organic light emitters. OLEDs have been developed on silicon by using both p-type and n-type silicon as anodes. The electroluminescence efficiency of n-Si anodes is typically lower than those of p-Silicon anodes.

(a) Organic Light Emitting Diodes with p-Si

Organic light emitting diodes have been developed on silicon during the early 1990s [50]. Typically in silicon based organic light emitting diodes, Si acts as the anode and the base substrate. p-Si typically offer good enhanced hole injection compared to indium tin oxide (ITO) anodes [52]. Typical ITO substrates have defects on the substrates, and there is a need for additional hole transport layers to overcome the shortcomings of ITO substrates. Authors in [52-54] have reported that imbalance of the hole and electron injection by the p-Si was a major limitation for improving the device efficiency. With

further development it was observed that hole injection, typically via a thin silicon dioxide (SiO_2) layer, enables better carrier balance in the diode [55]. Top emitting diodes have been demonstrated on p-Si by changing hole injection deposited onto silicon. Some groups have demonstrated that electron withdrawing fluorine can enhance the electron affinity of organic semiconductors and enhance the electron mobility. This would improve the efficiency of the devices with holes as the majority carriers [56]. In our system we use p-Si as the anode for hole injection into the diode system.

(b) Organic Light Emitting Diodes on n-Si

Organic light emitting diodes have been demonstrated on n-Si [54, 57] that have a power efficiency 0.01 lm/W, improved to 0.1 lm/W by coating n-Si with a thin layer of gold (Au). The efficiency of these systems is, however, lower than p-Si, which is on the order of 0.2 lm/W. This is typically attributed to the low hole injection from the n-Si anode compared to that of p-Si anode. Bulk n-Si has a strong absorption tendency for visible light; these results in part of the light emitted towards n-Si cannot be utilized for light emission. To effectively utilize this part of the light and improve the hole injection from n-Si, the n-Si films are typically doped with Au generation centers, and aluminum (Al) is deposited as a back mirror on the anode side of the device [58].

Despite their high quantum efficiencies, these organic structures are susceptible to atmospheric conditions, including moisture, thermal and electrochemical degradation [16, 21]. Organic emitters have recently been replaced with semiconductor nanocrystals. These have different emission colors, electron affinities and ionization potentials, and have different sizes as well. The color purity of nanocrystals is well defined, and the quality of light emission can be easily tuned.

2.3 COLLOIDAL QUANTUM DOT BASED LIGHT EMITTING DIODES

2.3.1 Quantum Dots

Quantum dots are semiconductor materials whose excitons are confined in all three dimensions [59]. They have properties that are in between bulk semiconductors and discrete molecules. The emission wavelength of the particle is controlled by the size of the nanoparticles of the same material (Figure 2.1). Quantum dots can be synthesized to emit anywhere from ultraviolet to visible all through to infrared regime. These particles have typical photoluminescence with a full width half maximum (FWHM) 30 nm or less (Figure 2.2). This narrow spectral distribution indicates the color purity of the emitted light.

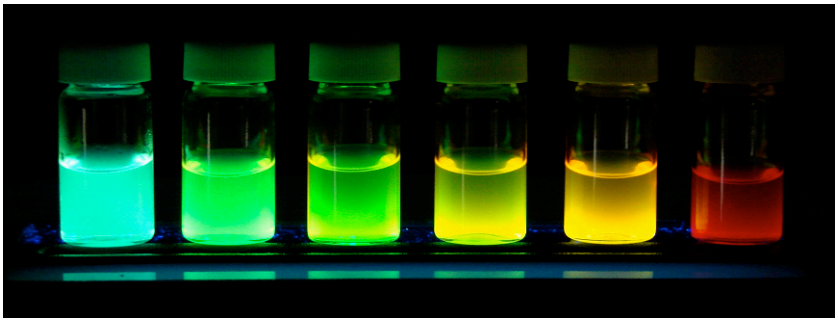

Figure 2.1: Synthesized Colloidal quantum dots made of the same material CdSe: ZnS [60].

There are two types of Quantum dots that are present: (a) Epitaxial and (b) Colloidal. Epitaxial quantum dots are formed when a semiconducting material is deposited via molecular beam epitaxy (MBE) on a substrate. The strain causes the top material to buckle and form quantum dots by the Stranski Krastanow growth method

[61]. MBE can also be used to deposit a capping layer and charge injection layer. Colloidal quantum dots, on the other hand, are synthesized from organometallic precursors injected into the organic solvent at high temperatures [62]. The temperature activates nucleation of small crystallites that continue to grow from the unreacted precursors until stopped by cooling. This process allows fine control on the quantum dot size and results in monodisperse solution. Colloidal quantum dots are preferred over expitaxial quantum dots, due to their low cost, ease of fabrication and integration.

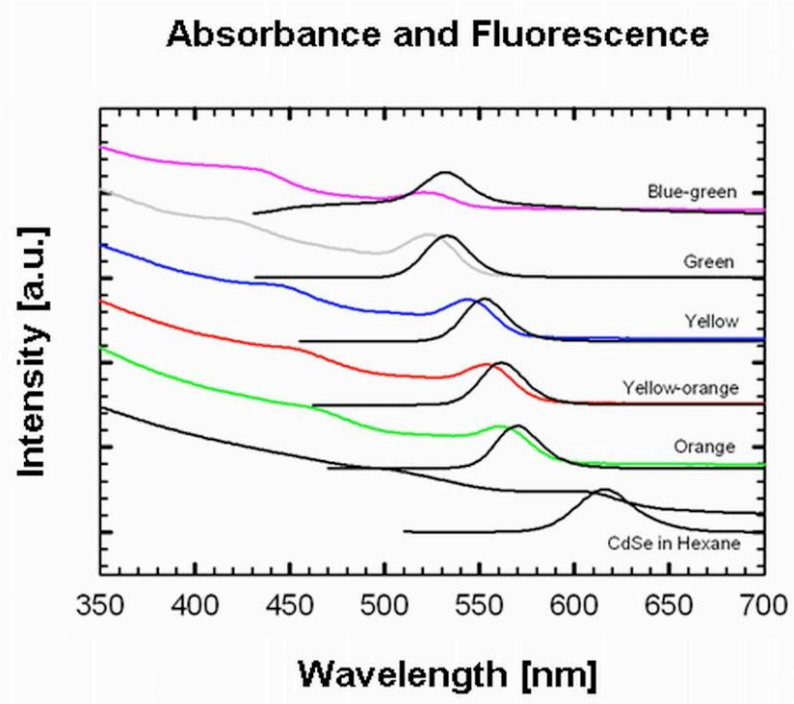

Figure 2.2: Absorption (vs.) Fluorescence of quantum dot with different emission wavelength [60].

Typical quantum dots that are used in the colloidal form have a core: shell structure with an organic capping layer. We will focus our discussion more on the Cadmium selenide (CdSe): Zinc Sulfide (ZnS) core: shell quantum dots that we use in this thesis. Organic capping is typically provided to prevent the aggregation or

precipitation of quantum dots (Figure 2.3). Organic compounds such as thiols, trioxtylphosphine oxide oleic acids have been used to create organic capping.

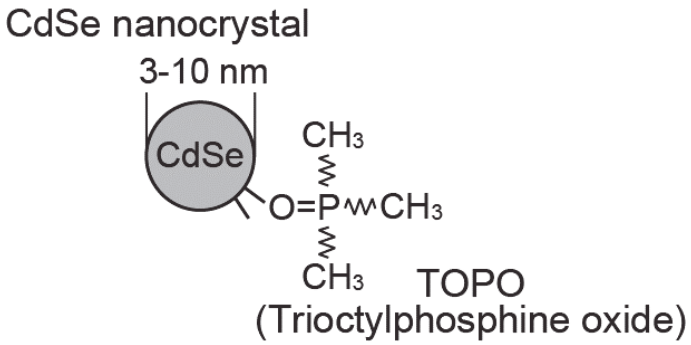

Figure 2.3: Core: Shell CdSe: ZnS configuration with outer TOPO or ligand layer [60].

Colloidal quantum dots have been used as light emitting material in LEDs due to their unique tunable luminescence properties [63-66]. Nanoparticle based light emitting structures with integrated organic layers have shown improved external quantum efficiencies, narrow bandwidth and high luminescence quantum yield [16, 67].

When the size of a semiconductor crystal becomes small enough that it approaches the size of the Exciton Bohr Radius, then the electron energy levels can no longer be treated as continuous. The energy levels must be treated as discrete, such that a small and finite separation between energy levels is present. This situation of discrete energy levels is called quantum confinement, and under these conditions, the semiconductor material ceases to resemble bulk, and instead can be called a quantum dot (Figure 2.4).

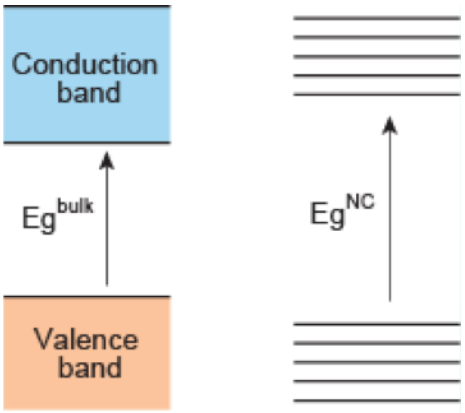

Figure 2.4: Band diagram comparison of bulk semiconductor CdSe vs. colloidal nanocrystal CdSe.

There have been a number of quantum dot based light emitting diodes that have been developed in literature. Multilayer quantum dot and quantum rod LEDs have been developed by spin coating the nanoparticles onto HTLs. Typically QDs with hydrophilic surfaces were deposited onto PVK by spin coating in aqueous solution. Incompatible solvents between QDs and HTLs can cause dewetting and aggregation of QDs, which is not desirable for the operation of the light emitting device [22, 68].

Alternate method for fabricating LEDs with quantum dots is by mist fabrication. This process deals with the assembly and patterning of quantum dots during the fabrication process. Good control over the thickness, composition and morphology of the particles is possible using this method. Multicolor deposition of nanoparticles was possible using shadow masks [69].

Some groups have demonstrated the creation of QD-LEDs on mechanically flexible substrates. These have been designed and fabricated on ITO coated poly

(ethylene terephtalate). The diodes developed by this method have luminous efficiency of 7070 Cd/m^2 and 2.57 Cd/A for red QD-LEDs and 3375 Cd/m^2 and 2.32 Cd/A for the green devices. Flexible LEDs have a critical bending radius of 5 mm [70].

2.3.2 Quantum Dot Patterning Methods

A number of approaches have been developed for depositing quantum dots onto substrates to create an LED. Quantum dots typically have a high fluorescence efficiency and tunable light emission depending on the size of the particle. Common quantum dot based light emitting devices consist of thin monolayers of nanoparticles or multilayers of particles embedded between two or more organic or inorganic support layers.

Some of the standard methods implemented are phase separation, spin coating, drop casting, electro deposition and Langmuir Blodgett methods have been used to create quantum dot thin films.

(a) Phase Separation

Coe et.al [71] developed a phase separation method for deposition of quantum dots. During the spin coating process the QDs separate from the small molecules and form a single monolayer on top of the organic top surface. The phase separation occurs between the quantum dots and the organic molecule TPD. These devices had a quantum efficiency of 2%. This method, however, has a shortcoming because it is necessary for the organic material to be a solvent that is compatible with the quantum dots. This method does not allow the capability of definition patterns while depositing.

(b) Spin Coating

Zhao et al.[72] demonstrated the spin-coating the QDs from chloroform solution onto a hydrophobic thermally cross-linked hole transport layer of polystyrene (PS) – *N*, *N*- diphenyl- *N*, *N* -bis (4-*n*-butylphenyl) – (1,1-biphenyl) - 4,4-diamine (TPD) –perfluorocyclobutane (PFCB). An electron transport layer was deposited on top of the QD layer to complete the device. The external quantum efficiency of these devices was 1.6% at 100 cd/m^2.

(c) Langmuir Blodgett Method

A novel fabrication method was introduced by combining colloidal quantum dots and metal organo-chemical vapor deposition (MOCVD) based systems. In this system a Langmuir Blodgett film of colloidal quantum dots is sandwiched between a p-type MOCVD GaN layer grown on sapphire and an n-type GaN layer grown using energetic neutral atom beam lithography/epitaxy. These diodes had EQE on the order of 0.001 to 0.01% [73].

(d) Micro-Contact Printing

Micro-contact printing is a method to form patterns using conformal contact of patterns of inked PDMS onto flat substrates. A number of micro-patterning methods have been developed in the past. Some of them are photolithography, inkjet printing, nano-imprinting and soft lithography has been used for microfabrication of various materials. Optical lithography is a fundamental tool in micro-fabrication. Nevertheless, these systems are not suitable for non-planar surfaces. Soft lithography has the advantage of high-resolution, low cost, and large area of operation.

Micro-contact printing has also been developed as an alternate method for depositing quantum dots. This method has been used to deposit close packed monolayers of alkane thiol Au nanoparticles [74, 75]. Micro-contact printing has also been used for deposition of ($Cd_xZn_{1-x}Se$) $Cd_yZn_{1-y}S$ core/shell on 4,40-N, N0-diphenylcarbazole (CBP) for fabrication of green diodes [76]. Typically in microcontact a polydimethylsiloxane stamp is inked with the polymer and is then transferred onto a solid substrate. PDMS substrates can make conformal contact with surfaces over large areas, enabling patterning in nanometer or micrometer size features.

PDMS stamps have a drawback, that they swell easily in contact with non-polar solvents such as toluene and chloroform solutions. In this case, conformal deposition becomes difficult. A number of methods have been developed to overcome this problem; Coe-Sullivan et al. have a modified surface of PDMS stamp by coating chemical vapor deposited Parylene-C layer [18]. The particles are then spin coated onto the PDMS surface, which is micro-contact printed onto the hard substrate. This enables uniform deposition of multilayer of quantum dots onto the substrates. The process has a drawback such that spin coating consumes a large amount of particles, thereby a significant amount of the material is wasted [77].

An alternate method was demonstrated by Bulovic [78] in which quantum dots can be inkjet printed onto the PDMS substrate. This is achieved by a thermal inkjet pico fluidic system developed by Hewlett Packard. Monolayers of particles can be easily achieved in this process. The drawback with the system is that the pattern variation cannot be easily achieved.

[79] also prepared a patterned ZnO film by simply printing a pattern using a PDMS mold on a sol–gel derived ZnO film. The ZnO films were spin coated onto the silicon substrate and heated to a certain temperature. Patterned PDMS was brought into contact with the surface and patterns on ZnO were obtained by removing the PDMS stamp. An alternate method to pattern ZnO films was developed by Yacaman et.al.[80]. In this method the assembly of nanoparticles was achieved by drying a small amount of colloidal ZnO nanoparticles suspended between a floating template (PDMS mold) and the substrate (silicon wafer).

We have developed a modified micro-contact printing method, where the nanoparticles re-suspended in hexane are used in a modified Langmuir Schaffer technique to create thin films of particles, which are picked up by PDMS stamps and micro-contact printed on silicon substrates [19, 20].

2.4 Structure and Energy Band Diagram

2.4.1 Structure Design

The structure of QD-based LEDs consists of multi-layers of inorganic materials: the combination of Gold (thickness: 5 nm) and Silver (12 nm) as the cathode, ZnO: SnO_2 (ratio 3:1, 40 nm) as the electron transporting layer, CdSe: ZnS particles as the light emission layer, 1 nm silicon dioxide and p-silicon as the bottom electrode (Figure 2.5).

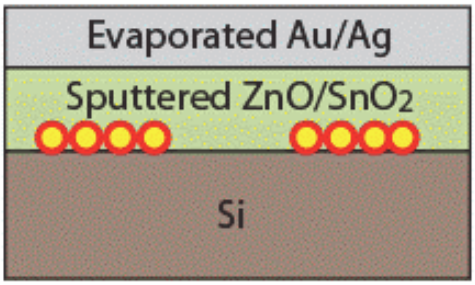

Figure 2.5: Schematics of silicon-based quantum dot light emitting diode design.

Resistivity of p-type silicon is 10-100 Ωcm. The emission is observed through the top metal cathode, similar to a top emitting organic light emitting diode (TEOLED).

2.4.2 Band Diagram

Figure 2.6 gives the structure and the energy band diagram of the inorganic light-emitting diode, where the holes are injected from the p-type silicon via silicon dioxide, and transported to the QDs. Similarly the electrons are injected from the Ag/Au negative electrode into ZnO: SnO_2 and transported to the QDs. The electron affinity and ionization energy for CdSe: ZnS QDs are taken from previous experimental data [65, 67].

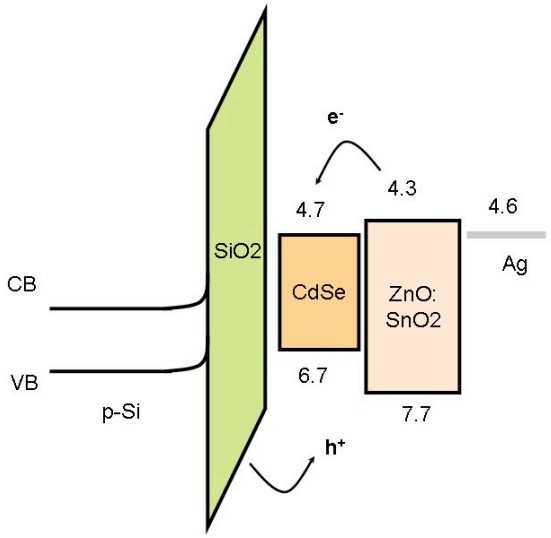

Figure 2.6: Schematic of the band diagram of the diode.

There are a number of advantages to using p-type silicon as a hole injection layer, as compared to ITO [55]. ITO is inefficient in injecting holes to polymer layers whereby an additional hole transporting layers is required before an emitting layer in the system [37, 65, 81]. Carrier injection from silicon electrode is improved because most of the electric field drop occurs across the highly resistive layer of thin SiO_2. The SiO_2 on silicon acts as a buffer layer for the system. The buffer layer will restrain the injected hole current and then improve the balance between hole- and electron-injection. Resulting high probability of radiative recombination consequently promote luminance and electroluminescence (EL) efficiency [3]. The Fermi level of the silicon is aligned to that of the electroluminescent material [50]. The excitons produced at QD layers can be easily quenched in close proximity to a metal electrode [82]. The ZnO: SnO_2 layer hence separates the electroluminescent QD layer from the metal layer where by increasing the radiative recombination. ZnO: SnO_2 layer improves the electron injection into the system and simultaneously acts as a hole-blocking layer. A band diagram of this device reveals that the barrier injection from ZnO layer into the emitting quantum dots is small. The thin SiO layer on p-silicon anode offers a strong hole injection (Figure 2.7).

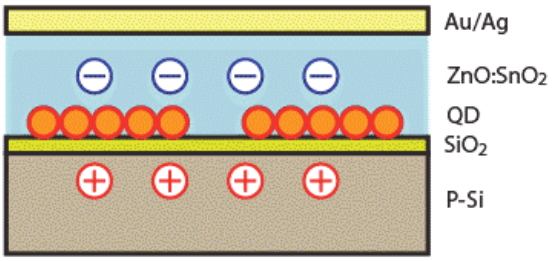

Figure 2.7: Device function on application of voltage to the device.

On application of voltage to the device, the anode injects holes into the hole transport layer while the cathode injects electrons into the electron transport layer

(Figure 2.8). The field across the device carries the electrons and holes to the quantum dot layer where the electrons and holes form excitons on the quantum dots. The excitons dissipate energy by emitting light corresponding to the optical band gap of the quantum dots.

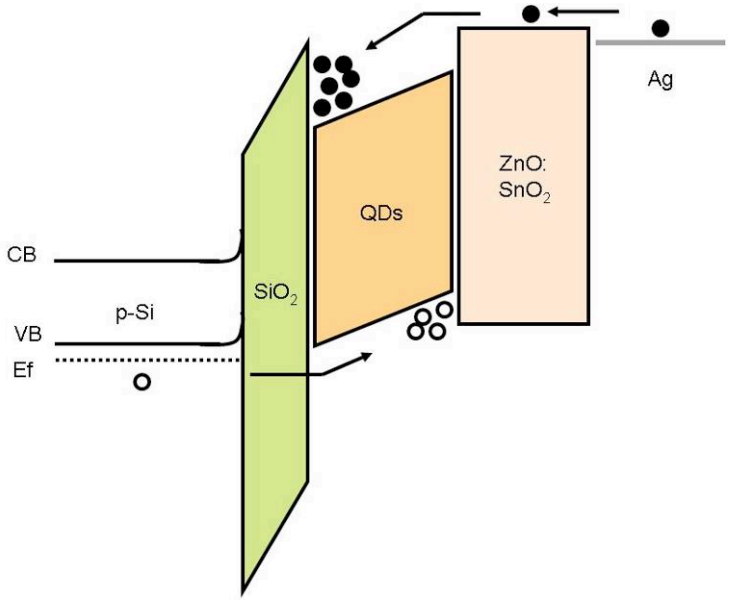

Figure 2.8: Band diagram of the device in forward bias.

2.5 SUMMARY

In this chapter we discussed the advantages of silicon that make it attractive for light emitting diode applications. Silicon can be fabricated into desired shapes and configurations using lithography and etching techniques. Uniform films consisting of arrays of CdSe: ZnS quantum dots were used as light emitters for the device. A number of methods to deposit CdSe: ZnS quantum dots have been developed. We implement the use of micro-contact printing to accurately deposit particles onto the silicon substrate. A

mixture of metal oxide was deposited onto the quantum dot layer that acts as the electron transport layer. A band diagram indicating the function of the device on application of voltage was also discussed. These devices can be integrated for a vast variety of applications in MEMS based systems.

CHAPTER 3: DEVICE FABRICATION

3.1 INTRODUCTION

In this chapter, we introduce the fabrication technique for patterning inorganic QD-based light emitting devices (QD-LEDs) through microcontact printing [74, 75] of quantum dots on p-type silicon substrates under room temperature. p-silicon in the QD-LED structure acts as the hole transport layer, since a p-type silicon anode with a thin layer of silicon dioxide as an energy barrier can enhance hole injection when compared to ITO as an anode in organic light emitting diodes [55]. The compatibility of microcontact printing with most of the existing silicon microfabrication techniques ensures the future opportunities of the QD-LED on silicon.

In addition, microcontact printing is potentially capable of patterning a few numbers of colloidal QDs with well-defined geometry [83]. Stamping-based microfabrication of a stable light emitting device will have a wide range of applications, from integrated circuits (ICs) compatible nanophotonics, to MEMS, to micro-total analysis systems for biomedical research, to future molecular electronics.

The structure of QD-based LEDs consists of multi-layers of inorganic materials: the combination of Au (thickness: 5 nm) and Ag (12 nm) or Al (15 nm) as the cathode, ZnO: SnO_2 (ratio 4:1) as the electron transporting layer, CdSe: ZnS particles as the light emission layer, 1 nm silicon dioxide and p-type silicon as the bottom electrode (Figure 3.1).

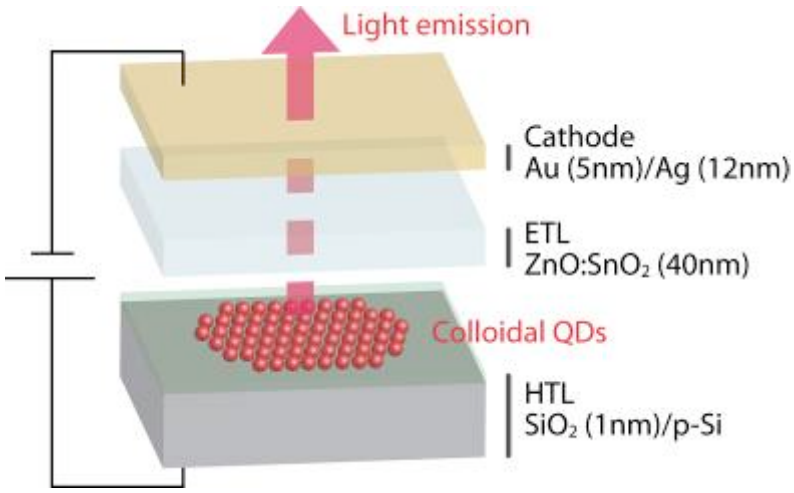

Figure 3.1: Schematic of silicon-based quantum dot light emitting diode.

3.2 DEVICE FABRICATION

Figure 3.2 shows the fabrication process. Patterned PDMS stamps were used to stamp monolayers of CdSe: ZnS core: shell QDs onto bare <100> p-type Silicon with 1nm-thick oxide. QDs for the microcontact printing process was prepared as follows: First, CdSe: ZnS QDs (Evident Technologies) were precipitated and re-suspended in hexane (Reagent grade-Sigma Aldrich) to remove excess ligands. A hydrophobic colloidal suspension of 15 μl of CdSe: ZnS particles in a 50:50 (v: v) solvent of 1,2-Dichloroethane (Sigma Aldrich) and hexane making a total of 400 μl solution was prepared. This solution was then pipetted onto a 20 mm diameter convex water surface pinned at the edge by a teflon disk (20 mm inner diameter, 2 mm thick) on a Petri dish. The solvent present on the surface of water evaporates, forming a uniform array of self-assembled nanoparticles due to capillary immersion and convective forces.

The film was then picked up by hydrophobic polydimethylsiloxane (PDMS) stamps with patterns (feature size: 20-100 μm) and deposited onto a substrate. This procedure was repeated with QDs with average diameters ranging from 7.8 nm, 8.4 nm, 9.0 nm, 9.8 nm, with corresponding photoluminescence peaks from 560 nm, 576 nm, 598 nm, and 618 nm.

The PDMS stamp was fabricated based on the rapid prototyping technique. SU8 photoresist (Microchem Corp [84]) is patterned photolithographically on a silicon wafer. Depending on the stamp height specification for our device, SU8-2100 (~100 μm thickness) or SU8-2025 (~25 μm thickness) was used. Microchem Corporation provides photolithography process specifications. PDMS (Sylgard 184, Dow Corning Corp [85].) is then poured over the SU8 master mold, cured at 70° C for ~30 min, and peeled off the mold to form the microstructures [86]. The PDMS stamps were treated with buffered oxide etchant (Ammonium Fluoride Solution with HF in a 6:1 ratio) for 1 min to prevent sticking onto the substrate during microcontact printing [82]. After stamping, the substrate was annealed at 140 °C for 15 min to remove excess organic solvents [87].

Besides organic materials, inorganic materials have been considered as a transport layer in organic or QD-LEDs. Inorganic materials enhance the stability of solution processed LEDs. MoS_2 [88]and NiO [89] have been used as hole transport layers in OLEDs or QD-LEDs respectively. Some recent publication reports also indicate the use of TiO_2[90, 91]and ZnO [89] as an electron transport layer in light emitting diodes. Here, a thin film mixture of ZnO: SnO_2 of 40 nm (thickness) was RF co-sputtered with a low deposition rate of 0.2 Å/s to avoid damage to the QD layer. Sputtered ZnO: SnO_2 without additional oxygen exposure during sputtering acts as an electron transport layer. A transparent top electrode with 120 Å of silver (Ag) and 50 Å of gold (Au) or 200 Å of Al was e-beam evaporated at 0.4 Å/s and 0.5 Å/s respectively.

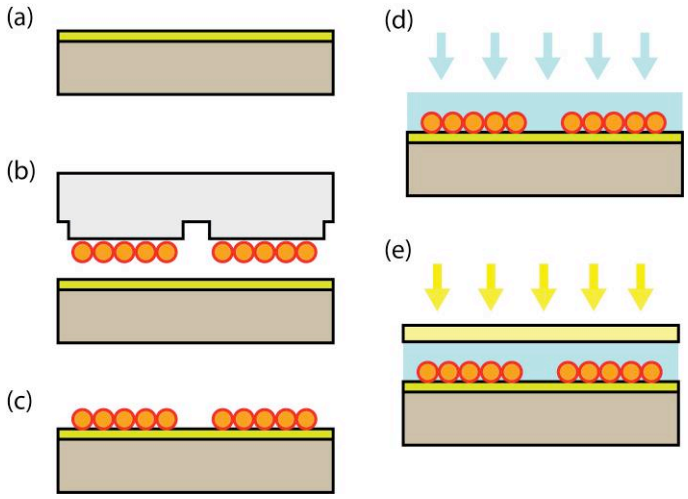

Figure 3.2: Fabrication process for quantum dot light emitting diode (a) <100> p type wafer with 1 nm silicon dioxide grown on surface. (b) Self-assembled quantum dot film was transferred onto a PDMS micropattern. (c) Transfer of quantum dot pattern onto silicon substrate. (d) Sputtering of 40 nm of ZnO: SnO_2 onto the quantum dot substrate. (e) E-beam evaporation of metal.

3.2.1. Silicon Substrate Preparation

p-Si wafer with resistivity (1-100 ohm-cm) was oxidized for 45 mins (WetOx1050). 500 nm thick grown oxide on the surface of p-Si was then patterned using photolithography. Spin coated AZ 5209 at a speed of 2200 rpm for 30 secs. We pre-baked the wafer at 90° C for 30 sec and then exposed it to UV for 4 secs (EVG Mask Aligner). The wafer was then post expose baked (PEB) at 90° C for 1.30 mins and developed for 50 secs. On complete development using AZ 726MIF the wafer was hard baked at 150° C for 5 mins. Oxide not covered by the photoresist was etched using BOE for 5-10 mins. On complete etching the resist was removed using piranha-cleaning

solution for 8 mins. The wafer was then diced to the desired size to obtain the flat substrate to perform micro-contact printing. The wafer pieces were again treated with BOE for 30 secs and piranha cleaning solution for 8 mins. The 500 nm thick p-Si acted as an insulator between p-Si and the top cathode deposited onto the devices.

3.2.2. Re-suspension of Quantum Dots

200 μl of CdSe:ZnS QDs initially suspended in toluene was pipetted into a centrifuge tube containing 5 ml of acetone. The solution was then ultrasonicated for 5 mins and then centrifuged for 15 mins at 3000 rpm. It was observed that CdSe:ZnS particles settled in the bottom of the tube. Excess acetone was removed and the particles were dried. 400 μl of hexane was pipetted into dried CdSe:ZnS QDs and ultrasonicated for 30 mins.

3.2.3. Sputtering Conditions

ZnO and SnO_2 were co-sputtered in Edwards Auto 500 sputtering system. The power for sputtering was varied from 30 W to 50 W and the rate of deposition varied from 0.1 Å/s to 0.4 Å/s. 40 nm of thin film was deposited for a time period of 20 mins. The chamber was pumped down to a pressure of 2.0e-4 mbar and sputtering was performed at a pressure of 5.0e-2 mbar. The RF plasma is generated at a pressure of 9e-2 mbar at a power of 50 W.

3.2.4. E-Beam Evaporation Conditions

Al cathode was deposited in the CHA e-beam evaporator. The chamber was pumped down to a pressure of 4e-6 Torr. The evaporation power was between 35-36% and the deposition rate varied from 0.5 Å/s to 1 Å/s. A total thickness of 20 nm was deposited onto the diodes.

120 Å of silver (Ag) and 50 Å of gold(Au) was e-beam evaporated at 0.4 Å/s and 0.5 Å/s. The chamber was pumped down to a pressure of 5e-6 Torr and deposition was performed onto the diodes with sputtered ZnO: SnO_2 films. The Au layer deposited was to prevent the oxidation of the Ag layer and hence act as a protective layer.

3.3 THIN FILM FORMATION

A hydrophobic colloidal suspension of 15 μl of CdSe: ZnS particles in a 50:50 (v: v) solvent of 1,2-Dichloroethane and hexane making a total of 400 μl solution was prepared. This solution was then pipetted onto a 20 mm diameter convex water surface pinned at the edge by a teflon disk (20 mm inner diameter, 2 mm thick) on a Petri dish (Figure 3.3). Controlling the volume of water used varied the convex water level curvature. After a series of experiments, we determined the optimum water level to be used consistently throughout the experiment. The radius of curvature of the convex water surface was optically determined to be approximately 40 mm. The film was formed after ~15 minutes of evaporation.

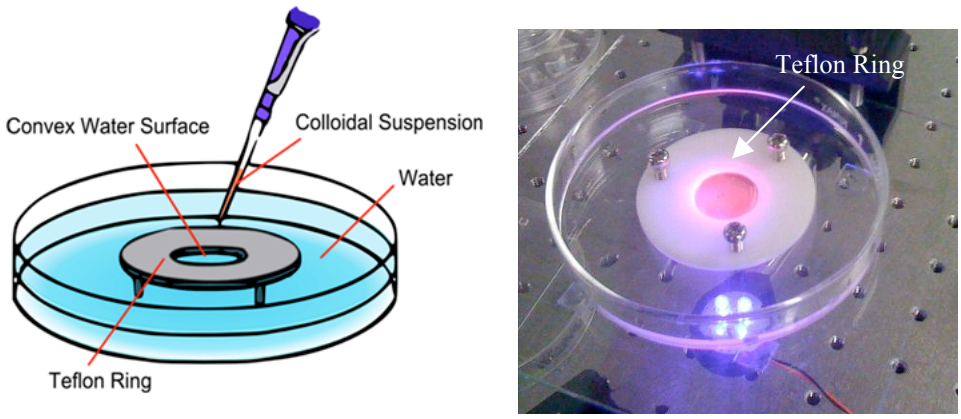

Figure 3.3: Experimental setup for monolayer formation. (a) Schematic of experimental setup indicating the teflon ring with inner diameter of 2 cm and outer diameter of 5 cm was placed in the center, pinning down the water and creating a slightly convex water shape in the middle. The hydrophobic colloidal suspension was slowly poured on top of this surface. (b) Picture of the actual setup with quantum dots excited by an ultraviolet light emitting diode (UV LED) source in the bottom. Emission wavelength of the particles is 606 nm.

3.3.1. Radius of Curvature of Water Level

The focal length of the lens (convex water surface pinned by the Teflon ring) in air can be calculated from the lens makers equation [92].

Lens makers formula is given by:

$$\frac{1}{f} = (n-1)\left[\frac{1}{R1} - \frac{1}{R2} + \frac{(n-1)d}{nR1R2}\right] \qquad (1)$$

Where f is the focal length, n is the refractive index of the material, R1 is the radius of curvature of the lens surface closest to the light source, R2 is the radius of

curvature of the lens surface farthest from the light source, d is the thickness of the lens. In this case R2= ∞, which reduces Equation 1 to the following:

$$\frac{1}{f} = (n-1)\left[\frac{1}{R1}\right] \qquad (2)$$

We assume the refractive index of water to be n=1.31, and the focal distance is measured using a measuring tape to be f=130. Hence the radius of curvature was found to be ~40 mm.

3.3.1 Theory of Thin Film Formation

Self-assembly of monolayers and multilayers of nanoparticles have been demonstrated on a variety of substrates, through deposition on surface modified glass and metal substrates [93, 94], self-assembly of multilayer polymer superlattices with incorporated nanoparticles [95], induced depositions with an electrical or magnetic field [96, 97], direct etching or growth of nanoparticles on substrates [62], and evaporation of nanoparticle dispersions on substrates or on a water surface (Langmuir-Blodgett films) [67, 98].

Position control of quantum dots attachment has yet to be thoroughly investigated to exploit the fascinating nature of colloidal quantum dots and their integration with existing micro-nanostructures. The applications of the above assembly methods have been limited by the quality of film, the lack of transferability after the thin film self-assembly or pre-treatments needed for nanoparticle functionalities. Recently, it has been demonstrated that monodisperse, spherical gold nanoparticles can be self-assembled on a convex water-air interface, and subsequently be transferred using the Langmuir-Schaeffer technique [74, 75].

The morphology of the semiconductor quantum dots film differs from that of the gold nanoparticles, due to their nonspherical crystalline structure [99]. Here we report a technique that would enable the controlled deposition of quantum dot nanoparticles. We expand the self-assembly method with the traditional Langmuir-Schaeffer technique to rapidly deposit monolayers of Cadmium selenide (CdSe): Zinc Sulfide (ZnS) quantum dots on flat substrates. A uniform film of quantum dots self-assembled on water was transferred using hydrophobic polydimethylsiloxane (PDMS) stamps with various micro-scale patterns, and was subsequently stamped on glass or silicon substrates.

The film of nanoparticles forms in a process similar to crystallisation [100] (Figure 3.4). First, the hydrophobic solvent holding the nanoparticles begins to evaporate. Because of the convex water surface, the layer in the centre of the surface is the thinnest, exposing the nanoparticles and forming solvent menisci between individual exposed nanoparticles (Figure 3.4A). As the solvent evaporates in the thinnest region, an attractive capillary immersion force collects the nanoparticles into densely-packed hexagonal arrays called the nucleus [101, 102] (Figure 3.4B). Then, as the solvent evaporates further, the contact line of the colloidal suspension and water grows outward radially and convective flow of the solvent attracts the nanoparticles from the colloidal suspension to the contact line, where they self-assemble onto the outer edge of the growing nucleus [103] (Figure 3.4C). As the contact line approaches the Teflon ring, where the water is pinned down, meniscus slope angle at the solvent and water interface increases from slope angle α at the slightly convex water surface that composes most of the surface inside the ring, to slope angle β at the edge where water is pinned down. As a result, multilayers are formed (Figure 3.4D).

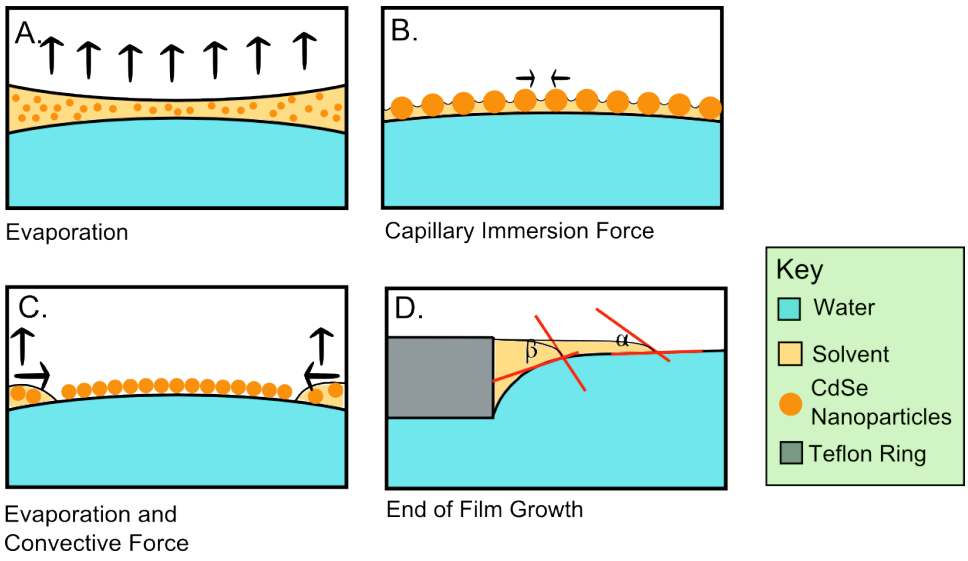

Figure 3.4: Self-Assembly Mechanism. (A) The solvent evaporates, thinning the layer of colloidal suspension throughout the water surface. (B) Menisci of solvent forms between the exposed nanoparticles and capillary immersion forces pack them together. (C) The contact line grows outward radially due to further evaporation and convective force that draws additional nanoparticles from the suspension to the edge of the growing film. (D) The meniscus slope angle increases, which cause multilayers of nanoparticles to form near the edge ($\beta > \alpha$).

3.3.2 Solvent Optimization

Solvents with different compositions of hexane, 1,2-Dichloroethane (EDC), and/or Dichloride methane (DCM) were tested. Hexane is very effective in dissolving and suspending the particles and is less dense but generates micron-sized objects at the evaporating front, due to formation of hexane-water micelles [74, 75]. Therefore, either EDC or DCM was added to prevent this. Because both EDC and DCM are denser than water, a balance of the excellent solvency of hexane and micelle-preventing characteristic

of EDC/DCM had to be met, while maintaining a density less than that of water. The optimal result was a 50:50 mixture of either EDC or DCM and hexane. EDC was chosen over DCM because of the consistency of results in films prepared with EDC.

3.3.3 Water Surface Curvature

Controlling the volume of water used varied the convex water level curvature. After a series of experiments, we concluded that the greater the curvature, the thinner and more fragile the film. With a higher curvature, the solvent in the center of the water surface is very thin, resulting in less time for convective flow to collect nanoparticles towards the center before the nucleus forms and the contact line begins to grow outward. Also, controlling initial film growth becomes increasingly difficult with greater curvature because the sensitivity of the curvature to the volume of water increases as well. The optimal volume of water used to get the required quantum dot monolayers was ~30ml. With the rapid airflow to induce a faster evaporation rate, there were several cases where the contact line appeared before colloidal suspension was completely dispensed onto the water surface.

3.3.4 Evaporation Rate

The rate of evaporation was controlled by placing the film making apparatus inside the fume hood, or in the middle of a well-circulated room. We observed improvements in the film thickness and uniformity when the film was self-assembled under a fume hood, leading us to believe more rapid evaporation aids in uniform film self-assembly. To obtain ~2 monolayers for particles with emission wavelength 600 nm,

it would take 15 mins for the solvent to completely evaporate under normal room conditions and 5 mins under a fume hood.

3.4 MICRO CONTACT PRINTING

First, a silicon master is patterned with SU8 photoresist using standard semiconductor processing techniques. Polydimethylsiloxane (PDMS) is mixed with curing agent (1:10 ratio), degassed, poured onto the master and degassed again. It is then allowed to cure at 70 C for 30 minutes. The PDMS "stamp" is then removed from the master and cut into the desired shape and size. The QD film that is formed on the convex water is then picked using the PDMS stamp. The inked stamp is then inverted onto a substrate using a setup shown in figure 3.5. A gentle pressure is applied for 30 seconds such that the particles transfer completely onto the substrate.

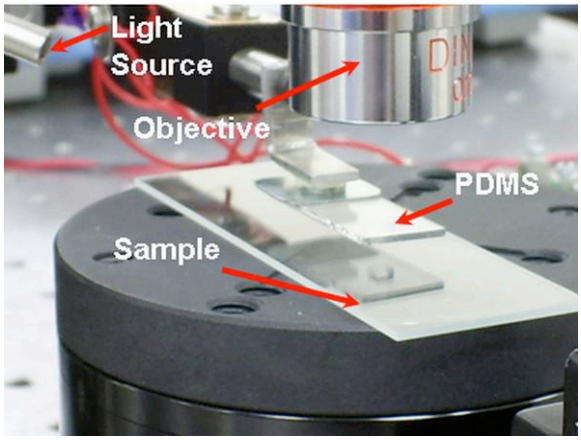

Figure 3.5: Microcontact printing of Quantum dots onto substrate.

3.4.1. Transfer of Particles

The process of transfer of particles onto the substrate is indicated in Figure 3.6. The quantum dot thin film is self-assembled onto water surface by dispensing a hydrophobic suspension of CdSe: ZnS quantum dots in a solvent mixture of 1,2-dicholoroethane and hexane. The uniform film is picked up by the PDMS stamps with micro features and deposited onto silicon substrate (Figure 3.6).

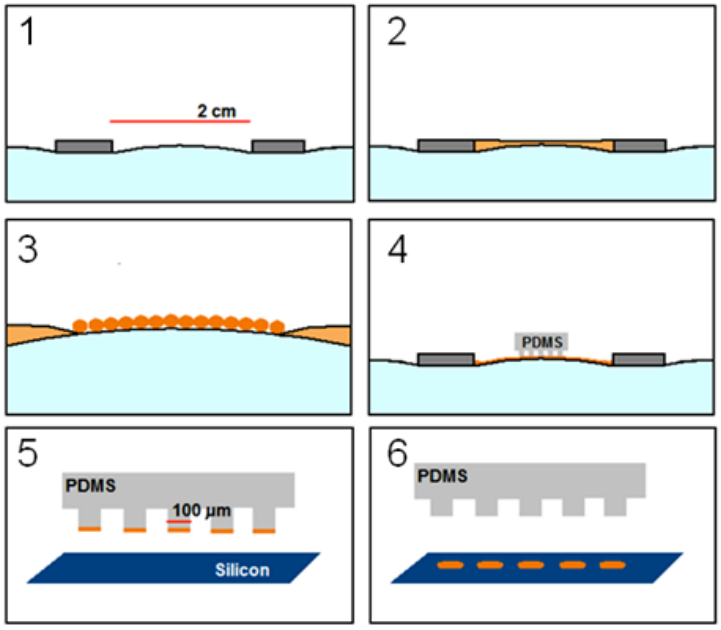

Figure 3.6: Principle of quantum dot film self-assembly and micro-contact printing. These steps illustrate total film self-assembly and microcontact printing process: 1. Convex water surface is created; 2. Colloidal suspension is poured; 3. Film is self-assembled; 4. Hydrophobic PDMS stamp is lowered, picking up the film; 5. PDMS stamp is lowered onto flat substrate; 6. Film is stamped onto the flat substrate.

Complete transfer of particles from the PDMS is observed after a time span of 30 sec. Figure 3.7 gives the image of PDMS before and after micro-contact printing.

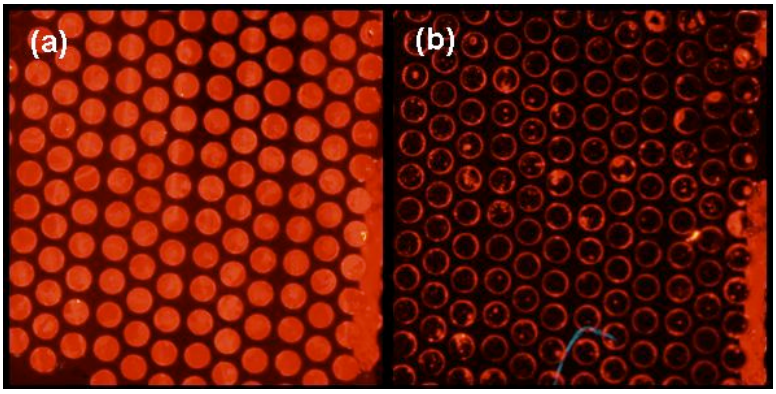

Figure 3.7: QDs on PDMS substrate (a) Before micro-contact printing and (b) After microcontact printing.

Uniform films of nanoparticles, stamped as 100 μm diameter circles on flat substrates, were produced for quantum dots with emission wavelengths 560 nm, 580 nm, 600 nm and 620 nm (Figure 3.8 a-d). Stamped fluorescence image of the University of Texas "Bevo"-pattern particles with emission wavelength 600 nm was also observed, as shown in figure 3.8e, indicating simple patterning capability using this method.

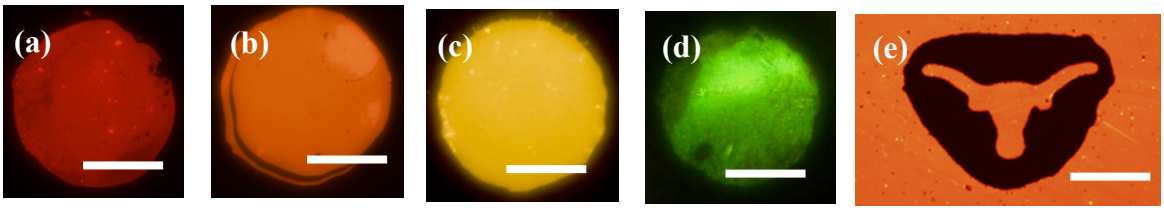

Figure 3.8: Photoluminescence of patterned quantum dots (a-d) PDMS stamps with 100 μm-diameter cylinders were used to stamp uniform, self-assembled films with quantum dots of emission wavelengths (from left) 620 nm, 600 nm, 580 nm and 560 nm (Scale: 50 μm). (e) Fluorescence image of Bevo with emission wavelength 600 nm and particle size 9.0 nm (Scale:50 μm).

3.5 SPUTTERED THIN FILMS

A mixture of ZnO: SnO_2 was co-sputtered (Edward Auto 500) simultaneously, power ranging between 30 W and 50 W in a pure argon environment at a pressure of 3.3 mTorr. This corresponds to a combined deposition rate varied between 0.2 Å/s to 0.5 Å/s, which are sufficiently slow to minimize the damage to the QD layer. ZnO: SnO_2 alloy is an n-type semiconductor where its conduction-band level allows injection of electrons into the CdSe: ZnS QD conduction band.

Optical transparencies of ZnO: SnO_2 films were measured (UV-VIS NIR Spectrometer Cary 5000) to be 90% (Figure 3.9). Depositing a thin transparent metal Au (5 nm)/Ag (12 nm) electrode reduces optical transmission to 60-40% between 500-700 nm emission wavelength, compared to using the ZnO: SnO_2 electrode.

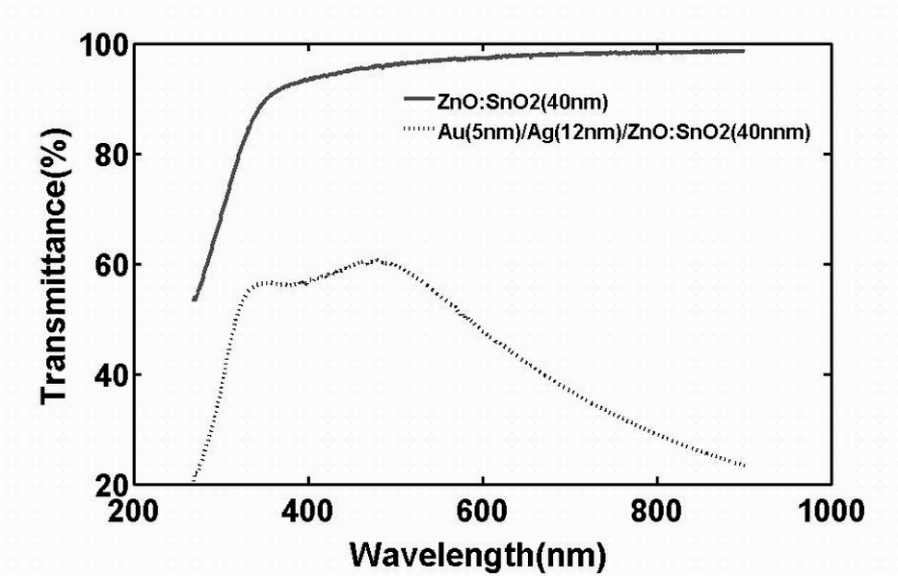

Figure 3.9: Optical transmittance spectrum of top inorganic layers indicated. Solid line: ZnO: SnO_2 (40 nm), Dashed line Au (5 nm)/Ag (12nm)/ ZnO: SnO_2 (40 nm).

3.6 METAL CATHODE FILMS

The inorganic light emitting diode created on silicon has a top emission configuration. The electroluminescence (EL) is coupled through a semitransparent thin cathode. The structure and composition of the transparent cathode and its deposition technique plays a significant role in the final performance of the device. We have created diodes with two different cathode configurations Al and Ag/Au.

Diodes with 20 nm Al as the top cathode makes it CMOS compatible. Those with Ag/Au as the cathode make the electrode more transparent compared to the diodes with Al as the top cathode. The top cathode was e-beam evaporated at deposition rate varying from 0.3 Å/s to 1 Å/s. The metals were deposited at a chamber pressure of 3e-6 Torr.

3.7 SUMMARY

Uniform films consisting of hexagonally packed array of CdSe: ZnS quantum dots were self-assembled by dispensing a hydrophobic colloidal suspension on top of a convex water shape. Adjusting three main parameters—solvent chemical composition, evaporation rate and water surface curvature—optimized this two-dimensional crystal growth mechanism. The concentration of nanoparticles in the suspension was also varied in an attempt to control the thickness of the self-assembled film. The combined QD thin film self-assembly and micro-contact printing technique were used to pattern the QD light emitters on the silicon substrate. Sputtering a mixture of ZnO and SnO_2

simultaneously and e-beam evaporating Ag/Au or Al as the thin cathode material completed the device. These devices can be integrated for vast variety of applications in molecular scale imaging and sensing.

CHAPTER 4: PROCESS CHARACTERIZATION

4.1 INTRODUCTION

In this chapter we introduce the characterization of thin films deposited to create an inorganic light emitting diode on silicon. This chapter also describes the optimal thickness of quantum dots for different emission wavelengths that would be required for good light emission from the LED. We further discuss the typical characteristics required for metal and metal oxide films deposited on top of the LED to create an efficient top emitting diode.

4.2 NANOPARTICLE CHARACTERIZATION

In optimizing the device structure of the QD-LEDs, it was found that the thickness of the QD layer played a critical role in electroluminescence efficiency and maximum luminance of the devices. The optimal quantum dot film thickness, or number of monolayers, for electroluminescence is dependent on its emission wavelength [63]. Research groups [63] have demonstrated that thinner emissive layers down to monolayer QDs, however, had increased leakage current through the QD layer without radiative recombination owing to the presence of voids, grain boundaries and interstitial spaces in the QD monolayers. Thicker QD layer lead to poor charge transport between the quantum dots. Using the idea previously established we determine the number of nanoparticles required to create a specific number of monolayers for our system. The amount of

nanoparticles needed to create the specific number of monolayers can be estimated as follows:

Area of each hexagonally packed particle is calculated as:

$$Area_{Hex} = \frac{3R^2}{\sin 60} \quad (1)$$

The number of hexagonally packed particles needed to completely fill the water surface area, with the desired number of monolayers, is calculated as:

$$Num_{Hex} = \frac{Area_{water} * Num_{ML}}{Area_{Hex}} \quad (2)$$

The number of hexagonally packed particles is converted into moles.

$$Mol = \frac{Num_{Hex}}{N_A} \quad (3)$$

R = Radius of particle

$Area_{Hex}$ = Area of the hexagonally packed particle

Num_{Hex} = Number of hexagonally packed particles

Num_{ML} = Number of monolayers wanted

N_A = Avogadro's constant

Mol = Number of moles to be added

The above estimation on the amount of nanoparticles (Table 4.1) needed to create the monolayers is based on the following assumptions: (1) Quantum dots were packed hexagonally [100]. (2) Each monolayer densely covered total available water surface

area. (3) The slightly convex curvature of available area of water surface is negligible in calculating the available water surface area.

S.No	Emission Color	Size of the Nanoparticle	Monolayers of Particles Needed	Volume Required
1	Red (620 nm) 8 nmol/mL	9.8 nm	2 ML	1.25 μL
2	Orange (600 nm) 13.59 nmol/mL	9.0 nm	2.5 ML	1.47 μL
3	Yellow (580 nm) 17.5 nmol/mL	8.4 nm	3.5 ML	1.714 μL
4	Green (560 nm) 31.7 3nmol/mL	7.8 nm	4 ML	1.261 μL

Table 4.1: Estimated concentration of quantum dots required to create thin monolayers.

4.2.1 Transmission Electron Microscopy

Transmission Electron microscopy (TEM) is a technique that uses a beam of electrons to pass through a very thin specimen sample [104]. The image that is formed is a result of the interaction of the electrons transmitted through the specimen. TEMs are capable of imaging higher resolution that helps resolve fine details such as a single atom.

Patterned CdSe: ZnS QDs were deposited onto transmission electron microscopy (TEM) grids with the previously described fabrication procedure. Figure 4.1 shows the TEM image of the circular-patterned (diameter 100 μm) particles with a 9.0 nm average diameter (emission wavelength: 598 nm). A well-defined area of packed QDs was observed, roughly suggesting the layer thickness to be a few monolayers. Similar characteristics were observed for particles with diameter 8.4 nm, 9.0 nm and 9.8 nm.

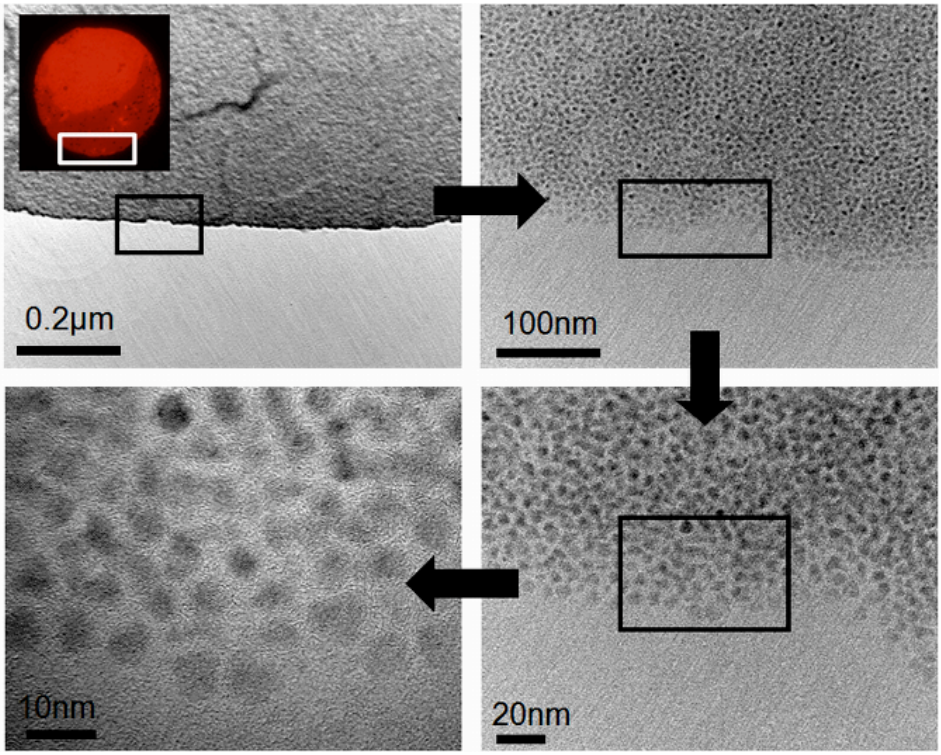

Figure 4.1: TEM images of stamped particles (9.0 nm average diameter) deposited using the microcontact printing technique (the arrows indicate the close-in view into the rectangular window).

4.2.2 Atomic Force Microscopy

Thicknesses of deposited particles were further assessed by atomic force microscopy (AFM). Atomic force microscopy is used to study the height of thin films as well as the surface quality of deposited materials [105]. In an AFM, a sharp silicon tip, with a radius of curvature of several nanometers is attached to a cantilever and brought close to the sample surface. The cantilever is oscillated near its resonant frequency. Force

between the sample surface and the tip varies the oscillation frequency of the silicon cantilever. Measuring the changes in oscillation frequency provides an image of the surface height and topography.

An example is shown in Figure 4.2. Particles with emission wavelength 576 nm and particle size 8.4 nm were deposited onto silicon and AFM measurement was performed. Peak to peak roughness of the stamped film was less than ~10 nm indicating controlled deposition of the nanoparticle film. The measured thickness of the film was 33nm indicating deposition of ~4 monolayers of particles. Thickness measurements using AFM were correlated with photoluminescence intensity data extracted from the optical micrographs. After measuring the thickness of the film stamped on silicon substrates (100 μm diameter stamps), the same sample was imaged under the fluorescence microscope. Fluorescence optical micrograph was processed via MATLAB®, by adding all red green blue (RGB) values per pixel to Thickness (vs) Fluorescence Correlation yield intensity values. Intensity values were obtained at 5 different points on each same stamped pattern and averaged. This was repeated for patterns with different particle thickness.

The thickness of the self-assembled film was correlated with its fluorescence intensity under the microscope, using the photoluminescence of quantum dots. After measuring the thickness of the film stamped on silicon substrates (100 μm diameter stamps) with atomic force microscopy, the same stamp was imaged under the fluorescence microscope. The fluorescence optical micrograph was processed via MATLAB®, by adding all RGB values per pixel to yield intensity values. Because the stamped film exhibited uniformity and evenness throughout each layer, it was assumed that the edge height measured with the AFM corresponded to the film thickness throughout the layer, whether the stamped film consisted of a single complete layer, or additional incomplete layers on top. Thus, the measured edge thickness was plotted

against the average fluorescence intensity throughout the corresponding layer (Figure 4.2).

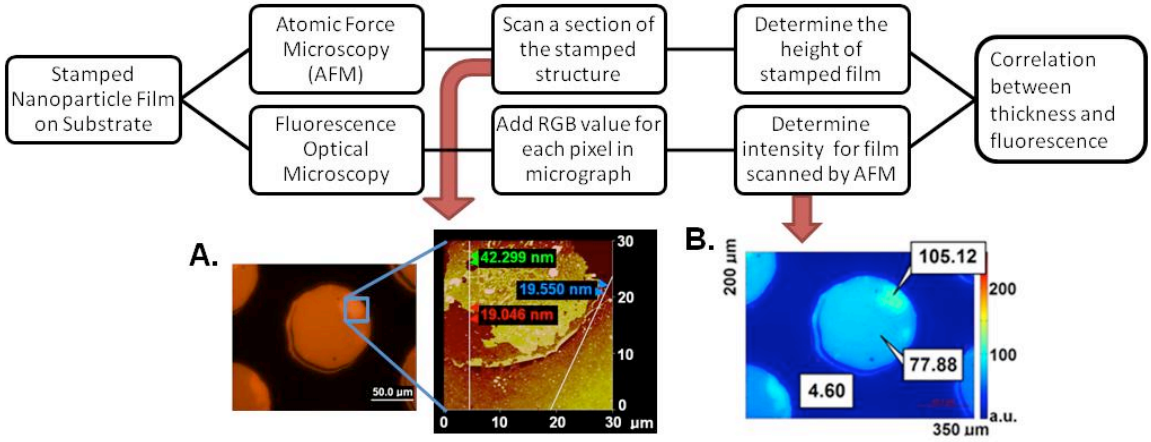

Figure 4.2: Numerical image processing flow to correlate thickness of stamped film to its photoluminescence. Samples of stamped quantum dot films using 100 μm diameter PDMS stamps were used to correlate the thickness of film to its fluorescence intensity, or photoluminescence. (a) Section analysis on the film edges was performed to measure thickness of the stamped film. (b) The fluorescence optical micrograph was processed by MATLAB® by first averaging RBG values per pixel to yield fluorescence intensity, then averaging the fluorescence intensity values inside each region of the film.This value was plotted with the corresponding film thickness.

Stamped films exhibited uniformity and evenness throughout each layer; it was assumed that the edge height measured with the AFM corresponded to the film thickness throughout the layer. As shown in Figure 4.3c, a strong positive, linear correlation between QD film thickness and photoluminescence was observed. As film thickness increases, the fluorescence intensity also increases. Increase in intensity was observed for

change in thickness as small as of ~10 nm. Deviations from this correlation can be attributed to the differences in the film density. These measurements indicated that the thickness of QDs varied from one monolayer to ten monolayers, depending on the amount of nanoparticles added to the colloidal suspension as well as the size of the particles used. Therefore, thickness distribution of the quantum dot layer can be estimated using the fluorescence images through the calibration curves shown in Figure 4.3c.

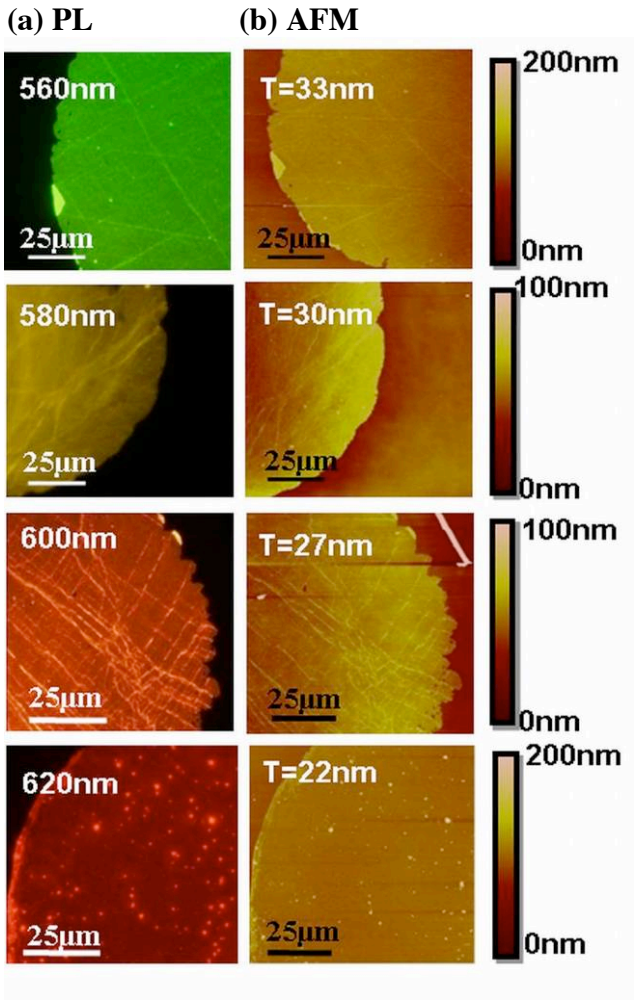

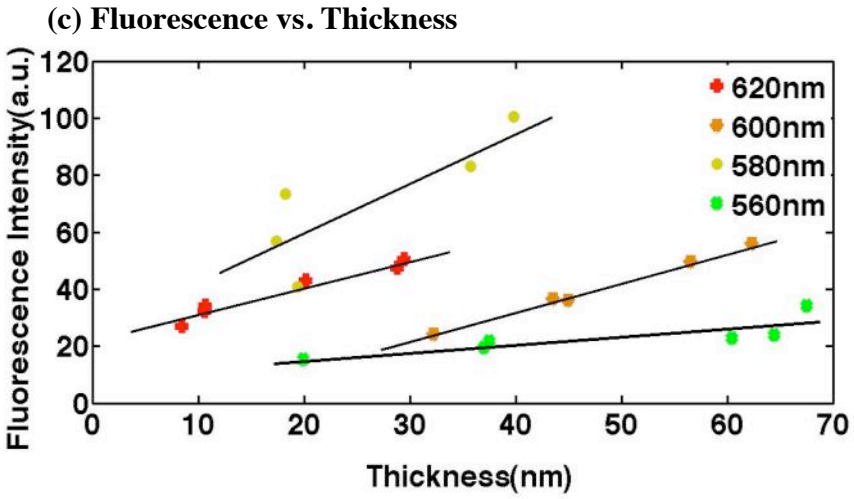

Figure 4.3: Patterned particles with 576 nm emission wavelength: (a) Fluorescence image. (b) AFM image indicating the height of deposition 33 nm. (c) Thickness of film measured by the AFM was plotted versus processed fluorescence intensity values. Using the plotted graph, thickness distribution of the quantum dot layer can be easily estimated from the fluorescence image without time taking AFM measurement. Positive linear correlations were seen in the films with all emission wavelengths tested.

4.2.3. Absorption Measurement

The optical absorption coefficient α is related to the threshold absorption energy (Eg) by $\alpha(h\nu) = A(h\nu - Eg)^{1/2}$ (Where A is a constant). The band gap energy Eg can be determined by extrapolation of the linear part of the plot of α^2 versus the excitation energy, $h\nu$. In order to estimate the bandgap of CdSe: ZnS particles we performed UV-Visible absorption spectrum measurement (UV-VIS NIR Spectrometer Cary 5000). Spectroscopic measurement was performed on solutions of QDs present in a cuvette in the spectroscopic system.

The absorption measurement curves are shown in figure 4.4.

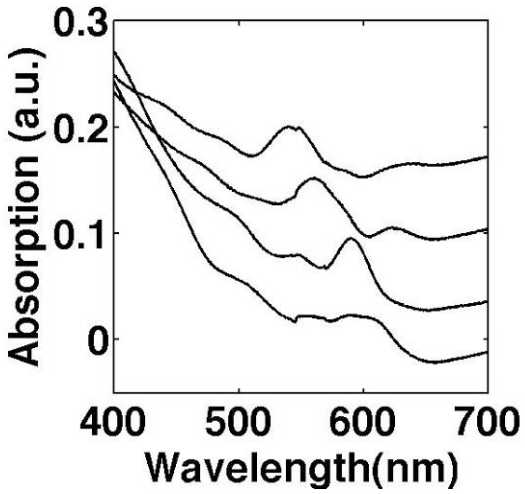

Figure 4.4: Absorption spectrum of the particles with emission wavelength (620 nm, 600 nm, 580 nm and 560 nm)

The bandgap energy of the particles with different emission wavelengths are given below.

Wavelength (nm)	Bandgap (eV)
560	2.125
580	2.0
600	1.98
620	1.91

Table 4.2: Bandgap energy of the Quantum dot particles.

4.2.3 Scanning Electron Microscopy

Patterned quantum dots on silicon substrates were imaged using scanning electron microscopy. We observed non-uniform distribution of the nanoparticles on the substrate. Certain portion of the deposited circular particles was dark and other portions were bright (Figure 4.5). This indicates one case of non-uniformity of the distribution of the particles that were picked up using the PDMS stamp. In this case it is obvious that the PDMS stamps tend to attract small water droplets, which can cause variations in particle density on evaporation. This non-uniform density of particles causes the dark and bright portions of the circular patterns. These conditions can be overcome by treating the PDMS to HF to prevent the attraction to water droplets.

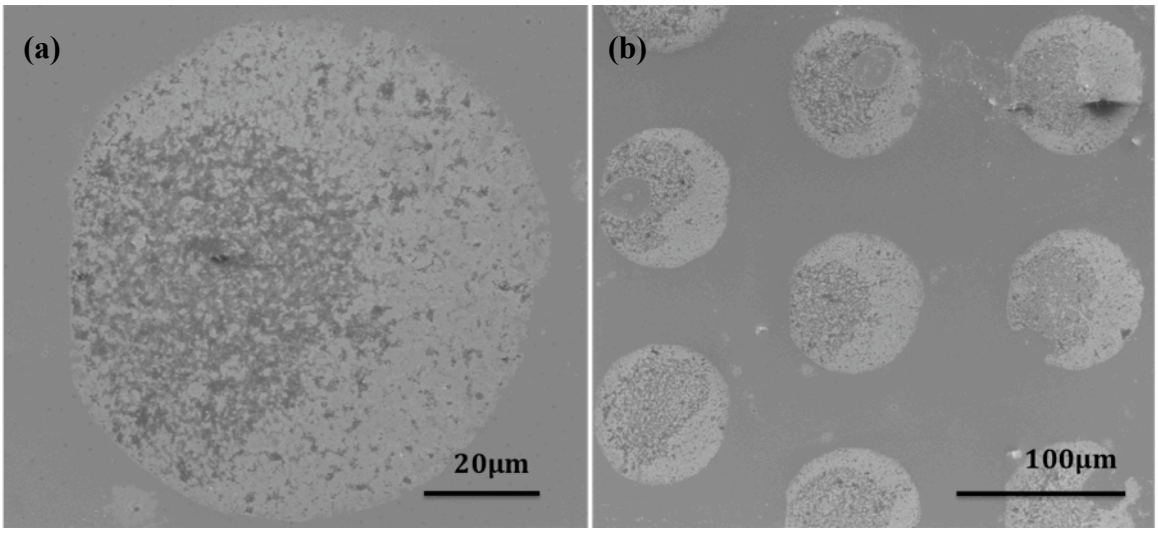

Figure 4.5: SEM images of stamped quantum dots. (a) Image of a single 100 μm diameter stamped pattern (b) Circular array pattern. The SEM images show that the quantum dot crystals are not very monodisperse or spherical, but that they can still form a closely packed and uniform monolayer.

4.3 NANOPARTICLE THIN FILM: OPTIMIZATION AND WORKING

The quantum dot thickness plays an important role in device functioning. Figure 4.6a shows the photoluminescence from a circular pattern of 9.8 nm particles deposited with some local thickness variation. Thickness distribution of the quantum dot layer was estimated using the fluorescence image. The RGB image of the photoluminescence was processed using MATLAB® to yield intensity values in figure 4.6c. This was correlated to the thickness values shown in figure 4.3. It was observed that left side of the circle was thinner (20 nm) compared to the right half (50 nm). On application of voltage across the system light emission was observed on the left side of the circle (Figure 4.6b). For figure 4.6b, driving voltage of 6 V was applied to observe electroluminescence from the left side of the device. Thicker quantum dot layer would result in an increase in operating voltage and decrease of carrier injection [63, 65, 106].

The presented technique allows the creation of CdSe: ZnS quantum dot thin film based LED with well-defined geometry and multi-color emission. The relative small non-uniformity of particle distribution is mainly attributed to two factors: (1) CdSe: ZnS nanoparticles are not perfectly spherical in shape, as shown in figure 4.1 TEMs. Therefore, they tend to cause a minor variation or cracks in the resulting thin film, which causes non-uniformity in the transfer of particles to the stamp. (2) During the manual operation of the stamps in picking up the film, PDMS stamps may attract small water droplets, which can cause variations in particle density. Due to the surface tension, water droplets tend to distribute quantum dots around its spherical surface. During the evaporation, the particles attached to the spherical surfaces interact and form multilayers. To further improve the homogeneity of the deposited film, highly localized and controlled version of microcontact printing is under development.

For QD-LED with organic transporting layers, a thickness of 2 monolayers (for particle size 9.8 nm) was reported to be optimal thickness for light emission [63]. In our case, it was observed that a thickness of 30 nm +/-5 nm (~3 monolayers), 40 nm +/-5 nm (~4 monolayers), 55 nm +/-5 nm (~6 monolayers) is sufficient for good light emission from particles of size 9.8 nm, 9.0 nm and 8.4 nm respectively. The values obtained were similar to those described in literature previously [63]. Carrier charge into smaller quantum dots has been shown to exhibit lower efficiency than that of larger quantum dots of the same composition. This is due to the mismatch between the highest occupied molecular orbitals (HOMOs) of the QDs and hole transport layers.

The quality of the quantum dots on the PDMS substrate depends on the film that is prepared on the convex surface of the water trough. The convex water level curvature was varied by controlling the volume of water used. After a series of experiments, we determined the optimum water level that was used consistently throughout the experiment. The radius of curvature of the convex water surface was optically determined to be approximately around 40 mm. The film was formed after ~15 minutes of evaporation. PDMS stamps, with an approximate total area of 25 mm^2, were used to deposit film.

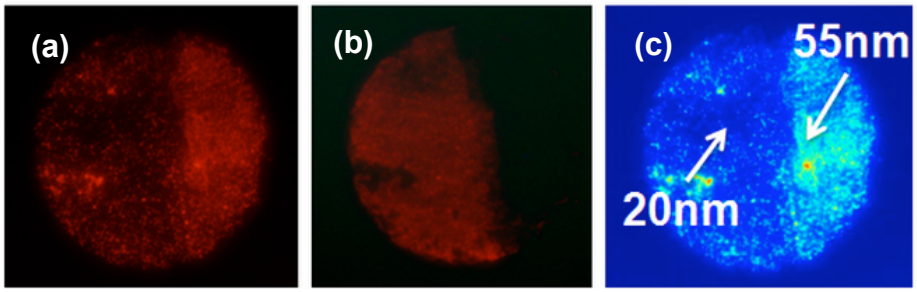

Figure 4.6: Photo/Electroluminescence from an identical circular pattern (circle diameter: 100 μm). (a) Photoluminescence image. (b) Electroluminescence observed from thinner portion of quantum dot layer. (c) Intensity plot of photoluminescence to estimate local thickness distribution.

4.4 METAL OXIDE OPTIMIZATION

Mixture ratio of the sputtered ZnO and SnO_2 was further optimized in our silicon inorganic light emitting diodes. SnO_2 acts as an n-type dopant for ZnO. Figure 4.7 indicates the impact of the emission from ZnO: SnO_2 on the QD EL spectrum for one set of light emitting devices. For a lower driving voltage, the spectrum is dominated by QD emission. As the voltage increases further, ZnO: SnO_2 emission was simultaneously observed along with particle emission. A broad emission was observed from ZnO: SnO_2. The inset image shows the orange light emission (600 nm) from particles and yellowish-white emission from ZnO: SnO_2. This is due to the imbalance between the electron and hole injection at the nanoparticle layer. This reduces the excitons density at the QD layer thereby reducing the emission intensity from particles. The mixture ratio of ZnO and SnO_2 was precisely controlled to obtain proper hole-electron recombination at the QD layer. Emission from ZnO: SnO_2 is typically observed at voltages on the order of 30 V -

50 V. Typical mixture ratio was maintained to be 40% Zn and 25% Sn to reduce operating voltage and thus avoid ZnO: SnO_2 emission.

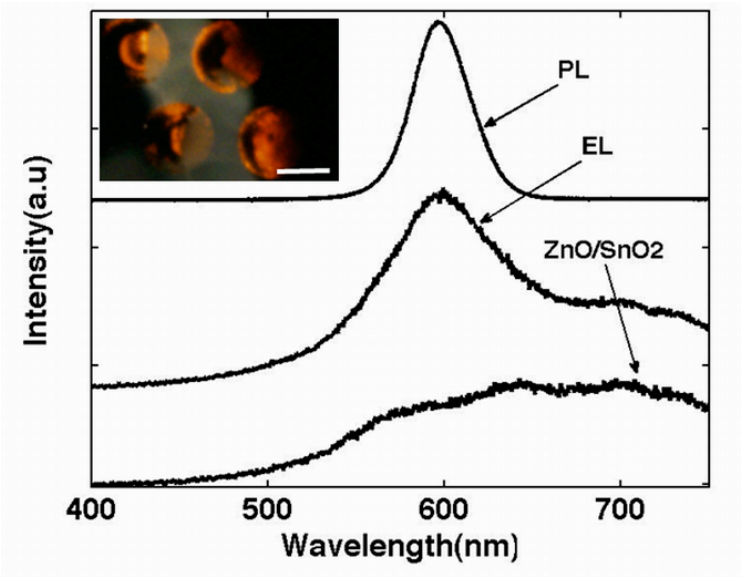

Figure 4.7: Simultaneous emission from ZnO and CdSe: ZnS nanoparticles. Photoluminescence observed from particles with emission wavelength of 598 nm. Electroluminescence identical to ZnO: SnO_2 (yellowish-white) emission was simultaneously observed along with particle emission (Orange) on application of voltage. (Embedded image: CdSe: ZnS and ZnO: SnO_2 emission (Scale bar: 100 μm).

Concentration of mixture was determined using energy dispersive x-ray (EDX) as shown in figure 4.8, where 40% Zn and 25% Sn was present. From the TEM image of the deposited film, white portions indicate presence of ZnO and dark areas indicate presence of SnO_2. The size of the ZnO particles in the mixture of ZnO: SnO_2 is comparable to that of the CdSe: ZnS particles used in the system.

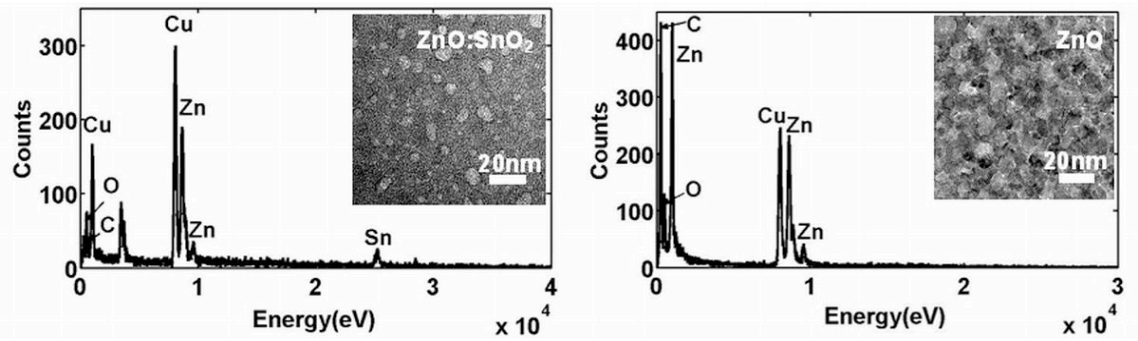

Figure 4.8: EDX data indicating 40% Zn and 25% Sn in ZnO: SnO_2 mixture (Inset: TEM image of 40 nm deposited film. Scale: 30 nm).

4.5 MEAL OXIDE FILM CHARACTERISTICS

4.5.1 X-Ray Diffraction

X-Ray diffraction is a system used to analyze the crystalline nature of materials. X rays are incident on the crystal with lattice planes spaced at a distance 'd' apart. These rays reflect off the faces of the crystals. The path difference between the reflections from the neighboring lattice places is given by the equation 2d sinθ. If the path difference of the reflected waves is equal to an integer number of wavelengths, it will constructively interfere. This is described by Bragg theory. If the material is crystalline at certain values of θ, then the reflections will be in phase. This would result in discrete and sharp peaks in an intensity (vs.) θ plot. Amorphous materials lack the periodic structure nature observed in crystalline structure [107].

ZnO film is polycrystalline in nature. Crystalline wurtzite ZnO has a unit cell dimension a = 3.250 Å and c = 5.207 Å. SnO_2 on the other hand is a tetragonal rutile structure with unit cell dimensions of a = 4.737 Å and c = 3.186 Å [108]. A mixture of the two materials would yield an amorphous film.

We aim at depositing amorphous charge transport layers since the defects or grain boundaries in a polycrystalline material causes shorts that is not desirable in the device [89].

Sputter deposition of pure ZnO onto silicon substrate indicate a certain amount of crystalline structure. 40 nm of pure ZnO was sputtered onto a 1 inch x 1 inch silicon substrate. XRD measurement revealed a peak at 33° indicating a certain degree of crystalline nature of the structure (Figure 4.9).

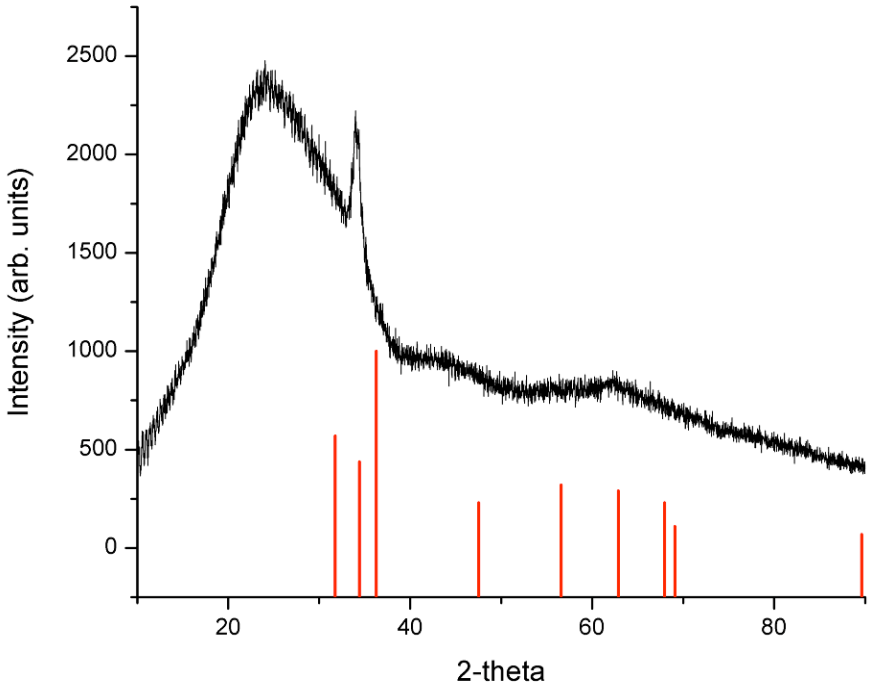

Figure 4.9: XRD of ZnO sputtered onto silicon substrate.

In order to obtain an amorphous film a mixture of 40 nm ZnO: SnO_2 that acts as a hole transport layer is deposited via sputtering. No significant peaks were observed for the sputtered film indicating amorphous nature of the film deposited (Figure 4.10). For efficient, inorganic QD-LEDs, the deposition of smooth and amorphous hole transport layers can prevent shorting and limit changes in mobility, which may arise from variations in film morphology [89].

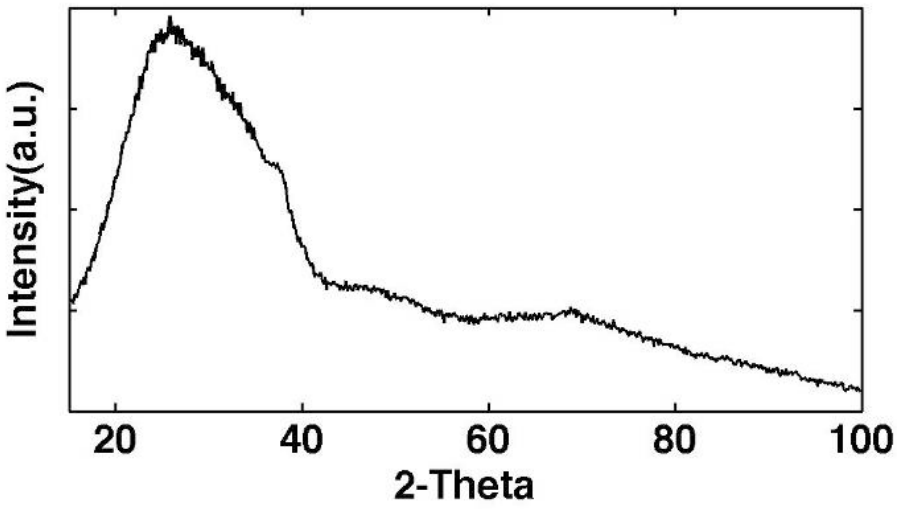

Figure 4.10: XRD image indicating the amorphous nature of the ZnO: SnO_2 mixture deposited over an area of 1 inch x 1 inch.

4.5.2 Atomic Force Microscopy

Pure ZnO or SnO_2 and certain portions of ZnO: SnO_2 films tend to be polycrystalline with pronounced grain boundaries, as shown in the AFM (Figure 4.11). The X-ray diffraction measurements indicate that ZnO: SnO_2 films are amorphous. The

AFM measurements indicate that the ZnO: SnO_2 films are relatively smooth (0.5 nm r.m.s. roughness) that has the likelihood of reducing morphologically induced electrical shorts in the device (Table 4.3).

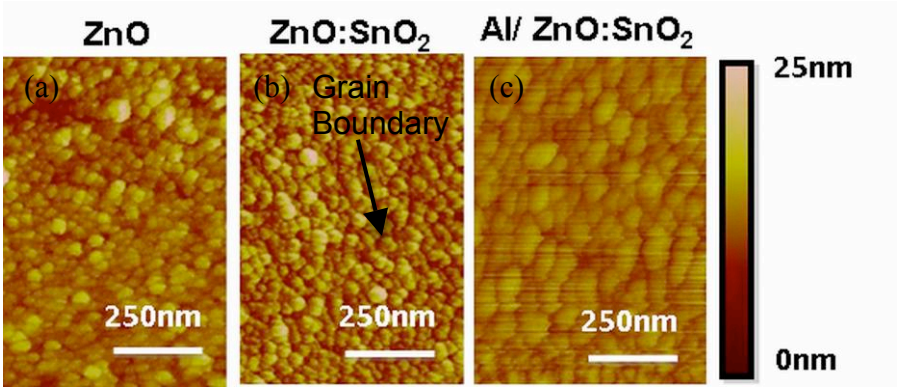

Figure 4.11: AFM of sputtered thin film (a) ZnO (b) ZnO: SnO_2 (c) Al/ZnO: SnO_2.

	Average Roughness	Film Thickness
ZnO	1.26 nm	40 nm
ZnO: SnO_2	2.39 nm	40 nm
Al/ZnO: SnO_2	2.75 nm	60 nm

Table 4.3: Metal/Metal oxide characteristics (a) Roughness (b) Film Thickness.

4.6 SUMMARY

In conclusion, the thickness of uniform monolayers of nanoparticles stamped onto to the substrate was determined by atomic force microscopy (AFM). This was then

repeated for quantum dots with diameters ranging from 7.3 nm to 9.8 nm, and corresponding emission wavelengths from 560 nm to 620 nm. Measurements were then correlated with fluorescence intensity optical micrographs, in which a linear relationship between film thickness and fluorescence intensity is observed. Once the particles were deposited a thin 40 nm metal oxide film was deposited at a low deposition rate to prevent the damage caused to the particles. The type of metal oxide (ZnO: SnO_2) film formed was an amorphous film. The top metal cathode that was deposited was thin enough to be transparent as well as conductive. Two device configurations were tested, (a) Ag/Au as the top cathode and (b) Al as the cathode that makes the device CMOS compatible.

CHAPTER 5: QDLED CHARACTERIZATION

5.1 INTRODUCTION

This chapter describes the measurement techniques used to observe the diodes. Various characteristics such as current-voltage, comparison of photoluminescence and electroluminescence and determination of the luminance were measured. These devices were tested in atmosphere with no specific packaging requirements like OLEDs. The current-voltage characteristics were recorded using a Lab View controlled power source meter. We also describe the post-processing capability of the diode making it CMOS compatible.

5.2 ELECTROLUMINESCENT CHARACTERISTICS

A positive bias is applied to the silicon and a negative bias is applied to the aluminum cathode. With modest turn-on voltage, electroluminescence is observed at room temperature. Most of the diodes demonstrated steady light emission for more than an hour of operation, proving the great stability of inorganic multilayer structure. Electroluminescence from QD-LEDs with different average QD diameters is shown in Figure 5.1. Emission from circular-patterned particles of size 7.8 nm and 9.8 nm with Ag/Au as the top electrode was observed. Figure 5.1(a-b) and 5.1(c-d) are for particles of size 9.8 nm (photoluminescence peak: 618 nm) and 7.8 nm (564 nm), respectively. For the electroluminescence in Figure 5.1d, one can observe slight emission of ZnO: SnO_2 mixture along with particle emission. A larger voltage was required to view light emission from smaller particles as 7.8 nm, resulting in simultaneous emission from ZnO: SnO_2 on the background.

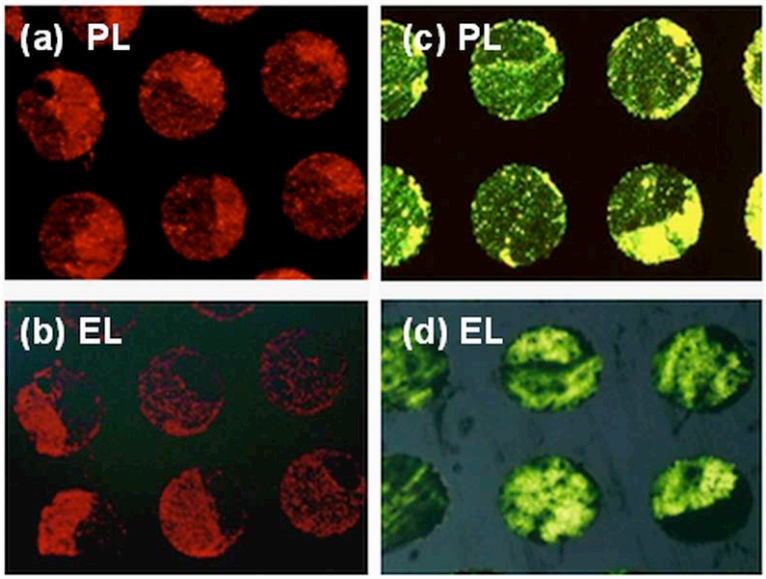

Figure 5.1: Photoluminescence and electroluminescence from patterned silicon substrate with the average diameters of (a, b) 9.8 nm and (c, d) 7.8 nm. (Circle pattern: diameter-100 μm).

A band diagram of the working of the device is illustrated in figure 5.2. When the device is forward biased the anode injects holes while the cathode injects electrons into the electron transport layer. The oxide layer acts like a buffer layer that will restrain the injected hole current and improve the balance between hole and electron injection. The field across the device carries holes and electrons to the QD layer. In this layer the electrons and holes form bound pairs, excitons, on the quantum dots. The excitons dissipate their energy by emitting light characteristics of the optical bandgap of the quantum dots.

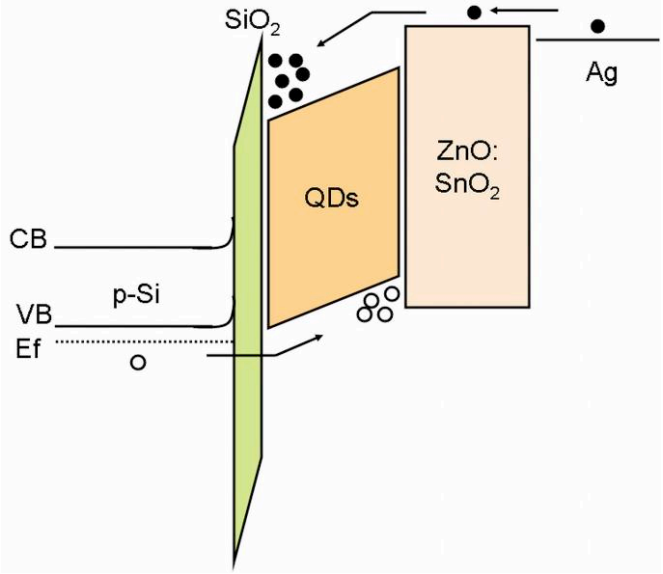

Figure 5.2: Band diagram of the quantum dot based light emitting diode on silicon working under forward bias conditions.

5.3 DIODE CHARACTERISTICS

The diodes that were fabricated on silicon substrates were tested with two different top electrodes: (a) silver (Ag)/gold (Au) and (b) aluminum (Al). A comparison of the working of each individual top electrode is described below.

5.3.1 Silver/Gold Cathode

Figure 5.3 shows the basic characteristics of the QD-LEDs with three different colors. Electroluminescence spectrum and image of the working device were observed indicating that the emission from the device is dominated by the emission from the quantum dots layer. Current–voltage characteristics are shown in Figure 5.3(a1-c1).

Forward bias is observed when p-type silicon is the positive electrode and Ag/Au electrode is grounded. A thin layer of Ag (12 nm) was deposited followed by gold (4 nm) to create the cathode. The gold layer was deposited to prevent the oxidation of Ag under normal atmospheric conditions. The thickness of Ag is sufficient for a cathode to conduct charge through the device, and the layer is sufficiently transparent to allow emission to be observed from the top of the diode.

Turn on voltages for LEDs with average particle size 9.8 nm, 9.0 nm and 8.4 nm were 2 V, 4 V and 5 V, respectively. It was observed that for all the devices forward current increases as the forward voltage increases. The smaller the particle, the larger the band gap, and so is the required turn on voltage for the device to show light emission. It was observed that the current required to view light emission was on the order of 40-50 $\mu A/mm^2$. Current-intensity plots in Figure 5.3(a2-c2) indicate a linear relationship between the increase in intensity and current flow through the device.

In literature it has been reported that luminance of 53 cd/m^2 at a current density 860 $\mu A/mm^2$ and at a voltage 14 V was observed for TOLED with Si anode [4]. In this paper the luminance of the device at 10 V with CdSe: ZnS nanoparticles, of particle size 9.8 nm, 9.0 nm and 8.4 nm was observed to be 482 cd/m^2, 375 cd/m^2 and 489 cd/m^2 for emission wavelength 622 nm, 598 nm and 576 nm for the particular emission area. The current density of 147 $\mu A/mm^2$, 120 $\mu A/mm^2$ and 375 $\mu A/mm^2$ was measured for 1 mm x 1 mm top electrode dimension for diodes with nanoparticles of size 9.8 nm, 9.0 nm and 8.4 nm respectively.

An example for calculating the intensity for quantum dots with emission wavelength 600 nm is given below. We observe the emission area using the spectrometer and determine the photon counts/sec. A 100x objective (Olympus BX51 microscope)

with 0.9 numerical aperture was used to observe the light emitting diode. Calculation for a single wavelength is shown below. This calculation works similarly for other wavelengths [9].

The emission wavelength was observed using a spectrometer to be 600 nm. Emission power *pe* of a single photon becomes:

$$pe = h\upsilon = \frac{hc}{\lambda}$$

pe=3.313 X 10^{-19}J

The photon counts of 2.18 *X* 10^7 [counts/s] at 10 V defines the emission power as

$$p = pe.counts$$

$$=(3.3 \text{ X } 10^{-19}) \cdot (2.18 \text{ X } 10^{7})$$

$$=7.195 \text{ X } 10^{-12} \text{ [W]}$$

Since we used a microscope objective with numerical aperture NA = 0.9 (sin θ = 0.9), the entire emission *P* of the LED is

$$P = \frac{p * 4\pi}{\left(2\pi \int_0^{\theta/2} \sin\varphi \cdot d\varphi \right)}$$

$$= 9.43 \text{ X } 10^{-11} \text{ [W]}$$

Thus, the luminous intensity is given by

$$P/4\pi = \text{[W/sr]}$$

$$= 7.498 \text{ X } 10^{-10} \text{ [W/sr]}$$

$$= 7.498 \text{ X } 683 \text{ X } 0.631 \text{ X } 10^{-10} \text{ [cd]}$$

The observed LED area is 20 μm x 45 μm and the luminance was observed 354 cd/m^2. Typical luminous intensity that we obtain is in W/sr that we convert to cd/m^2. Units in cd/m^2 are just to give a comparison with other LEDs demonstrated in literature.

The light emission observed from the LEDs created is darker compared to other conventional light emitting diodes described in literature. The enhancement in light emission can be accomplished by replacing the top electrode with a transparent material.

Figure 5.3 (a3-c3) shows the electroluminescence and photoluminescence of the LEDs plotted for particle size 9.8 nm, 9.0 nm and 8.4 nm, respectively. A strong electroluminescence band was observed from CdSe: ZnS particles with full width half maximum (FWHM) of ~40 nm. This was observed to be similar to that of photoluminescence. The electroluminescence emission peak was observed at 622 nm, 598 nm and 576 nm for the red, orange and yellow emitting devices, respectively. A slight red shift was observed between the photoluminescence (peaked at 618 nm) and electroluminescence (622 nm) spectra in Figure 5.3(a3). This is similar to the CdTe particles that have a red shift due to the trap filling or detrapping on the surface states [36]. The small red shift of ~5 nm and slight broadening of the electroluminescent spectra, when compared to the photoluminescence spectra, can also be attributed to effects such as energy and charge transfer among nanoparticles [67, 109]. It was also observed that the power consumed by these devices was typically small. For instance, devices with 9.8 nm particles consumed typically 5 mW power for an area of 1 mm x 1 mm.

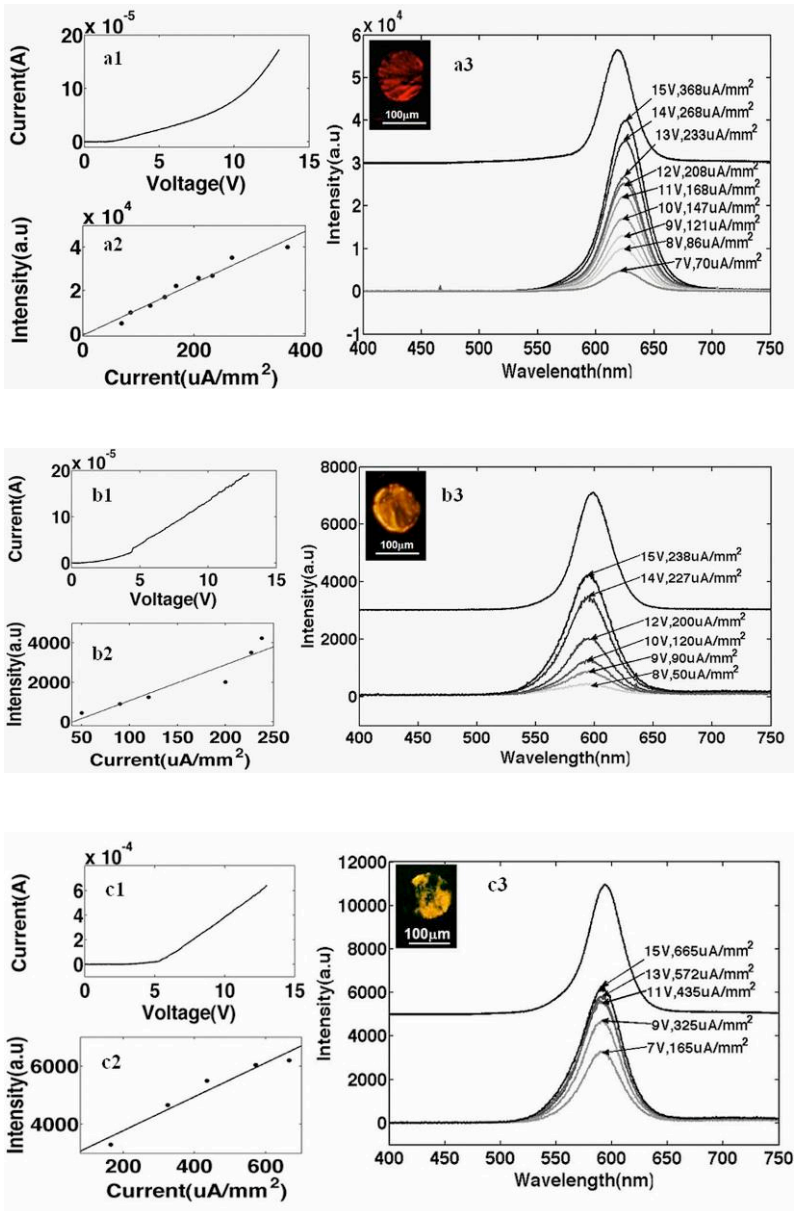

Figure 5.3: Basic characteristics of three different color (red, orange and yellow) LEDs. (a1, b1, c1): Current versus voltage. (a2, b2, c2): Luminance versus current characteristics. (a3, b3, c3): Photoluminescence and electroluminescence with different operating conditions. The inset images show electroluminescence for the QD-LED under operation.

5.3.2 Aluminum Cathode

To make the device CMOS compatible we deposited aluminum as the cathode instead of silver or gold. 20 nm of aluminum was e-beam evaporated onto the ZnO: SnO_2 layer. On application of positive voltage to the p-silicon and negative bias to the aluminum cathode, electroluminescence (EL) was observed. Turn-on voltages for the devices were measured (4.5, 4.4, 4.0 and 3 volts) for the average particle diameters (9.8 nm, 9.0 nm, 8.4 nm and 7.8 nm, respectively).

The electroluminescence emission peak was observed at 625 nm, 598 nm, 576 nm, 564 nm for the red, orange, yellow and green emitting devices, respectively (Figure 5.4). For ease of understanding we would refer the wavelengths as 620 nm, 600 nm, 580 nm and 560 nm instead of actual peak emission. A strong electroluminescence band was observed from CdSe: ZnS particles with full width half maximum (FWHM) of ~40 nm). This was observed to be similar to that of photoluminescence. An increase in electroluminescence intensity was observed with increase in applied voltage. The current flowing through the device was on the order of mA compared to μA current flowing through the device with Ag as the top electrode.

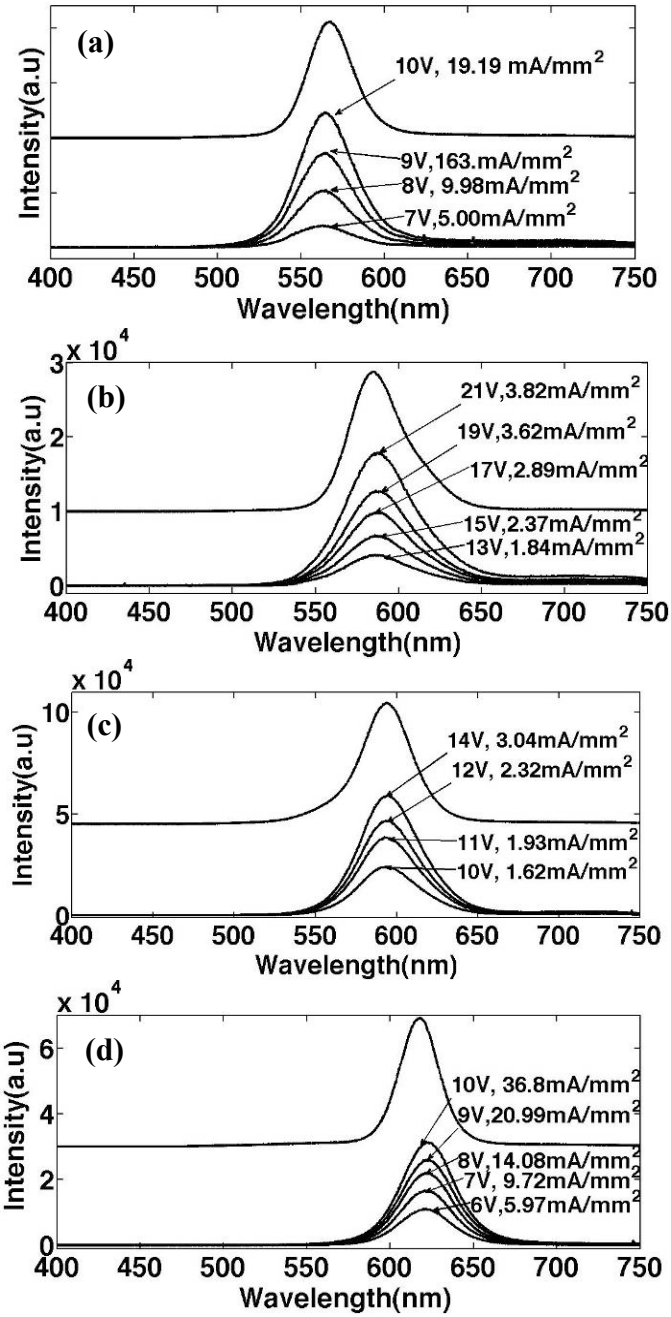

Figure 5.4: Intensity characteristics of four different color (red, orange, yellow, green) LEDs. (a, b, c, d): Photoluminescence and electroluminescence with different operating conditions.

The emission wavelength can be tailored by a choice of quantum dots with desired emission wavelengths. We have demonstrated multicolor light emitting diodes on silicon patterned by polymer stamp with quantum dots of different sizes in Figure 5.5. Smallest feature size of 500 μm x 500 μm was patterned and observed for particles with emission wavelength 560 nm and 600 nm. We were also able to observe light emission from 100 μm diameter arrayed circles. Different patterns can be obtained by varying the PDMS pattern used to create the light emitting diodes. To show different patterning capabilities we were able to pattern the 'Bevo' of feature size 500 μm.

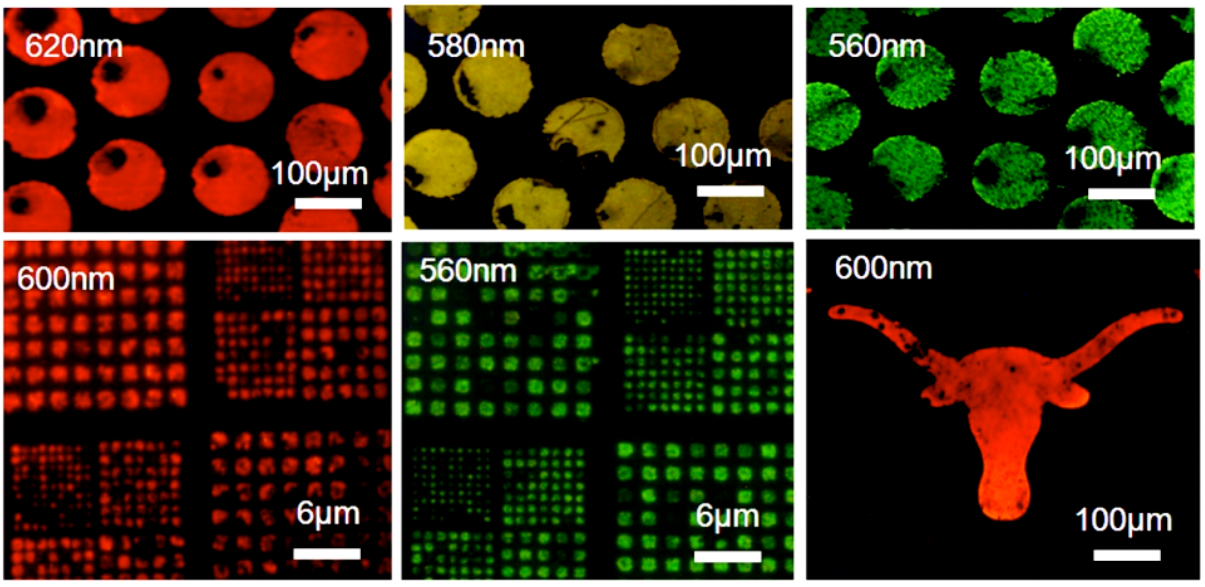

Figure 5.5: Electroluminescence observed from patterned quantum dots on silicon substrates. (Top row) Patterned light emission observed from circles of diameter 100µm with emission wavelength 620 nm, 580 nm and 560 nm. (Bottom row) Nano-patterned electroluminescence with smallest feature size 500 nm x 500 nm and emission wavelength 600 nm and 560 nm. Light emission was also observed from Bevo pattern.

It is observed that the light emission observed form diodes with Al, as a top electrode is darker in comparison to the diodes with Ag/Au as the top electrode. 60% of the light is trapped under the Al electrode compared to that of Ag/Au top electrodes. A comparison of the intensity values is listed in Table 5.1. The uniformity of light emission was observed to be better with Al as a top electrode when compared to that of Ag/Au. These are indicated in Figure 5.1 and Figure 5.5.

S.No	Wavelength (nm)	Color	QD-LED with Ag/Au Cathode (cd/m^2)	QD-LED with Al Cathode (cd/m^2)
1	560	Green	433	155
2	580	Yellow	489	135
3	600	Orange	375	487
4	620	Red	482	332

Table 5.1: Observed luminance of the device with different cathodes.

5.4 OPERATION CHARACTERISTICS

We observed that most diodes demonstrated steady light emission for more than five hours of operation with Al as the cathode, proving the great stability of inorganic multi-layer structure (Figure 5.6). Decrease in light emission with time was indicated for diodes having Ag/Au as the cathode fabricated previously [19]. Use of Al as the transparent top electrode enables better CMOS compatibility and post processing capability.

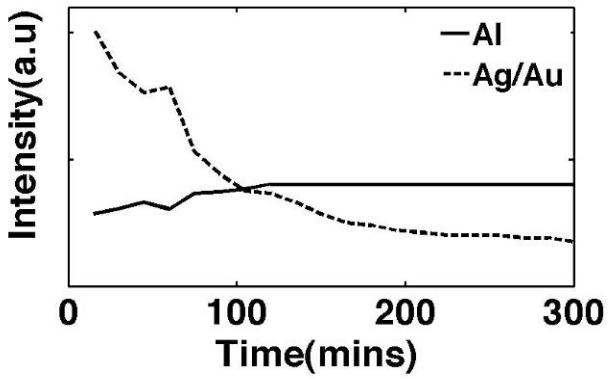

Figure 5.6: Variation of electroluminescence intensity versus time for light emitting diode with different metal cathode.

5.5 POST PROCESSING OF DIODE

Site-controlled patterning of light emitting diodes (LEDs) is important in applications such as high resolution arrays [110], large screen displays [111, 112], micro-electro-mechanical systems (MEMS)[8], optoelectronic systems [113], and multicolor excitation source in micro-total analysis systems (μ-TAS) [114]. Organic light emitting semiconductors have attracted the attention of researchers over the past decade due to its easy integration with large scale displays [48, 111, 112, 115, 116].

One of the biggest challenges in organic light emitting diodes (OLEDs) is the patterning technique. The most conventional photolithographic patterning have been very difficult for OLED fabrication due to the degradation or failure of the devices on being exposed to water, oxygen, solvents and developers used for the patterning and removal of photoresist [56, 117-119].

Typical patterning of OLEDs [18, 119] has been demonstrated using the shadow-mask technique [119, 120]. Other special techniques such as laser ablation [121] and stamping-induced lift off [122-125]have been also devised. Each of these methods has certain shortcomings. Shadow mask techniques have limited resolution because of shadow effects caused by the mask. The resolution is limited to several tens of microns [119]. Excimer photo-ablation of indium tin oxide (ITO) anode and metal cathode was used to create an array of 20 μm x 20 μm active area. The method is not suitable for a large screen display due to its low speed and low throughput [121]. Cold welding technique has been demonstrated for scalable electrode patterning by using contact stamping techniques [122-125]. These techniques require good pressure and temperature control in order to prevent damage to the organic layers [122-125], which requirement may not be suitable for large-area applications.

Alternate methods to pattern OLEDs have been demonstrated by patterning the active layer. The polymer-based light emitting diodes have been patterned utilizing screen printing [126], inkjet printing [127] and soft-lithography [128, 129]. The resolution in these patterning methods is not comparable with the far advanced photolithography process. Improved resolution of polymer patterning has also been carried out using capillary lithography techniques [130]. However, these are still limited in the size and the design. Heating the polymer above glass transition temperature could damage the organic polymer in the device.

Photolithography is the commonly used process in the fabrication of microelectronic integrated circuits (ICs) as well as semiconductor photonic components. Standard techniques such as photolithography, reactive ion etching and chemical etching have been used to fabricate the silicon devices. Such patterning techniques for the most advanced devices enable controlled feature size better than the order of 100 nm. These

have seen wide applications such as CMOS compatible very large scale integration (VLSI) systems or MEMS.

5.5.1 Fabrication Process

The device comprises a p-silicon that acts as the hole transport layer, with 1 nm SiO2 that acts as the buffer layer as shown in Figure 5.7. We deposit modified Langmuir–Schaefer films (2-3 monolayers) of CdSe: ZnS colloidal quantum dots via microcontact printing (Figure 6.1a-b) using PDMS, as discussed previously. The electron transport layer in this device is co-sputtered ZnO and SnO_2 (Figure 5.7c). The structure is completed by e-beam evaporating a 15 nm thick Al cathode onto the ZnO: SnO_2 (Figure 5.7c) layer. Use of Al as the transparent top electrode enables better complementary metal oxide semiconductor (CMOS) compatibility and post processing capability.

The diode fabricated was then post processed using conventional lithographic techniques. Tools commonly used for fabricating silicon devices are used without any modifications. AZ 5209A photoresist was spin coated at 2200 rpm (Figure 5.7 d) for 1min onto the device and exposed to UV light for 2 sec (EVG Mask Aligner) (Figure 5.7e). Patterns with feature size 5 μm were developed for 30 sec using AZ 726 MIF. The device was then baked at 90 °C for 1.5 mins.

The pattern was then etched into the device using reactive ion etching technique. A mixture of CF_4 and Cl_2 were used at a power of 250 W (Figure 5.7e) to etch the aluminum layer. Typically etching time of 1.5 min was sufficient to etch through the aluminum layer. With a longer etching time, ZnO: SnO_2 layer as well as the QD layer was observed to be etched as shown in Figure 5.7.1f. The residual resist was removed by

triple rinsing the device in acetone, methanol and isopropyl alcohol followed by oxygen plasma cleaning (March Asher) at 300 W for 2 mins. On completing the device, a positive bias was applied to the p-silicon and negative bias to the aluminum cathode.

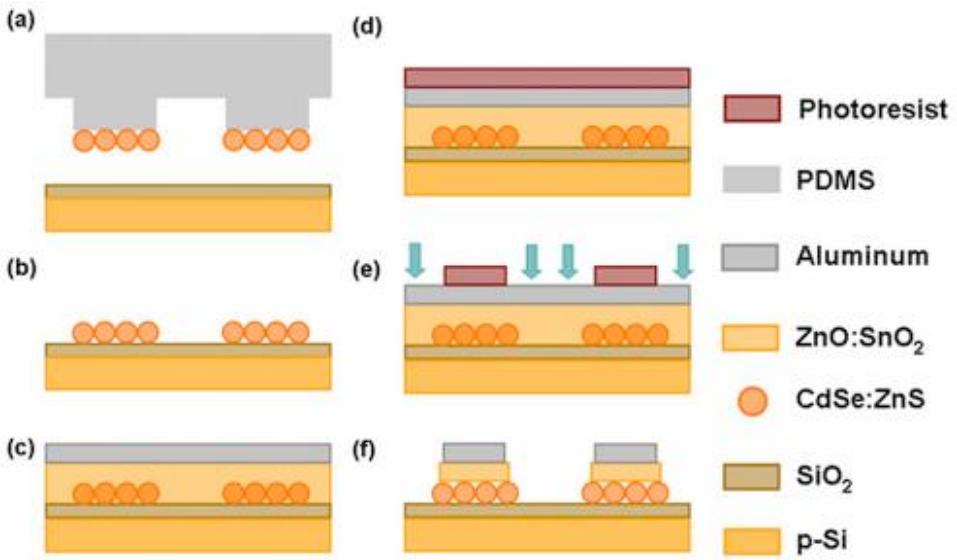

Figure 5.7: Fabrication process of QD-LED. (a) Microcontact printing of monolayer's of quantum dots onto SiO_2/p-Si substrate. (b) Transfer of particles. (c) Sputter deposition of ZnO: SnO_2 (10 nm) and e-beam evaporation of Al (15 nm).(d) Spin coating of AZ 5209A. (d) Pattern, develop and reactive ion etching of the device. (f) Completed inorganic light emitting diode.

Optical transparencies of the ZnO: SnO_2 films for the visible wavelengths were measured to be more than 90 %. The cathode is the thin transparent Al (15 nm) electrode, which reduces optical transmission to 20–10 % between 500 nm and 700 nm emission wavelength (Figure 5.8).

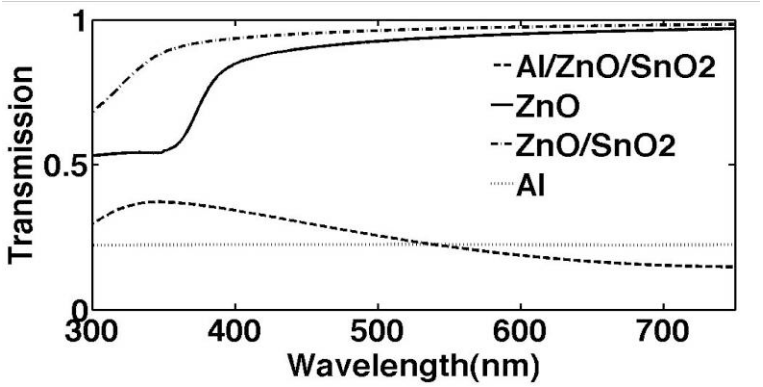

Figure 5.8: Optical transmission of the various films deposited.

5.5.2 Electroluminescence Characteristics

The light emitting area can be defined either by the patterning of the QD layer or the cathode. A combined patterning technique where the top electrode is patterned over patterned monolayers of QDs was used to form a QD-LED. Figure 5.9a shows electroluminescence of the fabricated diode.

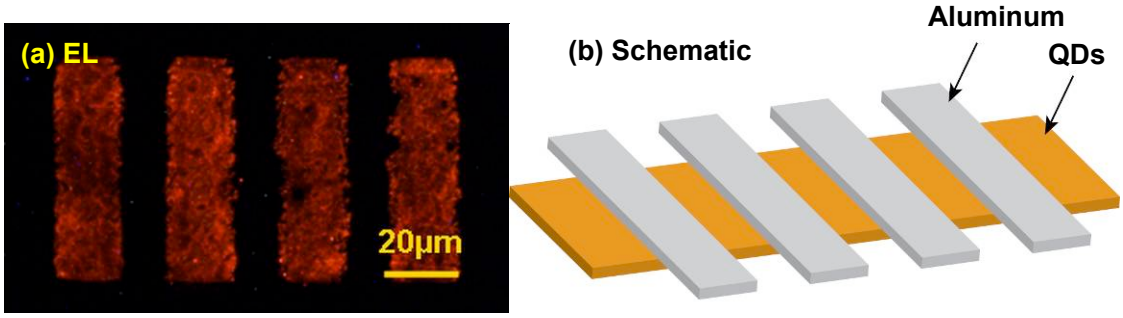

Figure 5.9: Patterned top aluminum electrode. (a) Electroluminescence observed for patterned top electrodes with feature size 20 μm; (b) Schematic of patterned nanoparticles and Top Aluminum electrode.

Arrayed patterns of 100 μm wide grating structure of monolayers of CdSe: ZnS particles of size 9.0 nm were microcontact printed onto silicon substrate. The PDMS stamp transfers the pattern of the QD layer. The ZnO: SnO_2 and aluminum layers were then deposited as described above. Finally, the aluminum cathode was patterned to form 20 μm-wide lines perpendicular to the QD pattern. Figure 5.9b gives the schematic of the patterned device. Light emission was observed at 4 V.

Circular arrayed patterns of CdSe: ZnS with emission wavelength 620 nm and 580 nm were patterned onto the same silicon substrate. The top Al cathodes were aligned and patterned onto the diode as shown in Figure 5.10a. On application of a bias to each electrode we were able to electrically excite the diode and observe light emission from each individual color at a particular voltage. Light emission for particles with emission wavelength 620 nm was observed at 12 V (Figure 5.10b) and for particles with emission wavelength 580 nm light emission was observed at 15 V. We were able to successfully pattern two individual colors on the same substrate and excite them individually.

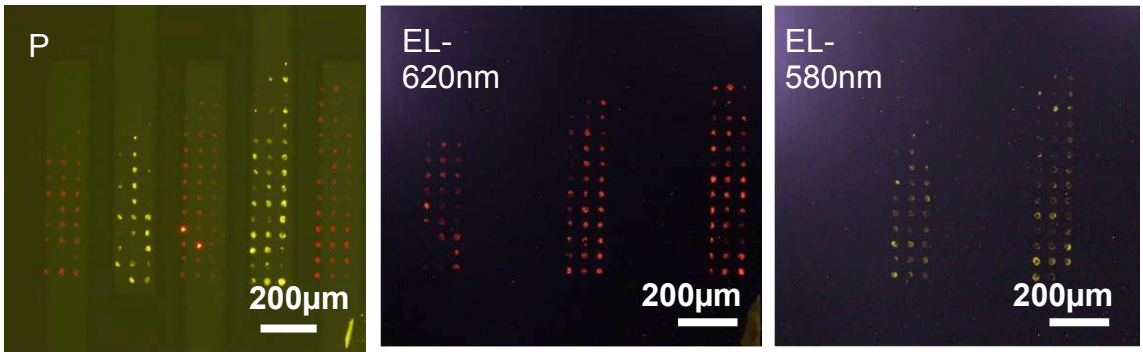

Figure 5.10: Patterned electrode emission from two colors. (a) Photoluminescence from 620 nm and 580 nm patterned quantum dots. (b) Electroluminescence observed from particles with emission wavelength 620 nm at a voltage of V = 12 V.(c) Electroluminescence observed from particles with emission wavelength 580 nm at 15 V.

LEDs with different QD diameters, namely 9.8 nm, 9.0 nm, 8.4 nm and 7.8 nm, for emission wavelength 620 nm, 600 nm, 580 nm and 560 nm, respectively were tested with the same device configuration. The corresponding photoluminescence (PL) and electroluminescence (EL) spectra for 600 nm and 560 nm LEDs are shown in Figure 5.11. The EL spectra measured from QD-LEDs are well correlated to the PL spectrum. An increase in electroluminescence intensity was observed with increased current injection in the device. The full width half maximum of the electroluminescence spectrum was ~40 nm (Figure 5.11).

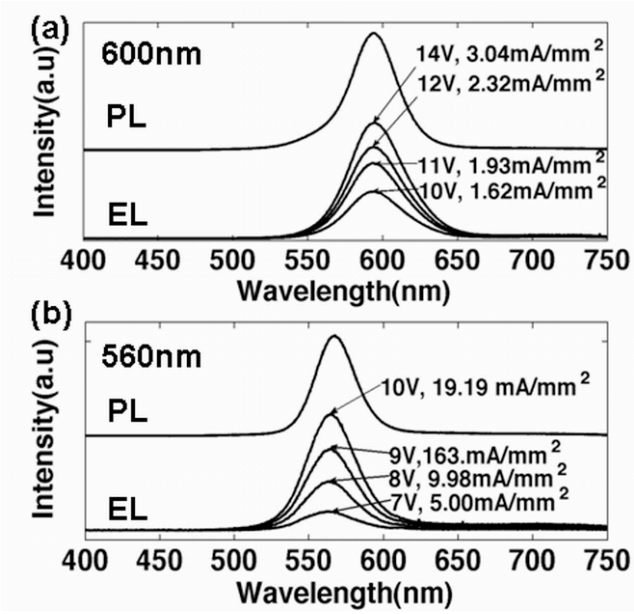

Figure 5.11: Electroluminescence and Photoluminescence (PL) observed from particle size of (a) 9.0 nm and (b) 7.8 nm.

Figure 5.12 shows the current density versus voltage and electroluminescence intensity characteristics of the device. The inset gives the current versus the intensity of the light emitting diode for particle size 9.0 nm and emission wavelength 600 nm.

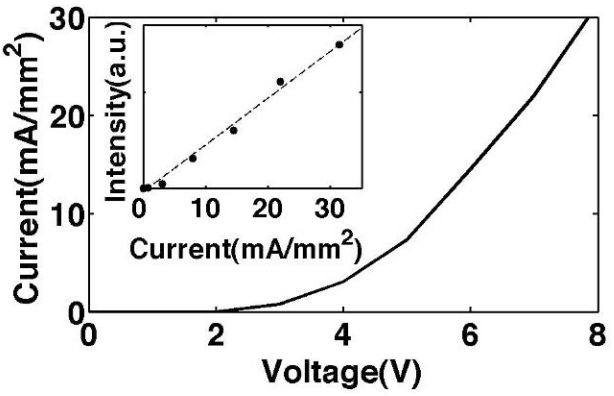

Figure 5.12: Current density versus voltage characteristics of a 2 mm^2 area inorganic light-emitting device. Inset: Electroluminescence intensity variation with current flowing through the device (Emission wavelength of the diode 600 nm). The completed device consists of 15 nm thick Al/10 nm thick ZnO: SnO_2 top of 25 nm thick CdSe: ZnS nanoparticles /SiO_2/p-Si.

The luminance of the devices for emission wavelength 620 nm, 600 nm, 580 nm and 560 nm was measured at 10 V and calculated to be 332 cd/m^2, 487 cd/m^2, 135 cd/m^2 and 155 cd /m^2. The measured emission area was 100 μm x 100 μm. The current density of 12.3 mA/mm^2, 10.9 mA/mm^2, 12.0 mA/mm^2 and 19.9 mA/mm^2 with 1 mm × 2 mm top electrode was measured for 620 nm, 600 nm, 580 nm and 560 nm diodes respectively. Turn-on voltages were 3.5 V, 4.0 V, 4.5 V and 5.5 V for the average particle diameters 9.8 nm, 9.0 nm, 8.4 nm and 7.8 nm, respectively.

5.6 NANO-PARTTERNING TO DEFINE LIGHT SOURCE

It is important to control patterning of both the light emitting layer and the top metal cathode. In this way it is possible to define multicolor light sources with designs of several degrees of freedom. We studied the limitation of the two patterning methods,

namely (a) nano-pattern stamping which defines the area of the patterned quantum dots and (b) photolithographic patterning the top metal cathode that defines the area of the charge injection.

PDMS nano-pattern stamps were used to transfer QDs onto the substrate. The stamps (500 nm feature size) were replicated from the silicon masters, which were fabricated by e-beam lithography and following reactive ion etching. The nano-atamps were created from patterned silicon samples that acted as master molds for PDMS. AFM image of one such pattern is given in Figure 5.13. The patterns were created onto silicon surface using e-beam lithography.

25 nm of chromium was deposited onto the silicon substrate that acted as the hard mask. ZEP520A (Spin speed 2200 rpm) was patterned using EBL system. The patterns were then developed using ZED N50 for 1 min followed by isopopyl alcohol for 1 min. Chromium was initially etched using ZEP520A as the hard mask. Then the pattern on chromium was transferred to silicon substrate using reactive ion etching up to 1 μm deep using CF_4 gas mixture.

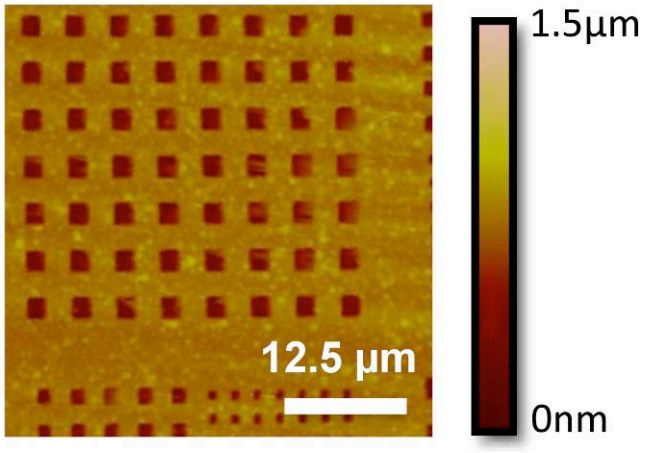

Figure 5.13: AFM of the master mold for nano-stamps

Successful nano-scale electroluminescence from QD-LEDs with different average QD diameters and emissions was observed as shown in Figure 5.14.

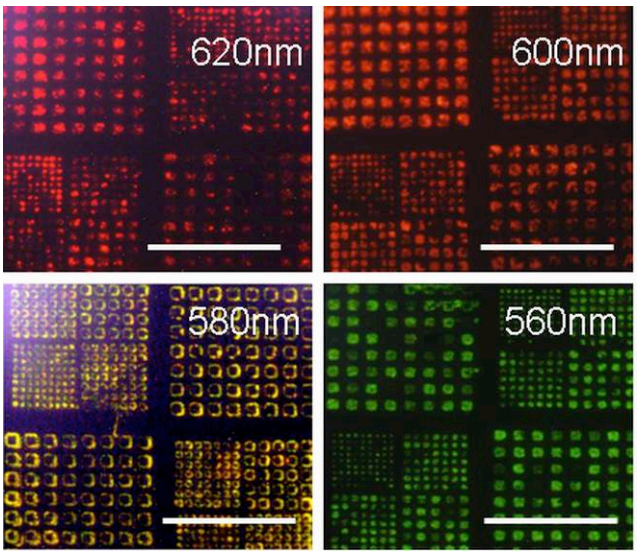

Figure 5.14: Electroluminescence observed for different emission wavelength. (Scale: 25 μm)

The variation in light intensity observed from the pattern was due to non-uniformity in thickness of QDs deposited onto the substrate. As discussed previously, thicker quantum dots (thickness of ~50 nm for particle size 9.0 nm) require more injection current, as they are highly resistive in nature [19]. A very thin layer (~10 nm) of quantum dot particles is insufficient for good light emission. Hence it is required to have optimal thickness (~35 nm for emission wavelength 600 nm) of particles for uniform light emission.

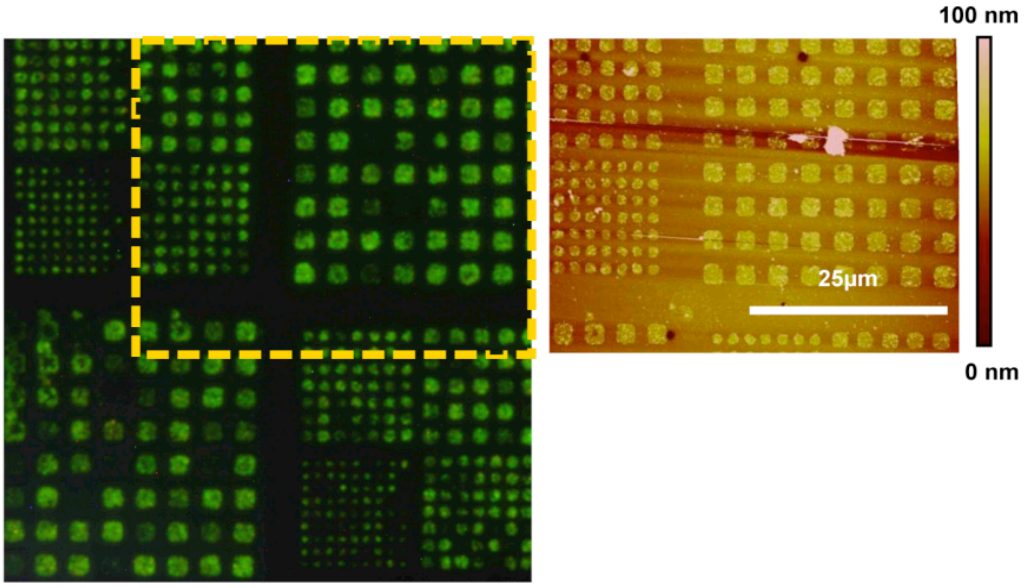

Figure 5.15: (Left) Electroluminescence of particles with emission wavelength 560 nm. (Right) Dotted lines give the exact area where AFM was performed.

Atomic force microscopy (Digital Instruments AFM 3000) was performed on the nano-patterned LED after observing electroluminescence from the device (Figure 5.15). The scanned feature size was varied from 500 nm x 500 nm to 800 nm x 800 nm. The variation in the size of patterned QD islands could be due to the difficulty of creating a perfect PDMS replication of the nanopatterns, while the thickness distribution is attributed to our modified Langmuir-Schaefer film formation process.

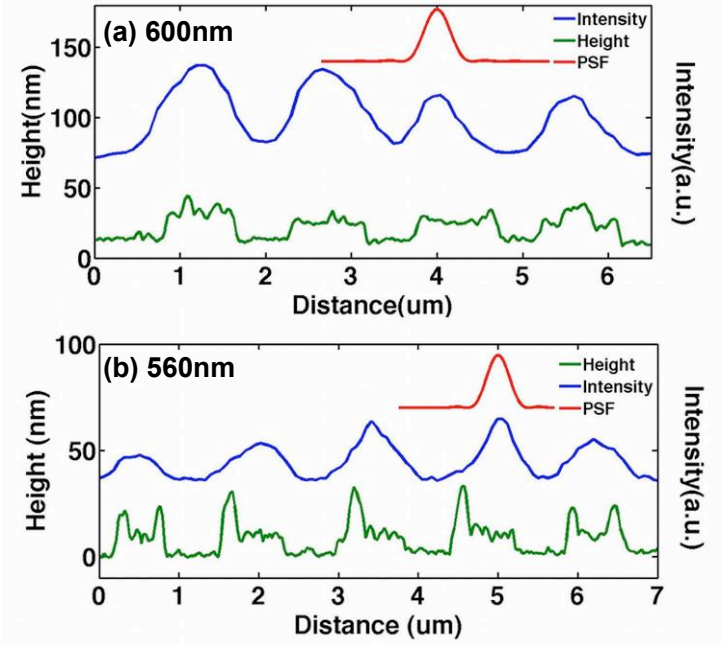

Figure 5.16: AFM versus electroluminescence for nanopatterned light emitting diodes observed from particle size of (a) 9.0 nm and (b) 7.8 nm.

The height observed using AFM (~20 nm) was correlated with the electroluminescence intensity measured for the exact same region (Figure 5.16). The electroluminescence intensity along with the AFM-measured profiles is shown for particles with emission wavelength 600 nm and 560 nm (particle size 9.0 nm and 7.8 nm. respectively). The microscope acts as a diffraction limited optical system [131]. The resolving power of the objective is determined by the Airy disk point spread function (PSF), which is expressed as the Bessel function of the first kind. Measured optical intensity is the convolution of the actual emitting area and the PSF. The Airy pattern radius *r* from the central peak to the first minimum is given by the equation [132]:

$$r = \frac{1.22\lambda}{2NA} \qquad (1)$$

Where *r* is the Airy radius, λ is the wavelength of illuminating light, and *NA* is the objective numerical aperture. In our case the λ (wavelength) is given by the emission wavelength of the light emitting diode (e.g., 600 nm or 560 nm). These intensity patterns were compared with the Airy pattern that was theoretically calculated for our microscope objective (100x Olympus M Plan N, numerical aperture 0.9). The numerical aperture of the objective used here is among the highest available with an air medium. For certain cases, the emission profile was comparably small as the point spread function calculated (Figure 5.16) indicating that the smaller numbers of particles were electrically excited compared to the area of particles deposited. The profile of emission is mainly defined by the point-spread function of the microscope. The actual emitting areas are roughly estimated to be smaller than 100 nm. The minimum number of QDs required for light emission can be as few as a single molecular order (less than 10). In other cases the electroluminescence intensity peak profile was larger than the AFM measured profile, indicating that the entire 500 nm x 500 nm area of particles were electrically excited. The EL profiles for those cases are still largely affected by the PSF. For the photolithographically patterned light emitting diodes, the smallest feature size of the electrode was 5 μm (Figure 5.17). In this device a large area (2 mm x 2 mm) of quantum dots were microcontact printed and then subsequently ZnO: SnO_2 and Al were deposited. The diodes were then post processed to etch the aluminum layer as well as the QD layer. After subjecting the diode to photoresist, developer and reactive ion etching no significant damage to the device was observed during the process, proving that our device is robust enough for most of the standard device fabrication processes.

On application of voltage (~3.5 V) to the diode, light emission was observed from the patterned top aluminum electrode. QDs with emission wavelength 600 nm were used. AFM measurement was performed on the patterned electrode and correlated with the electroluminescence intensity. Double-lined edges can be found on the sides of each line

in the AFM image (Figure 5.17c). This can be also observed as two steps in the AFM profile of an edge (Figure 5.17). While the electroluminescence measurement corresponds to the inside 5 μm-wide stripe pattern (Figure 5.17b), the photoluminescence measurement does to the outside 8 μm-wide pattern (Figure 5.17a). This suggests that the inside stripes are the aluminum layer and the outside pattern the QD layer. The QD layer had a height of ~25 nm and the total layers had a height of 45 nm. The increasing and decreasing profile edge of the EL is similar to that of the point spread function of the microscope. This indicates that the actual emitting area is comparable to the step function defined only by the geometry of patterned aluminum.

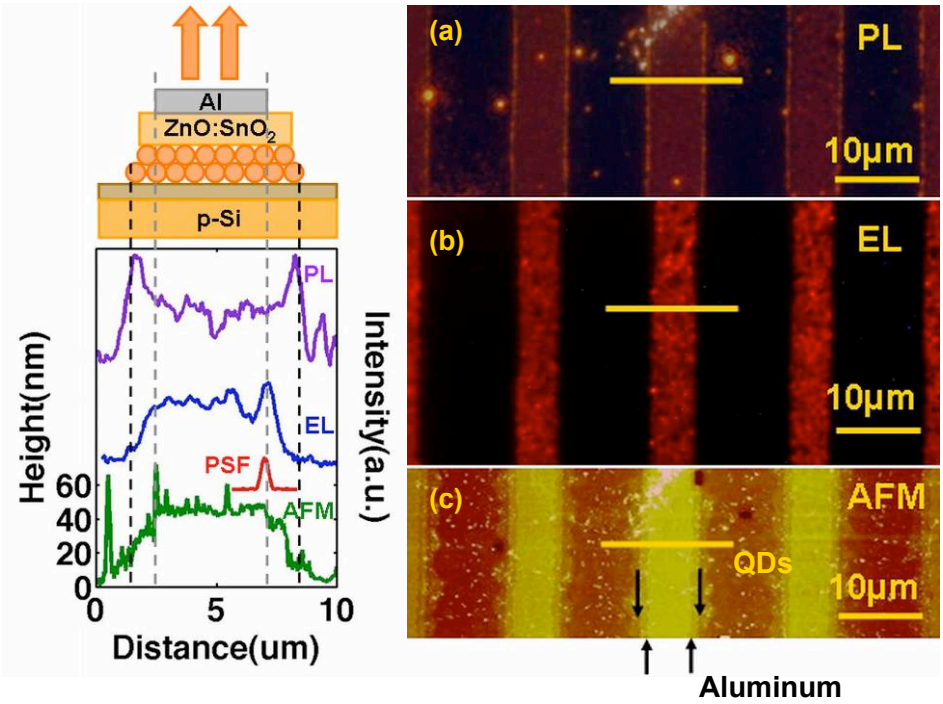

Figure 5.17: (Left) Schematic of patterned aluminum electrode and measured values of PL, EL and AFM at the yellow lines indicated in the images on the right. (Right) Patterned top metal cathode (a) Photoluminescence (b) Electroluminescence and (c) Atomic force microscopy of etched aluminum electrode with 5μm feature size. Arrows in the bottom indicate aluminum step and the arrows on top indicate the quantum dot step. (The profile measurement on the left figure was measured at the orange bar indicated.)

5.7 SUMMARY

When voltage was applied to the QD-LED with Ag/Au as the top electrode, electroluminescence (peaked at 622 nm, 598 nm and 576 nm) identical to the photoluminescence (618 nm, 598 nm and 576 nm) was observed depending on the average diameter of the used QDs (9.8 nm, 9.0 nm and 8.4 nm, respectively). For devices with Al as the top electrode the luminance of the devices for emission wavelength 620 nm, 600 nm, 580 nm and 560 nm was measured at 10 V and calculated to be 332 cd/m^2, 487 cd/m^2, 135 cd/m^2 and 155 cd/m^2. The LED demonstrated steady light emission for hours of operation, proving the great stability of inorganic multilayer structure. The ease of fabrication and processing of colloidal QD on silicon, through microcontact printing and further integration with metal oxides, open up the possibilities for creating nanophotonic microsystems with mass reproducibility and enable robust, compact and tunable imaging, sensing and display applications.

We also demonstrated photolithographical patterning the metal cathode of the top emitting quantum dot based inorganic light emitting diodes on silicon. The feature size of 5 μm was achieved using UV photolithography and reactive ion etching. The stability of inorganic silicon materials and metal oxide based diode structure offers excellent advantages to the device, with no significant damage observed during the patterning and etching steps.

The actual emitting area is mainly defined by three factors: (1) The top cathode geometry, which can be potentially smaller than 100 nm with the state-of-the-art silicon processing technology; (2) the area of the patterned quantum dots, which can be deposited via microcontact printing. The feature size of the light emitting area that can be patterned is as small as 500 nm x 500 nm, with the number of light emitting QDs

estimated to be single molecular order (<100 nm or 10 QDs). The nanostamping technique [19] we developed previously can potentially deposit a fewer number of colloidal QDs with well-defined geometry; (3) the point spread function (PSF) of the microscope. In our experiments, the rising and falling edge of the EL peak was governed by the PSF of the microscope for the emission wavelengths of 560 nm and 600 nm. Therefore, the fineness of the emitting area is mainly limited by the resolution of the observing microscope.

The combination of micro-scale lithographic patterning and nanostamping methods make it possible to accurately define diffraction-limited multicolor light sources on a single silicon substrate with great accuracy. We demonstrated steady light emission for more than five hours of operation with Al as the metal cathode. The ease of fabrication and post processing of quantum dot based light emitting diode (QD-LED) open up the possibilities for creating robust micro imaging systems integrating nanophotonics and CMOS electronics for advanced displays, spectral analysis, medical imaging and micro-total analysis systems in biomedicine.

CHAPTER 6: APPLICATION OF QD-LED

6.1 INTRODUCTION

In this chapter we introduce applications of quantum dot based light emitting diodes on silicon. The diodes fabricated on flat substrate have been translated to two possible applications. Here we describe the possible applications that have been investigated with the diodes created: (a) Nano-light emitting diodes for near field scanning optical microscopy and (b) Multispectral light sources for point of care detection devices. We start out discussing the translation of QD-LEDs onto three dimensional silicon substrates to create nano-light emitting diodes for near field applications. Second we describe the integration of multicolor sources on a single substrate as excitation sources for cancer diagnostics.

6.2 NANO-LEDS FOR NSOM APPLICATION

Near field scanning optical microscopy (NSOM) is a microscopic technique for investigating structures that breaks the far field resolution limit. The fundamental limit to imaging resolution is caused by diffraction. The typical diffraction limit is given by Rayleigh criterion[133]:

$$d = 0.61\frac{\lambda}{NA} \tag{1}$$

Where: λ is the wavelength of light

NA is the numerical aperture

Typically optical microscopes are diffraction limited. They cannot resolve sample features with later spacing smaller than 200 nm for visible wavelength. NSOM enables the optical observation below the diffraction limit of a standard optical microscope [134].

Typical NSOM consists of four major parts [135]: (a) Illumination source and probe; (b) Scanning and feedback system; (c) Optical Detection system and (d) Optics. The illumination source is a laser beam typically coupled to the scanning probe for near field imaging. The scanning and feedback system enables control of the sample position, keeping it at a constant distance from the probe. The optical detection consists of a photodiode that transforms the optical radiation into information that can be used for further analysis.

Probes used for NSOM typically have a conical shape to ensure coupling of the light to or from the aperture to the sample. Typical probes are fabricated by pulling optical fiber under heat or etching of the fiber tip. Other methods to create such probes have been developed by micromachining from silicon nitride or other materials. Once these probes have been developed they are typically coated with metals such as aluminum (Al) or silver (Ag) or gold (Au) using vapor deposition. Apertures at the tip of these probes are created by focused ion beam method. Typical probes created by such methods have aperture size on the order of 50-200 nm. These probes have transmission efficiencies on the order of 10^{-6}-10^{-9} depending on the wavelength used [135].

Typically an NSOM system can be operated with an aperture or a non-aperture mode. Apertured tips have many issues associated with the tips such as heating, artifacts, contrast, sensitivity, topology and interference amongst others. Conventional NSOM has a resolution that is directly related to the size of the probe used. NSOM have been used for a number of wide applications such as molecular feature characterization of organic

interfaces, polymers and optical recording for data storage devices. Conventional NSOM is a powerful tool for exploring nanoscale features in thin films. The major drawback with this system is the manual assembly process of the probe with an illuminating fiber that reduces its capability for large-scale applications. Also the requirement of an external light source for each probe increases the complexity. A number of techniques for miniaturizing the NSOM probes have been developed using MEMS based systems. Light absorbing gold particles, fluorescent beads, etc. have been attached to the scanning tips. The resolutions of these have been determined by the amount of light coupled to the tip. This requires an external laser source for excitation.

Creation of 'apertureless' small light sources will directly lead to resolution improvement. Secondly, the light source is built-in on tip and a compact system can be made without any external light sources [136]. Vertical-cavity surface-emitting lasers on the NSOM probes were reported to integrate a light source, but the light emitting areas were larger than several micrometers, and the probes still required a metal coating with an aperture to obtain the diffraction's limited resolution [137]. Integration of organic light emitting diodes on the scanning probe has also been reported recently, and the size of the light emitting diode (LED) was approximately 10 μm x 10 μm. This light source would be too large to work in near field applications.

We believe that creating a small light emitting diode with semiconductor quantum dots as the light emitter would improve the resolution of the near field imaging system. The resolution of the system is mainly defined by the size and position of the LED. Another advantage of using the QD-based light source is that multicolor emission can be observed by varying the QDs incorporated into the system. These near field imaging systems have potential applications in nano-drug distribution measurement in biomaterials [138].

In order to create an inorganic light emitting diode we initially fabricated them on flat silicon test substrates (Figure 6.1). The emission wavelength was tailored by a choice of quantum dots used. The creation of the light emitting diodes on the flat silicon substrate was then translated to silicon probes [9] that were fabricated using conventional silicon fabrication techniques [10].

Our experiments and efforts reveal that the multicolor colloidal quantum dot based light emitting diodes fabrication process is compatible with traditional CMOS processing in the semiconductor industry thus enabling integration with near field imaging or point of care detection systems while significantly reducing fabrication costs and barriers to market acceptance.

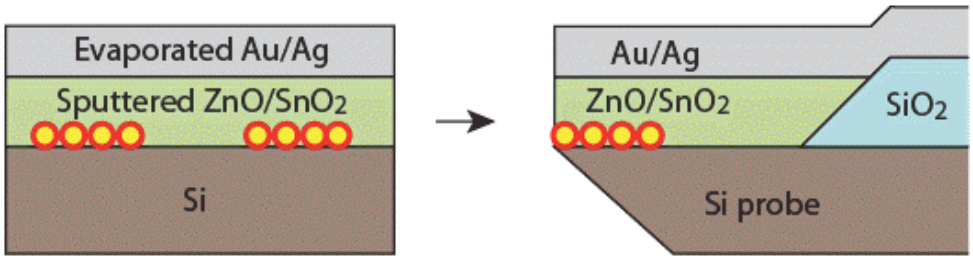

Figure 6.1: Translation of LED on flat substrate to 3D probe structure on silicon substrates.

6.3 Micro-contact Printing of QDs onto Silicon Probe Tips

QD-LEDs also offer great promise for fluorescence measurements. In particular, it is an excellent choice as the light source for scanning microscopy, due to the sub-10 nm dimensions that has been already utilized in several labeling applications. In previous

efforts, we reported on fabrication of patterned QD-LEDs on flat silicon substrates through a microcontact printing technique, which is highly advantageous because of the compatibility with well-studied silicon based MEMS. In this chapter, we extended the technique to create an electrically pumped excitation source at the tip of a silicon microprobe for near-field optical microscopy (NSOM).

The fluorophore is a colloidal CdSe: ZnS QDs stamped on the tip. Firstly, a monolayer of the QD film is formed by a modified Langmuir-Schaefer technique and transferred on a PDMS stamp [19]. The film is then picked up on the scanning probe tip by compressing the stamp.

The microcontact printing method can be controlled such that controlled deposition of the particles onto the probe tip is possible. Control of the QD thickness is essential in creating efficient LEDs. With the guidance of the fluorescence microscopic observation, a desirable portion of the QD film can be transferred to the probe. The thickness of the transferred film is measured by using the void QD pattern that remains on the PDMS after stamping (Figure 6.2 (c), (d) and (f)). The measurement in Figure 6.2 (g) shows the film thickness to be 10-20 nm, which corresponds to 1-2 monolayers of QDs (diameter: 9.0 nm). The thickness is comparable with our previous QD-LEDs fabrication demonstrated on flat silicon substrates. Electroluminescence is observed from the active area of the tip (Figure 6.2(e)) fabricated as described in the following section.

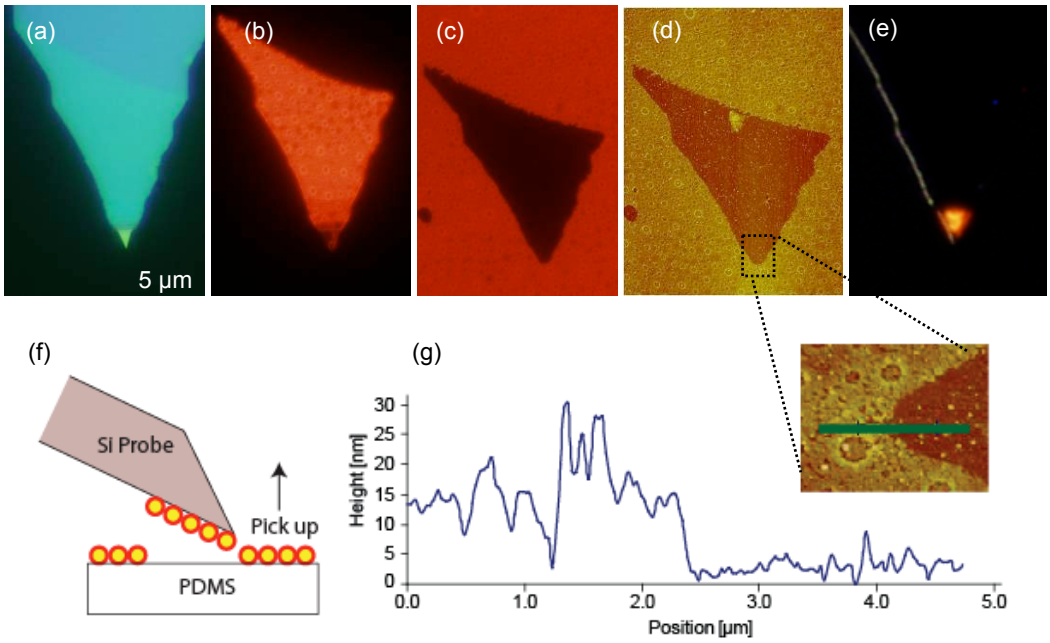

Figure 6.2: Quantum dot stamping on the probe tip. (a) Bright field image of the silicon probe. (b) Photoluminescence image of the probe stamped with QDs. (c) Photoluminescence "void" pattern of the PDMS stamp after the film is picked up by the probe. (d) AFM image of the void pattern. (e) Electroluminescence from the probe tip. (f) Illustration showing the stamping process (g) AFM profile of the QD void pattern showing the film thickness. The embedded picture shows the scan line, taken from the tip part of the AFM image (d)[6].

6.4 Multicolor Light Emitting Sources on Silicon Probes

The previously described stamping technique is performed during the fabrication steps of our QD-LED, which is created at the tip of microprobe. Chemical wet-etching of a single-crystal silicon wafer is used to form the probe body, which is doped with phosphorous ions to be utilized as a charge transporting substrate. The probe was made of a Silicon-on-Insulator (SOI) wafer with a 2 µm thick device layer, which was doped by

phosphorous oxychloride. First, the electrode pattern, as well as the probe body, were created through wet etching (Figure 6.3).

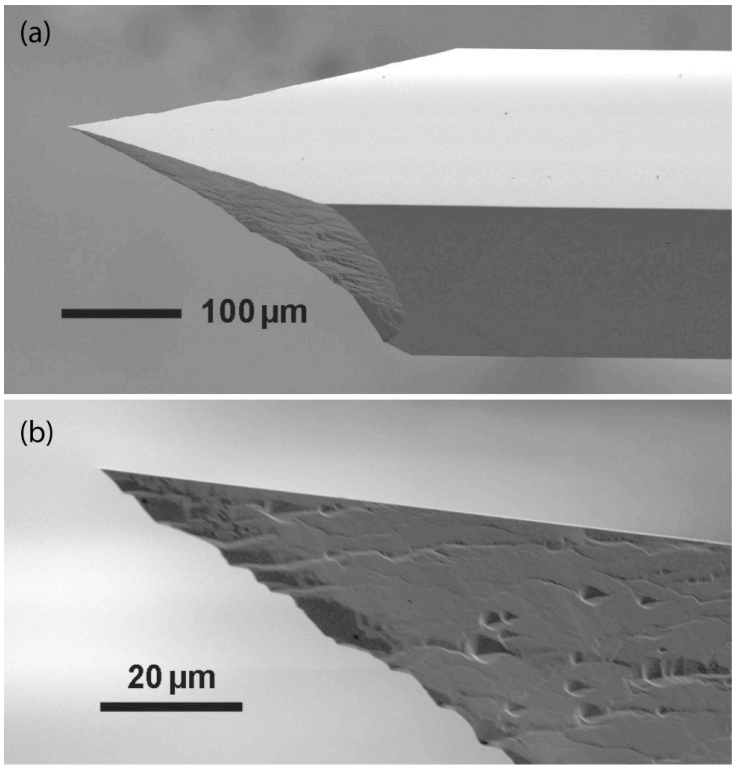

Figure 6.3: Chemically wet etched silicon probe tips.

The LED consists of multi-layers of inorganic materials [5]. The detailed structure, as shown in Figure 6.4, consists of Al (thickness: 15 nm) as the cathode, ZnO: SnO_2 (ratio 1:3, 40 nm) as the electron transporting layer, CdSe:ZnS QDs as the light emission layer, NiO (20 nm) as the hole transporting layer and Pt (20 nm) as the cathode. After the QD layer is stamped on the focused ion beam (FIB) patterned hole-transporting layers, the electron-transporting layer and the top cathode is deposited. The emission is

observed through the top metal cathode, similar to a top emitting organic light emitting diode (TEOLED).

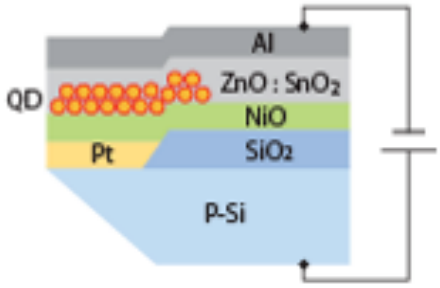

Figure 6.4: Schematic of LED created on silicon probe tips.

Figure 6.5 shows the electroluminescence observed from QD-LED probes with different emission wavelengths, ranging from 580 nm to 600 nm. Measured electroluminescence spectra from the QD-LED probes are shown in Figure 6.6(a). Figure 6.6(b) shows an example of the relationship between the current-voltage (I-V). Driving voltages of 5-10 V are applied and the current was measured to be typically lower than 10 μA.

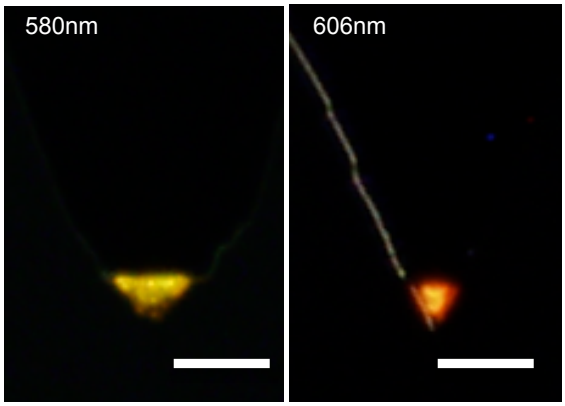

Figure 6.5: Electroluminescence (EL) from QD-LED probe tip. Emission wavelengths peak ranged from 580 nm to 620 nm. Scale bars = 50 μm.

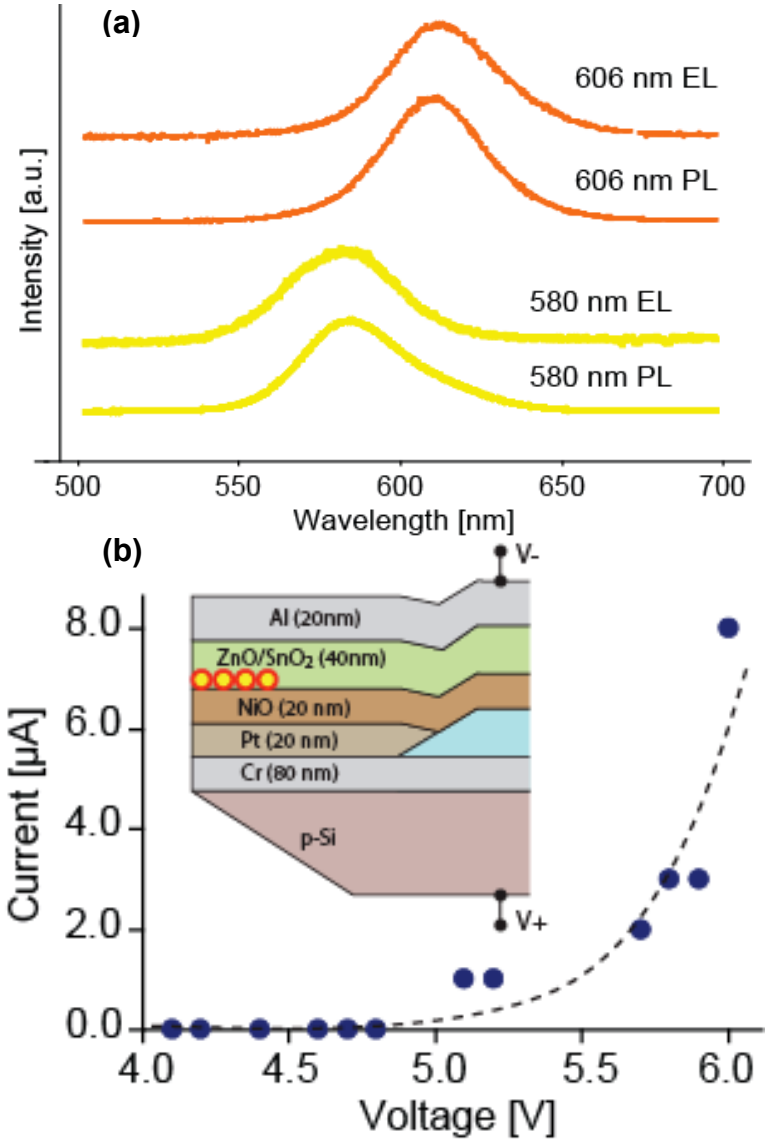

Figure 6.6: Characteristics of the on-probe QD-LEDs. (a) EL spectra measured from QD-LEDs at probe tips. (b) Typical current-voltage (I-V).

The probes were tested in a standard NSOM setup (Veeco Aurora) shown in Figure 6.7. The silicon probe was attached to a quartz tuning fork as introduced by [139]

and controlled in shear-force feedback to perform simultaneous topographic and optical imaging (Figure 6.7).

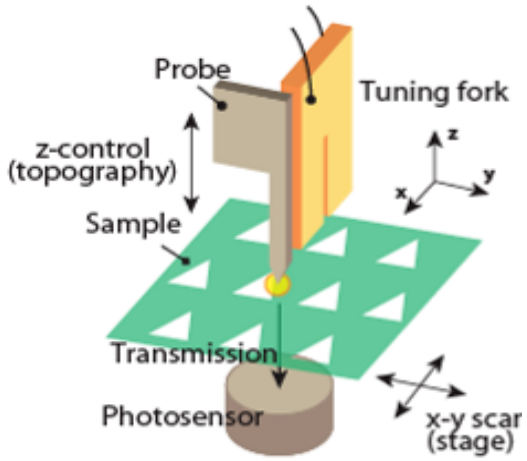

Figure 6.7: Nano-LED mounted on an NSOM setup.

The NSOM probe is attached to a tuning fork and oscillated by a peizo-actuator at resonant frequency. As the probe approaches the sample surface, a drag force acting on the tip damps the oscillation. This signal is used as the feedback signal for tip sample distance control. Optical excitation for near field would be provided by the nano-LED created on the tip. A microscope objective located below the sample would be used to collect the light that is subsequently imaged into a photon counting detector. When the probe scans the sample surface simultaneous optical and topographic measurements can be made. The sample is an approximately 1μm-thick pattern of CdTe:ZnS core:shell QDs with the emission peak at 800 nm (QD 800). The pattern is prepared on a transparent glass cover slip using a microcontact printing technique. The QD-LED 600 scanning light source is fixed in the focal point of the 60x objective, and the QD 800 sample is displaced

by the XYZ piezoelectric scanning stage. Energy transfer between QDs has been drawing attention for several applications. Chemical sensing with nano-scale spatial resolution, creation of broad band emitting light sources, quantum logic devices, etc are among the potential applications to utilize such energy transfer. Our method could lead to future single particle based optical measurement. The electrically pumped QD light source paves a way for highly controlled direct excitation and observation based on the colloidal QD labeling.

6.5 ON CHIP INTEGRATED SPECTROMETER

In this chapter we also introduce the integration of multicolor light sources on silicon as a multispectral source for bio-detection. Multicolor sources created by site-controlled patterning of light emitting diodes on silicon overcome the use of filter cubes or laser sources that are typically used in microscopes. Multiple light sources are suitable for easy to use on site diagnostic tools.

Integrated systems using light emitting diodes for biomedical applications have been demonstrated previously by incorporating organic light emitting diodes (OLEDs)[31, 35, 36]. OLEDs are placed on the rear side of the glass substrate and a microfluidic channel made out of polydimethylsiloxane (PDMS) on the front side. The emission wavelength of the OLED is 520 nm and has a relatively wide peak of 70 nm. Visual inspection of excitation of fluorescent dye Rhodamine B was demonstrated [37].

OLEDs with a 0.3 mm-thick interference filter combined with a 400 μm pinhole to achieve effective excitation with the appropriate wavelength have also been used [35]. Detection of the emission light was achieved by an optical fiber coupled to a PMT, giving

a detection limit of 3 μM for the Alexa 532 fluorescent dye. The current drawbacks of OLEDs are due to low irradiance and light purity. The OLEDs typically require an additional excitation filter that would enable excitation from a narrow bandwidth light source. The emission full width half maximum (FWHM) of OLEDs is typically broad. These devices have to have special enclosures to make sure there is no contact with oxygen or moisture since the devices are susceptible to damage under these circumstances. An integrated lab-on-a-chip would have impact in many areas including: (1) diagnostics, (2) environmental and (3) biomedical research by reducing costs for expensive projects such as genomics or proteomics measurements.

However, despite advances in the field, the use of such OLED based sensors, in particular for monitoring multiple analytes or biosamples, is limited due to issues such as elaborate fabrication, cost, portability and the need for trained operators. The emissions from OLED sources have broad emission compared to QD-LED sources. Also these sources require additional emission filters to acquire the exact excitation wavelength.

We have developed quantum dot based LEDs that are planar and easy to integrate to on-chip systems compared to commercial systems. The light emitting area in these diodes can be defined by a combination of (a) micro-contact printing (b) post processing the cathode of the device. These diodes were then post processed to define the cathode thereby defining multicolor sources on a single substrate. Multicolor LEDs on a single substrate offer a unique capability to excite cells with individual excitation sources in a single substrate for on-chip multicolor imaging. The size of the diode can be controlled depending on the kind of imaging requirement. Sizes of the light-emitting source can be varied to the size of the individual cell that we plan on imaging.

In order to show the excitation capability of the device we integrated the QD-LEDs with two cancer cells lines. Excitation from multiple light sources allowed us to determine the nucleus-to-cytoplasm ratio, the key characteristics to determine the properties of cancer cells.

6.6 QD-LEDs Integrated with Biosamples

A schematic of well-confined localized electroluminescence for multicolor illumination of cancer cells on a single chip is given in Figure 6.8. The stained cancer cell sample is placed over the multicolor QD-LED source and observed using a microscope to image the cells under different excitation wavelength. In this setup we observed that the absorption of different parts of the cells varied with the excitation wavelength that was used in the system. We have imaged MDA 435 and PC 3 cancer cell samples excited by the quantum dot based inorganic light emitting diodes on silicon to demonstrate the capabilities of the device created.

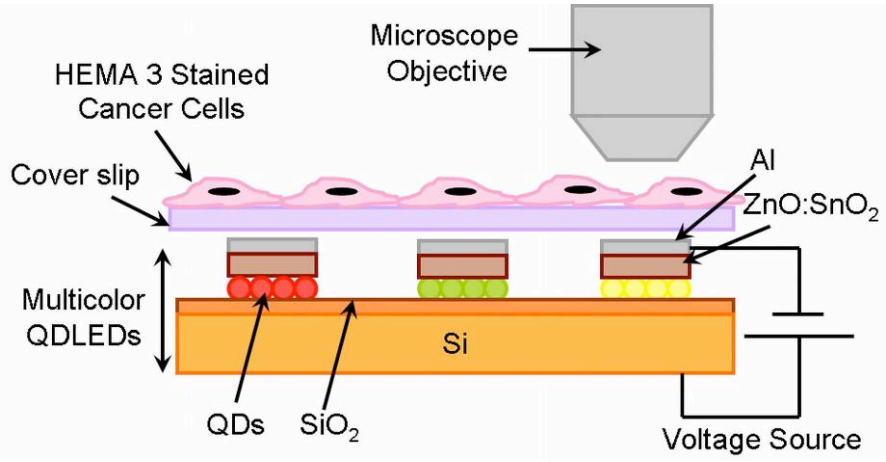

Figure 6.8: Schematic of integrated bio-imaging system.

6.6.1 Cancer Samples

(a) MDA 435 Cell Lines

MDA 435 cell line was derived in 1970 from a female patient with breast cancer [140], and has been shown to be highly metastatic in mice [141, 142]. This cell line has been used for a large number of studies in biology and biomedical applications of breast cancer [143]. Globally, breast cancer is the most common cause of death by cancer in women, accounting for 16% of cancer mortalities. The importance of early detection by screening enables studying the dependence of survival rates on the stage at which the disease was diagnosed. We use MDA 435 as the primary cancer cell line to observe the absorption at different wavelengths when stained with HEMA 3 dye. MDA 435 cells were from MD Anderson and cultured using standard procedure discussed in literature [41, 144]. The MDA 435 cell line was maintained in DMEM/F12 cell culture medium containing 5% fetal bovine serum. Coverslips were cleaned and placed in the Petri dish for cell culture. These cells are then stained using HEMA 3 to stain the nucleus and cytoplasm. A white light illumination image of the stained sample is shown in Figure 6.9.

(a) PC 3 Cell lines

PC 3 is a prostate cancer cell line that is derived from advanced bone metastasized prostate cancer [42]. This human prostate cancer cell line was maintained in standard culture conditions (RPMI/10% fetal bovine serum at 37°C). An image of the cultured cell is shown in Figure 6.9.

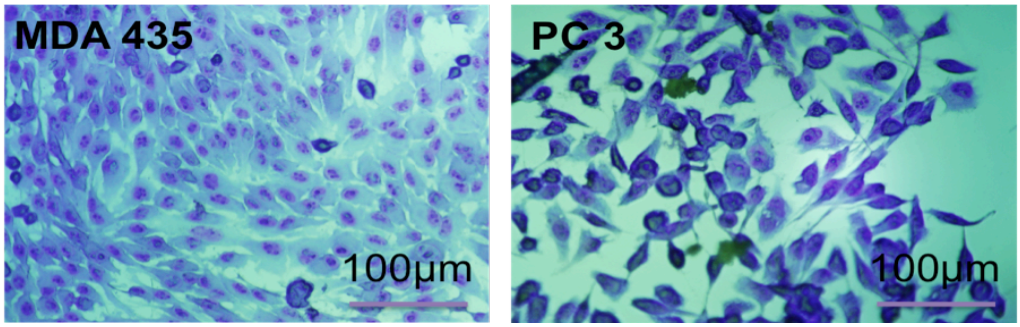

Figure 6.9: Cultured and stained. (Left) MDA 235. (Right) PC 3 cells on glass slides.

(b) HEMA 3 Stain

HEMA 3 stain is a modified quick Wright-Giemsa staining method [145]. The staining process takes 30 seconds and the samples are air-dried. Typical cell samples would be on glass slides that are dipped in solution 1, which is the fixative for 5 seconds and then dipped into solution 2 and solution 3 for 5 seconds each that stain the various portions of the cell. Fixative (Solution 1) used for fixing the cells is methanol. Solution 2 is a mixture of sodium azide, potassium phosphate monobasic, podium phosphate dibasic, eosin Y and water that stains the cytoplasm and collagen part of the cell. Solution 3 is a combination of azure A, sodium azide, potassium phosphate monobasic, sodium phosphate dibasic, methylene blue and water that stains the nucleus of the cell. The absorption and transmission of the dye was observed using UV-Visible spectrum measurement system. It was observed that the stain absorbs at wavelength 560 nm (Figure 6.10).

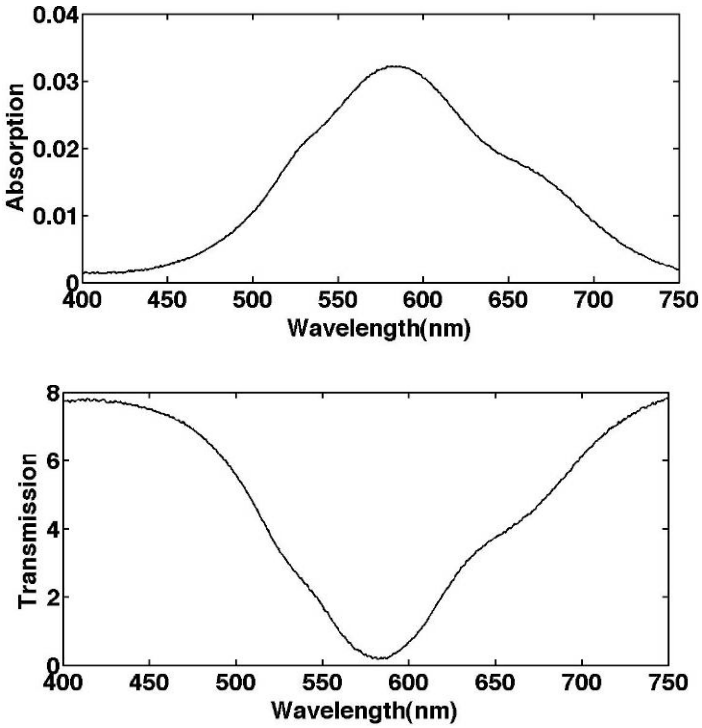

Figure 6.10: HEMA 3 stains. (a) Absorption measurement. (b) Transmission measurement.

6.6.2 Excitation of Cells

The cultured cancer cells were integrated as shown in the schematic in Figure 6.8. Excitation from patterned QD-LED light source with feature size 100 μm is given in Figure 6.11. An arrayed pattern of QD-LED with emission wavelength 580 nm excited the stained slides placed near the substrate. The excitation voltage for diode with emission wavelength 580 nm was 7 V at a current 6 mA. This indicates that we were able to observe the cells under the excitation from QD-LED source. The cells that were cultured on cover slips were placed very close to the QD-LED surface. The distance between the sample and the diode was maintained within 100 μm. Figure 6.11 indicates the diode with and without the cultured cell line on top of the diode.

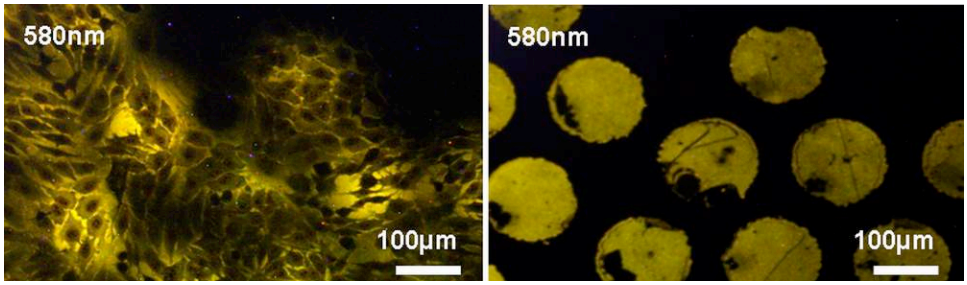

Figure 6.11: Excitation of MDA 435 using multicolor colloidal quantum dot based LED. (a) Transmission observed from the MDA 435. (b) Electroluminescence from QD-LED observed.

Patterned substrates give the flexibility to image a single cell under different excitation wavelength. The size of the individual patterned QD-LED source can be fabricated to be on the order of a single cell (10μm). In order to obtain a better understanding of the absorption characteristics of the QD-LED via cancer cells, we integrated the cells with a larger sized LED. The sizes of the LEDs were 1 mm x 1 mm. Emission wavelengths 560 nm, 580 nm and 600 nm were used as excitation sources for imaging cells. The electroluminescence spectrums of three excitation sources are plotted in a single graph. On excitation with different light sources, we observed that the nucleus absorbs at 560 nm (QD-LED excitation) and passes 600 nm (QD-LED excitation). The results are very similar to the data obtained for the absorption of light emission from the dye in Figure 6.10. Different portions of the cell absorbed at different wavelengths. Images of excitation from different light sources (560 nm, 580 nm) with feature size 100 μm are given in Figure 6.12. The cells in the bottom row of Figure 6.12 were excited by larger LED sources 1 mm x 1 mm.

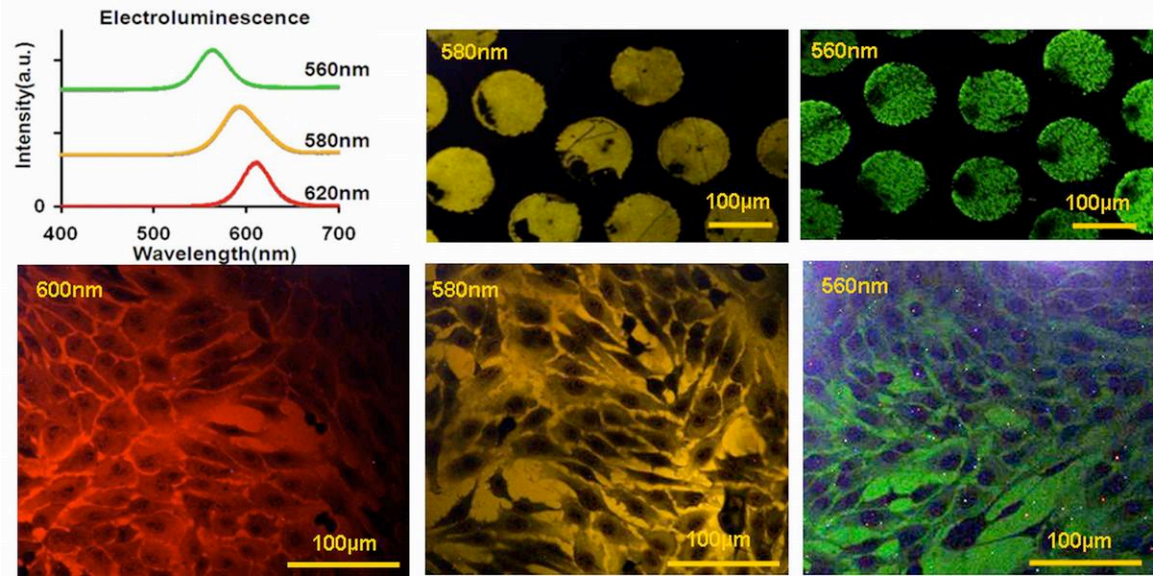

Figure 6.12: (a) Electroluminescence spectrum of individual excitation sources. (b) QD-LED with emission wavelength 580 nm. (c) 560 nm (d-f) MDA 435 cancer cells excited by QD-LED.

The QD-LED was used to excite a number of different cell lines. Cell lines MDA 231 and PC 3 were excited using QD-LED excitation sources, as indicated in Figure 6.13. PC 3 is a prostate cancer cell line that is derived from advanced bone metastasized prostate cancer. These cell lines were stained using HEMA 3 stain solution.

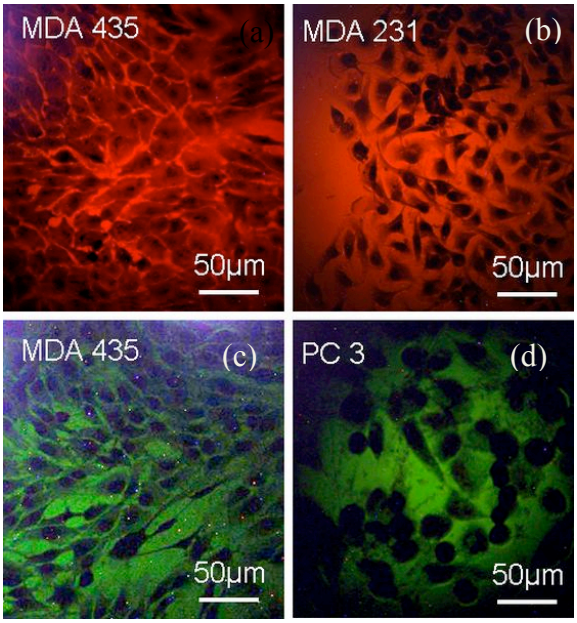

Figure 6.13: QD-LED excitation of (a,c) MDA 435 (b) MDA 231 (d) PC3

HEMA 3 stain is a modified quick Wright-Giemsa staining method. This dye contains Eosin Y that stains the cytoplasm of the cell and Methylene Blue that stains the nucleus. The transmission via HEMA 3 and the excitation from the QD-LEDs is shown in Figure 6.14.

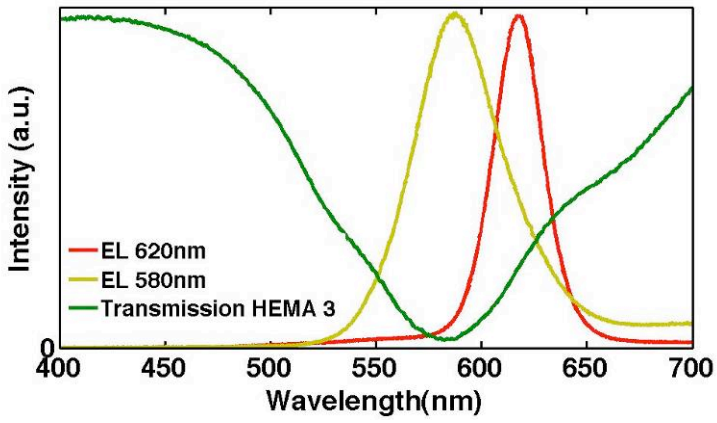

Figure 6.14: Measured transmission of the dye along with the electroluminescence from QD-LED (a) 620 nm and (b) 580 nm.

Excitation of the similar area of the exact glass slide would enable better understanding of the inside of the cells. An example of excitation of similar regions of the cells is indicated in Figure 6.15. The cells excited in this image are MDA 435 breast cancer cell lines. From Figure 6.15 it was observed that the nucleus absorbs excitation wavelength 560 nm. The cytoplasm transmits the green color excitation to pass through the cell. Excitation from multiple light sources allows us to determine the nucleus-to-cytoplasm ratio. Nucleus of cancer cells tends to absorb at 560/580 nm excitation. Excitation with 600/620 nm helps observe the cytoplasm and the inside of the nucleus without absorption. This allows us to distinguish the cancer cells more clearly.

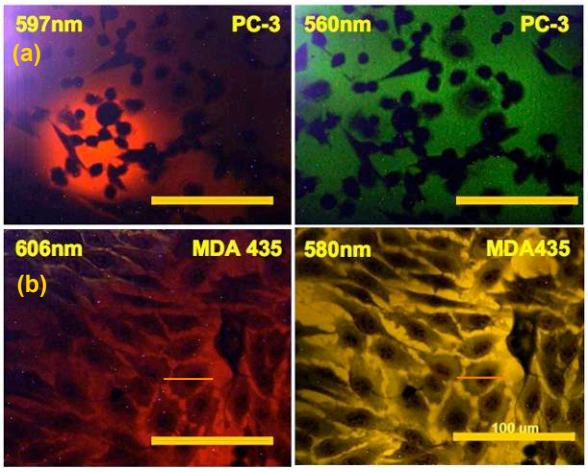

Figure 6.15: Excitation of the exact same region using two excitation sources. (a) PC 3 cells. (b) MDA 435 cells (Scale 100 μm) [Orange line indicates intensity variation].

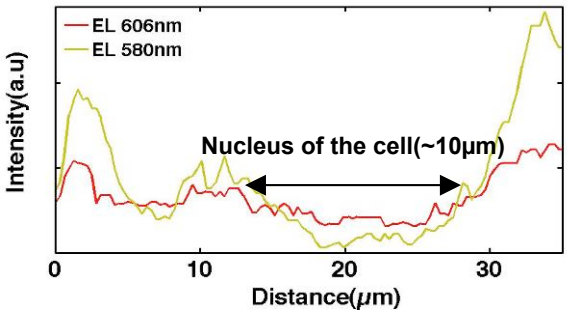

Figure 6.16: Intensity variation in a single cell excited by two-excitation source (a) 580 nm (b) 606 nm (MDA 435 cells).

MDA 435 and PC 3 were further excited, each at two wavelengths: 580 nm and 600 nm (Figure 6.16). Figure 6.16 shows the comparison of the intensity variation between a single MDA 435 cells on excitation from two sources. The nucleus absorbed 580 nm excitation source indicating decrease of intensity at the nucleus compared to 600 nm. For PC 3 cells it was observed that the size of the nucleus and cytoplasm was the same on excitation from two different light sources. MDA 435 cells have a smaller nucleus compared to the cytoplasm and cell division is observed distinctly inside the nucleus on excitation from 600 nm. The measured nucleus-to-cytoplasm ratio indicates the developmental stage of the cancer cells**.** This technology opens up exciting opportunities for on-chip fluorescence based tumor cell identification for early cancer detection. We were able to estimate the nucleus to cytoplasm ratio of MDA 435 to be 0.001 and that of PC 3 cells to be 0.66.

The QD-LED excitations were compared with commercial LEDs available in the market. A single cell was excited with QD-LEDs with three different emission wavelengths 560 nm, 580 nm and 600 nm. The same cell was excited with commercial LEDs with red and green excitation. It was observed that the nucleus of the cell absorbed significantly with green excitation compared to the red excitation. A comparison of the two-excitation sources is given in Figure 6.17.

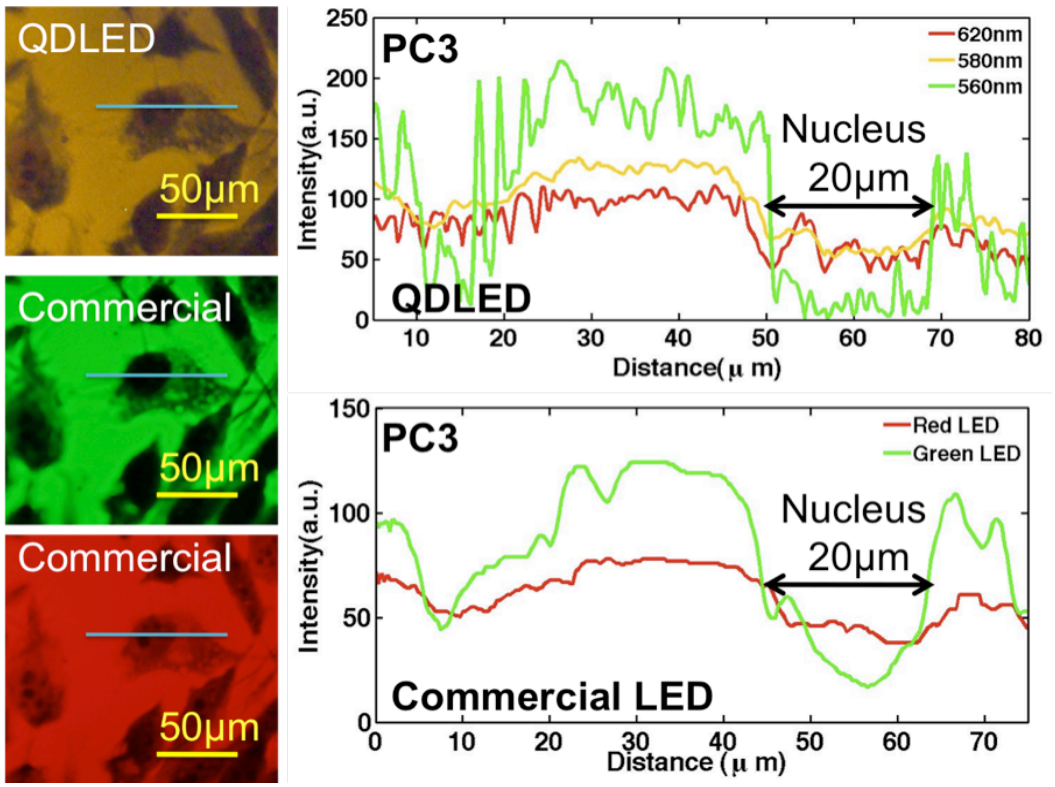

Figure 6.17: Intensity variation in a single PC 3 cell excited by (a) QD-LED on silicon and (b) Commercial LED.

6.7 SUMMARY

In this chapter we discussed the application of QD-LEDs in two different fields of imaging. We directly fabricated quantum-dot based inorganic light emitting diodes on scanning microprobe tip. The deposition of quantum dot monolayer was performed using microcontact printing via PDMS. We have shown that the number of stamped QDs can be controlled as small as a single molecular order. Multicolor light emission was observed on the probe tips indicating the translation of the technology from flat substrate to three-dimensional substrate. The tunable dimension and emission wavelengths of the QD-LEDs open up the possibilities of highly integrated nanophotonic imaging probes for

the new generation of near-field scanning optical microscopy. This scanning capability has potential applications in a number of biomedical applications.

In this chapter we also describe the application capability of the integrating light-emitting source that we have created with biological samples as potential spectroscopy sources. We have imaged MDA 435/PC 3 cancer cell samples excited by the quantum dot based inorganic light emitting diodes on silicon to demonstrate the capabilities of the device created. It was observed that the nucleus absorbs excitation wavelength 560 nm and passes through other excitation wavelength through the cells. A patterning technique enables site-controlled patterning and controlled feature size of light emitting area with greater accuracy. We utilize a stamping technique for patterning colloidal QDs with well-defined geometry. It is possible to accurately define multicolor light sources on a single substrate, which open up the possibilities for creating microsystems for imaging and sensing cancer cell lines.

CHAPTER 7: CONCLUSIONS AND FUTURE WORK

Conclusions:

In this thesis we have demonstrated the novel capability to create inorganic light emitting diodes with silicon as a charge injector and patterned quantum dots as light emitters in QD-LEDs. Controlled patterning of light emitting diodes is important in applications such as high-resolution arrays, large screen displays, micro-electro-mechanical systems, optoelectronic systems, and multicolor excitation source in micro-total analysis systems.

We demonstrated a technique of creating inorganic quantum-based patterned light emitting devices at room temperature on silicon substrate, through microcontact printing. Self-assembly and microcontact printing techniques were used to deposit quantum dots onto silicon substrate. The film was self assembled onto water surface by dispensing a hydrophobic colloidal suspension of CdSe: ZnS, a solvent of 1,2-dichloroethane and hexane. The uniform thin film was then picked up by hydrophobic polydimethylsiloxane stamps with nano-scale features and deposited onto the silicon substrate. The electron transport layer was co-sputtered ZnO and SnO_2 onto the quantum dots. The structure was completed by e-beam evaporating thin aluminum cathode onto ZnO: SnO_2. We were able to observe multicolor light emission on application of voltage across the device. On application of positive voltage to the p-silicon and negative bias to the aluminum cathode, electroluminescence (EL) was observed.

We also demonstrate the photolithographic patterning capability of metal cathode for top emitting quantum dot based inorganic light emitting diodes on silicon substrates. Since the device consists of clean-room compatible inorganic material such as metals, silicon and silicon/metal oxides, standard microfabrication processes can be applied. Lithographic patterning technique enables site-controlled patterning and controlled feature size of the electrode with greater accuracy. The feature size of 5 μm was achieved using UV photolithography and reactive ion etching. The stability of inorganic silicon materials and metal oxide based diode structure offers excellent advantages to the device, with no significant damage observed during the patterning and etching steps. The ease of fabrication and processing a long life, multicolor QD-LED opens up the possibilities for creating nanophotonic microsystems that are robust and compact for tunable imaging, sensing, MEMS based CMOS devices and micro-total analysis systems.

Efficient electrical excitation of QDs was first tested on flat silicon test substrates by two methods described above: (a) Micro-contact printing of quantum dots and (b) photolithographic patterning of the cathode to define the light-emitting regime of the diode. The technique was translated to create localized QD-based light sources on arbitrary three-dimensional structures as well. These LEDs acted as nano-light emitting diodes for near filed scanning optical microscopy. The light source size was controlled by a combination of focused ion beam (FIB) milling and stamping control of QDs transferred to the probe tip.

The dissertation also presents imaging results from cultured cancer cells that can be translated towards other types of cancer cells. The QD-LEDs were used as excitation sources under stained cancer cells. The absorption of different portions of the cells on excitation with different excitation wavelength was observed. This allowed us to distinguish different parts of the cancer cells.

We have developed and demonstrated the translation of photonics MEMS based system towards two platforms: (a) Near field imaging and (b) On chip spectroscopy. The technology developed has other potential applications, such as imaging circulating tumor cells in microfluidic systems, creating an integrated immuno sensor system and using QD-LEDs as potential chemical sensors and solar cells (Figure 7.1).

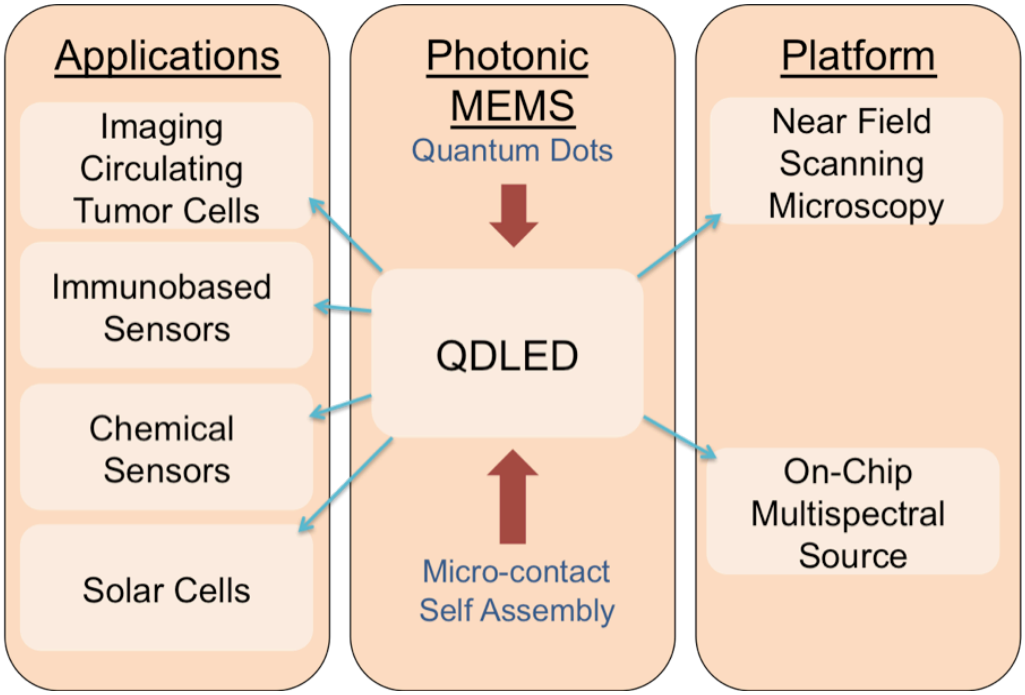

Figure 7.1: Towards translation research.

Future Work:

7.1 Point of Care systems in Biomedical Imaging

The experimental results of this dissertation provide several key insights into the future directions that this research can move forward. The multicolor light source on a single chip proposed can be used for further research in three different ways. First the device can be used in a modified hyperspectral-imaging source to image circulating tumor cells that are captured using microfluidic systems. Multicolor light sources driven by CMOS circuitry can be incorporated in future. Further modifications to the system would include an emission filter and a photodetector on the same system to improve the handheld portable capability for point of care diagnosis.

7.2 Near Field Imaging Systems as Optical Sensors

Secondly the devices that have been translated to nano-light emitting diodes for NSOM measurement can be used as fluorescence resonance energy transfer systems to image protein interactions. Fluorescence measurement at nanoscale can also enable better understanding of the transport phenomena of the ion through the cells as well as inherent properties of the cells within.

7.3 Energy

Third these devices exhibit photovoltaic capabilities and could be used for solar cell applications. Modifying the metal layers could potentially enable better trapping of solar energy. The quantum dot layers have been proved to enhanced capture of solar energy and improve the efficiency of the system.

References

[1] K. D. Hirschman, L. Tsybeskov, S. P. Duttagupta, and P. M. Fauchet, "Silicon-based visible light-emitting devices integrated into microelectronic circuits," 1996.

[2] Y. Huang, X. Duan, and C. M. Lieber, "Nanowires for integrated multicolor nanophotonics," *Small*, vol. 1, pp. 142-147, 2005.

[3] H. Rong, A. Liu, R. Jones, O. Cohen, D. Hak, R. Nicolaescu, A. Fang, and M. Paniccia, "An all-silicon Raman laser," *Nature*, vol. 433, pp. 292-294, 2005.

[4] P. LeMinh, J. Holleman, H. Wallinga, J. W. Berenschot, N. R. Tas, and A. Berg, "Novel integration of a microchannel with a silicon light emitting diode antifuse," *Journal of Micromechanics and Microengineering*, vol. 13, p. 425, 2003.

[5] P. LeMinh and J. Holleman, "Silicon light-emitting diode antifuse: properties and devices," *Journal of Physics D: Applied Physics*, vol. 39, p. 3749, 2006.

[6] K. Hoshino, A. Gopal, and J. X. Zhang, "Contact printing of quantum dot light emitting diode on silicon probe tip," presented at CLEO, 2010.

[7] K. Hoshino, A. Gopal, and X. Zhang, "Near-field scanning nanophotonic microscopy—breaking the diffraction limit using integrated nano light-emitting probe tip," *IEEE Journal of Selected Topics in Quantum Electronics*, vol. 15, p. 1393, 2009.

[8] K. Hoshino, L. J. Rozanski, D. A. V. Bout, and X. Zhang, "Near-field scanning optical microscopy with monolithic silicon light emitting diode on probe tip," *Applied Physics Letters*, vol. 92, p. 131106, 2008.

[9] K. Hoshino, D. A. V. Bout, and X. J. Zhang, "Direct fabrication of nanoscale light emitting diode on silicon probe tip for scanning microscopy," *Journal of Microelectromechanical Systems*, vol. 17, pp. 4-10, 2008.

[10] K. Hoshino, A. Gopal, D. A. V. Bout, and X. Zhang, "Near-field scanning optical imaging with monolithic silicon light emitting diode on probe tip," presented at 8th IEEE Conference on Nanotechnology (IEEE NANO 2008), Arlington, TX, 2008.

[11] T. Dekorsy, J. M. Sun, W. Skorupa, B. Schmidt, and M. Helm, "Light-emitting silicon pn diodes," *Applied Physics A: Materials Science & Processing*, vol. 78, pp. 471-475, 2004.

[12] M. R. Krames, O. B. Shchekin, R. Mueller-Mach, G. O. Mueller, L. Zhou, G. Harbers, and M. G. Craford, "Status and future of high-power light-emitting diodes for solid-state lighting," *Journal of Display Technology*, vol. 3, pp. 160-175, 2007.

[13] Z. H. Lu, D. J. Lockwood, and J. M. Baribeau, "Quantum confinement and light emission in SiO_2/Si superlattices," *Nature*, vol. 378, pp. 258-260, 1995.

[14] N. Lalic and J. Linnros, "Light emitting diode structure based on Si nanocrystals formed by implantation into thermal oxide," *Journal of Luminescence*, vol. 80, pp. 263-267, 1998.

[15] P. O. Anikeeva, J. E. Halpert, M. G. Bawendi, and V. Bulovi, "Electroluminescence from a mixed red- green- blue colloidal quantum dot monolayer," *Nano Letters*, vol. 7, pp. 2196-2200, 2007.

[16] V. L. Colvin, M. C. Schlamp, and A. P. Alivisatos, "Light-emitting diodes made from cadmium selenide nanocrystals and a semiconducting polymer," *Nature*, vol. 370, pp. 354-357, 1994.
[17] K. Ray, R. Badugu, and J. R. Lakowicz, "Metal-enhanced fluorescence from CdTe nanocrystals: a single-molecule fluorescence study," *Journal of the American Chemical Society*, vol. 128, pp. 8998-8999, 2006.
[18] L. A. Kim, P. O. Anikeeva, S. A. Coe-Sullivan, J. S. Steckel, M. G. Bawendi, and V. Bulovic, "Contact printing of quantum dot light-emitting devices," *Nano Letters*, vol. 8, pp. 4513-4517, 2008.
[19] A. Gopal, K. Hoshino, S. Kim, and X. Zhang, "Multi-color colloidal quantum dot based light emitting diodes micropatterned on silicon hole transporting layers," *Nanotechnology*, vol. 20, p. 235201, 2009.
[20] A. Gopal, K. Hoshino, and X. Zhang, "Photolithographic patterning of subwavelength top emitting colloidal quantum dot based inorganic light emitting diodes on silicon," *Applied Physics Letters*, vol. 96, p. 131109, 2010.
[21] P. Fenter, F. Schreiber, V. Bulovic, and S. R. Forrest, "Thermally induced failure mechanisms of organic light emitting device structures probed by X-ray specular reflectivity," *Chemical Physics Letters*, vol. 277, pp. 521-526, 1997.
[22] R. A. M. Hikmet, P. T. K. Chin, D. V. Talapin, and H. Weller, "Polarized-light-emitting quantum-rod diodes," *Advanced Materials*, vol. 17, pp. 1436-1439, 2005.
[23] J. M. Caruge, J. E. Halpert, V. Wood, V. Bulovic, and M. G. Bawendi, "Colloidal quantum-dot light-emitting diodes with metal-oxide charge transport layers," *Nature*, vol. 4, pp. 4-6, 2008.
[24] X. Jiang, F. L. Wong, M. K. Fung, and S. T. Lee, "Aluminum-doped zinc oxide films as transparent conductive electrode for organic light-emitting devices," *Applied Physics Letters*, vol. 83, p. 1875, 2003.
[25] S. T. Lee, Z. Q. Gao, and L. S. Hung, "Metal diffusion from electrodes in organic light-emitting diodes," *Applied Physics Letters*, vol. 75, p. 1404, 1999.
[26] B. Hecht, B. Sick, U. P. Wild, V. Deckert, R. Zenobi, O. J. F. Martin, and D. W. Pohl, "Scanning near-field optical microscopy with aperture probes: Fundamentals and applications," *The Journal of Chemical Physics*, vol. 112, p. 7761, 2000.
[27] P. F. Barbara, D. M. Adams, and D. B. O'Connor, "Characterization of organic thin film materials with near-field scanning optical microscopy (NSOM)," *Annual Review of Materials Science*, vol. 29, pp. 433-469, 1999.
[28] J. Teetsov and D. A. V. Bout, "Near-field scanning optical microscopy (NSOM) studies of nanoscale polymer ordering in pristine films of poly (9, 9-dialkylfluorene)," *Journal of Physical Chemistry B*, vol. 104, pp. 9378-9387, 2000.
[29] M. Sasaki, K. Tanaka, and K. Hane, "Cantilever probe integrated with light-emitting diode, waveguide, aperture, and photodiode for scanning near-field optical microscope," *Japanese Journal of Applied Physics*, vol. 39, pp. 7150-7153, 2000.
[30] T. Kalkbrenner, M. Ramstein, J. Mlynek, and V. Sandoghdar, "A single gold particle as a probe for apertureless scanning near-field optical microscopy," *Journal of Microscopy*, vol. 202, p. 72, 2001.

[31] K. S. Shin, Y. H. Kim, K. K. Paek, J. H. Park, E. G. Yang, T. S. Kim, J. Y. Kang, and B. K. Ju, "Characterization of an integrated fluorescence-detection hybrid device with photodiode and organic light-emitting diode," *IEEE Electron device letters*, vol. 27, pp. 746-748, 2006.
[32] S. Khalfallah, C. Gorecki, J. Podlecki, M. Nishioka, H. Kawakatsu, and Y. Arakawa, "Wet-etching fabrication of multilayer GaAlAs/GaAs microtips for scanning near-field optical microscopy," *Applied Physics A: Materials Science & Processing*, vol. 71, pp. 223-225, 2000.
[33] O. Hofmann, X. Wang, A. Cornwell, S. Beecher, A. Raja, D. D. C. Bradley, A. J. Demello, and J. C. Demello, "Monolithically integrated dye-doped PDMS long-pass filters for disposable on-chip fluorescence detection," *Lab on a Chip*, vol. 6, pp. 981-987, 2006.
[34] M. F. Garcia-Parajo, J. A. Veerman, S. J. T. Van Noort, B. G. De Grooth, J. Greve, and N. F. Van Hulst, "Near-field optical microscopy for DNA studies at the single molecular level," *Bioimaging*, vol. 6, pp. 43-53, 1998.
[35] B. Yao, G. Luo, L. Wang, Y. Gao, G. Lei, K. Ren, L. Chen, Y. Wang, Y. Hu, and Y. Qiu, "A microfluidic device using a green organic light emitting diode as an integrated excitation source," *Lab on a Chip*, vol. 5, pp. 1041-1047, 2005.
[36] V. Savvate'ev, Z. Chen-Esterlit, J. W. Aylott, B. Choudhury, C. H. Kim, L. Zou, J. H. Friedl, R. Shinar, J. Shinar, and R. Kopelman, "Integrated organic light-emitting device/fluorescence-based chemical sensors," *Applied Physics Letters*, vol. 81, p. 4652, 2002.
[37] S. Camou, M. Kitamura, G. Jean-Philippe, F. Hiroyuki, A. Yasuhiko, and F. Teruo, "Organic light emitting device as a fluorescence spectroscopy's light source : one step towards the lab-on-a-chip device," 2003.
[38] J. B. Edel, N. P. Beard, O. Hofmann, J. C. Demello, D. D. C. Bradley, and A. J. Demello, "Thin-film polymer light emitting diodes as integrated excitation sources for microscale capillary electrophoresis," *Lab on a Chip*, vol. 4, pp. 136-140, 2004.
[39] J. A. Chediak, Z. Luo, J. Seo, N. Cheung, L. P. Lee, and T. D. Sands, "Heterogeneous integration of CdS filters with GaN LEDs for fluorescence detection microsystems," *Sensors & Actuators: A. Physical*, vol. 111, pp. 1-7, 2004.
[40] K. Misiakos, P. S. Petrou, S. E. Kakabakos, H. H. Ruf, E. Ehrentreich-Förster, and F. F. Bier, "A bioanalytical microsystem for protein and DNA sensing based on a monolithic silicon optoelectronic transducer," presented at Journal of Physics, 2005.
[41] S. K. Khaldoyanidi, V. V. Glinsky, L. Sikora, A. B. Glinskii, V. V. Mossine, T. P. Quinn, G. V. Glinsky, and P. Sriramarao, "MDA-MB-435 human breast carcinoma cell homo-and heterotypic adhesion under flow conditions is mediated in part by Thomsen-Friedenreich antigen-galectin-3 interactions," *Journal of Biological Chemistry*, vol. 278, p. 4127, 2003.
[42] *http://en.wikipedia.org/wiki/PC3*.
[43] *http://en.wikipedia.org/wiki/Light-emitting_diode*.
[44] N. A. Sobolev, A. M. Emel'Yanov, E. I. Shek, and V. I. Vdovin, "Extended structural defects and their influence on the electroluminescence in efficient Si

light-emitting diodes," *Physica B: Condensed Matter*, vol. 340, pp. 1031-1035, 2003.
[45] M. Kittler, M. Reiche, T. Arguirov, W. Seifert, and X. Yu, "Silicon-based light emitters," *Physica Status Solidi (a)*, vol. 203, pp. 802-809, 2006.
[46] M. A. Green, J. Zhao, A. Wang, P. J. Reece, and M. Gal, "Efficient silicon light-emitting diodes," *Nature*, vol. 412, pp. 805-808, 2001.
[47] A. J. Kenyon, "Erbium in silicon," *Semiconductor Science and Technology*, vol. 20, p. R65, 2005.
[48] A. Halimaoui, C. Oules, G. Bomchil, A. Bsiesy, F. Gaspard, R. Herino, M. Ligeon, and F. Muller, "Electroluminescence in the visible range during anodic oxidation of porous silicon films," *Applied Physics Letters*, vol. 59, p. 304, 1991.
[49] A. Richter, P. Steiner, F. Kozlowski, and W. Lang, "Current-induced light emission from a porous silicon device," *IEEE Electron Device Letters*, vol. 12, p. 691, 1991.
[50] H. H. Kim, T. M. Miller, E. H. Westerwick, Y. O. Kim, E. W. Kwock, M. D. Morris, and M. Cerullo, "Silicon compatible organic light emitting diode," *Journal of Lightwave Technology*, vol. 12, pp. 2107-2113, 1994.
[51] http://en.wikipedia.org/wiki/OLEDs.
[52] W. Q. Zhao, G. Z. Ran, W. J. Xu, and G. G. Qin, "Passivated p-type silicon: Hole injection tunable anode material for organic light emission," *Applied Physics Letters*, vol. 92, p. 073303, 2008.
[53] G. L. Ma, G. Z. Ran, A. G. Xu, Y. H. Xu, Y. P. Qiao, W. X. Chen, L. Dai, and G. G. Qin, "Improving charge-injection balance and cathode transmittance of top-emitting organic light-emitting device with p-type silicon anode," *Applied Physics Letters*, vol. 87, p. 081106, 2005.
[54] G. Z. Ran, Y. H. Xu, G. L. Ma, A. G. Xu, Y. P. Qiao, W. X. Chen, and G. G. Qin, "Organic light-emitting diodes with n-type silicon anode," *Semiconductor Science and Technology*, vol. 20, p. 761, 2005.
[55] X. Zhou, J. He, L. S. Liao, M. Lu, Z. H. Xiong, X. M. Ding, X. Y. Hou, F. G. Tao, C. E. Zhou, and S. T. Lee, "Enhanced hole injection in a bilayer vacuum-deposited organic light-emitting device using a p-type doped silicon anode," *Applied Physics Letters*, vol. 74, p. 609, 1999.
[56] G. G. Qin, A. G. Xu, G. L. Ma, G. Z. Ran, Y. P. Qiao, B. R. Zhang, W. X. Chen, and S. K. Wu, "A top-emission organic light-emitting diode with a silicon anode and an Sm/ Au cathode," *Applied Physics Letters*, vol. 85, p. 5406, 2004.
[57] W. Q. Zhao, G. Z. Ran, W. J. Xu, and G. G. Qin, "Inverted top-emission organic light-emitting device with n-type silicon as cathode," *Journal of Physics D: Applied Physics*, vol. 41, p. 035106, 2008.
[58] Y. Z. Li, G. Z. Ran, W. Q. Zhao, and G. G. Qin, "Au generation centres doped n+-Si: hole-injection adjustable anode for efficient organic light emission," *Journal of Physics D: Applied Physics*, vol. 41, p. 155107, 2008.
[59] A. P. Alivisatos, "Semiconductor clusters, nanocrystals, and quantum dots," *Science*, vol. 271, p. 933, 1996.
[60] K. Hoshino, A. Gopal, D. Ostrowski, L. Rozanski, R. Patel, A. Heitsch, B. Korgel, D. VandenBout, and X. J. Zhang, "Single monolayer nanocrystal LED on probe tip for near-field molecular imaging and patterning," presented at

International Conference on Micro-electro-mechanical Systems (MEMS '08), Arizona, USA, 2008.
[61] D. Bimberg, M. Grundmann, and N. N. Ledentsov, *Quantum Dot Heterostructures*: Wiley, 1999.
[62] B. O. Dabbousi, J. Rodriguez-Viejo, F. V. Mikulec, J. R. Heine, H. Mattoussi, R. Ober, K. F. Jensen, and M. G. Bawendi, "(CdSe) ZnS core-shell quantum dots: synthesis and characterization of a size series of highly luminescent nanocrystallites," *Journal of Physical Chemistry B*, vol. 101, pp. 9463-9475, 1997.
[63] Q. Sun, Y. A. Wang, L. S. Li, D. Wang, T. Zhu, J. Xu, C. Yang, and Y. Li, "Bright, multicoloured light-emitting diodes based on quantum dots," *Nature Photonics*, vol. 1, pp. 717-722, 2007.
[64] W. K. W. Seth Coe and V. B. Moungi Bawendi, "Electroluminescence from single monolayers of nanocrystals in molecular organic devices," *Nature*, vol. 420, pp. 800-803, 2002.
[65] M. C. Schlamp, X. Peng, and A. P. Alivisatos, "Improved efficiencies in light emitting diodes made with CdSe (CdS) core/shell type nanocrystals and a semiconducting polymer," *Journal of Applied Physics*, vol. 82, p. 5837, 1997.
[66] A. H. Mueller, M. A. Petruska, M. Achermann, D. J. Werder, E. A. Akhadov, D. D. Koleske, M. A. Hoffbauer, and V. I. Klimov, "Multicolor light-emitting diodes based on semiconductor nanocrystals encapsulated in GaN charge injection layers," *Nano Letters*, vol. 5, pp. 1039-1044, 2005.
[67] B. O. Dabbousi, M. G. Bawendi, O. Onitsuka, and M. F. Rubner, "Electroluminescence from CdSe quantum dot/polymer composites," *Applied Physics Letters*, vol. 66, p. 1316, 1995.
[68] S. Chaudhary, M. Ozkan, and W. C. W. Chan, "Trilayer hybrid polymer-quantum dot light-emitting diodes," *Applied Physics Letters*, vol. 84, p. 2925, 2004.
[69] T. Zhu, K. Shanmugasundaram, S. C. Price, J. Ruzyllo, F. Zhang, J. Xu, S. E. Mohney, Q. Zhang, and A. Y. Wang, "Mist fabrication of light emitting diodes with colloidal nanocrystal quantum dots," *Applied Physics Letters*, vol. 92, p. 023111, 2008.
[70] J. Xu, Z. Tan, C. Zhang, F. Zhang, S. Pickering, and A. Y. Wang, "Colloidal nanocrystal-based light-emitting diodes fabricated on plastic–towards flexible quantum dot optoelectronics," *Nano Letters*, vol. 7, p. 2196, 2007.
[71] S. Coe-Sullivan, J. S. Steckel, W. K. Woo, M. G. Bawendi, and V. BulovicÂ, "Large-area ordered quantum-dot monolayers via phase separation during spin-casting*," *Advanced Functional Materials*, vol. 15, pp. 1117-1124, 2005.
[72] J. Zhao, J. A. Bardecker, A. M. Munro, M. S. Liu, Y. Niu, I. K. Ding, J. Luo, B. Chen, K. Y. J. Alex, and D. S. Ginger, "Efficient CdSe/CdS quantum dot light-emitting diodes using a thermally polymerized hole transport layer," *Nano Letters*, vol. 6, pp. 463-467, 2006.
[73] M. Achermann, M. A. Petruska, D. D. Koleske, M. H. Crawford, and V. I. Klimov, "Nanocrystal-based light-emitting diodes utilizing high-efficiency nonradiative energy transfer for color conversion," *Nano Letters*, vol. 6, pp. 1396-1400, 2006.

[74] V. Santhanam and R. P. Andres, "Microcontact printing of uniform nanoparticle arrays," *Nano Letters*, vol. 4, pp. 41-44, 2004.
[75] V. Santhanam, J. Liu, R. Agarwal, and R. P. Andres, "Self-assembly of uniform monolayer arrays of nanoparticles," *Langmuir*, vol. 19, pp. 7881-7887, 2003.
[76] J. S. Steckel, P. Snee, S. Coe-Sullivan, J. P. Zimmer, J. E. Halpert, P. Anikeeva, L. A. Kim, V. Bulovic, and M. G. Bawendi, "Color-saturated green-emitting QD-LEDs," *Angewandte Chemie*, vol. 118, pp. 5928-5931, 2006.
[77] A. Rizzo, M. Mazzeo, M. Palumbo, G. Lerario, S. D'Amone, R. Cingolani, and G. Gigli, "Hybrid light-emitting diodes from microcontact-printing double-transfer of colloidal semiconductor CdSe/ZnS quantum dots onto organic layers," *Advanced Materials*, vol. 20, pp. 1886-1891, 2008.
[78] J. Yu, J. Chen, H. Huang, M. Bawendi, and V. Bulovic, "Microcontact printing of quantum-dot LEDs using an inkjet-assisted patterning method."
[79] C. Y. Kuan, J. M. Chou, C. Leu, and M. H. Hon, "Sol–gel-derived ZnO coating with nanopatterns fabricated by nanoimprinting," *Journal of the American Ceramic Society*, vol. 91, pp. 3160-3166, 2008.
[80] S. Sepulveda-Guzman, B. Reeja-Jayan, E. De la Rosa, U. Ortiz-Mendez, C. Reyes-Betanzo, R. Cruz-Silva, and M. Jose-Yacaman, "Room-temperature deposition of crystalline patterned ZnO films by confined dewetting lithography," *Applied Surface Science*, 2009.
[81] I. D. Parker, "Carrier tunneling and device characteristics in polymer light-emitting diodes," *Proceedings of SPIE*, vol. 2144, p. 51, 1994.
[82] I. A. Larkin, M. I. Stockman, M. Achermann, and V. I. Klimov, "Dipolar emitters at nanoscale proximity of metal surfaces: Giant enhancement of relaxation in microscopic theory," *Physical Review B*, vol. 69, p. 121403, 2004.
[83] K. Hoshino, T. C. Turner, S. Kim, A. Gopal, and X. Zhang, "Single molecular stamping of a sub-10-nm colloidal quantum dot array," *Langmuir*, vol. 24, pp. 13804-13808, 2008.
[84] Y. Cui, Q. Wei, H. Park, and C. M. Lieber, "Nanowire nanosensors for highly sensitive and selective detection of biological and chemical species," *Science*, vol. 293, p. 1289, 2001.
[85] http://www.dowcorning.com/.
[86] J. R. Anderson, D. T. Chiu, R. J. Jackman, O. Cherniavskaya, J. C. McDonald, H. Wu, S. H. Whitesides, and G. M. Whitesides, "Fabrication of topologically complex three-dimensional microfluidic systems in PDMS by rapid prototyping," *Anal. Chem*, vol. 72, pp. 3158-3164, 2000.
[87] H. Mattoussi, L. H. Radzilowski, B. O. Dabbousi, E. L. Thomas, M. G. Bawendi, and M. F. Rubner, "Electroluminescence from heterostructures of poly (phenylene vinylene) and inorganic CdSe nanocrystals," *Journal of Applied Physics*, vol. 83, p. 7965, 1998.
[88] G. L. Frey, K. J. Reynolds, and R. H. Friend, "Novel electrodes from solution-processed layer-structure materials," *Advanced Materials*, vol. 14, pp. 265-268, 2002.
[89] J. M. Caruge, J. E. Halpert, V. Bulovi, and M. G. Bawendi, "NiO as an inorganic hole-transporting layer in quantum-dot light-emitting devices," *Nano Letters*, vol. 6, pp. 2991-2994, 2006.

[90] S. A. Haque, S. Koops, N. Tokmoldin, J. R. Durrant, J. Huang, D. D. C. Bradley, and E. Palomares, "A multilayered polymer light-emitting diode using a nanocrystalline metal-mxide film as a charge-injection electrode," *Advanced Materials*, vol. 19, pp. 683-687, 2007.
[91] S. H. Kang, C. K. Kumar, Z. Lee, K. H. Kim, C. Huh, and E. T. Kim, "Quantum-dot light-emitting diodes utilizing CdSe/ ZnS nanocrystals embedded in TiO thin film," *Applied Physics Letters*, vol. 93, p. 191116, 2008.
[92] E. Hecht, "Optics/E. Hecht," 2002.
[93] G. Chumanov, K. Sokolov, B. W. Gregory, and T. M. Cotton, "Colloidal metal films as a substrate for surface-enhanced spectroscopy," *The Journal of Physical Chemistry*, vol. 99, pp. 9466-9471, 1995.
[94] H. O. Finklea, "Of thiols and related molecules on electrodes," *Electroanalytical Chemistry: A Series of Advances: Volume 19*, p. 109, 1996.
[95] J. Schmitt, G. Decher, W. J. Dressick, S. L. Brandow, R. E. Geer, R. Shashidhar, and J. M. Calvert, "Metal nanoparticle/polymer superlattice films: fabrication and control of layer structure," *Advanced Materials (Weinheim)*, vol. 9, pp. 61-65, 1997.
[96] M. Giersig and P. Mulvaney, "Preparation of ordered colloid monolayers by electrophoretic deposition," *Langmuir*, vol. 9, pp. 3408-3413, 1993.
[97] J. Rybczynski, U. Ebels, and M. Giersig, "Large-scale, 2D arrays of magnetic nanoparticles," *Colloids and Surfaces A: Physicochemical and Engineering Aspects*, vol. 219, pp. 1-6, 2003.
[98] T. P. Bigioni, X. M. Lin, T. T. Nguyen, E. I. Corwin, T. A. Witten, and H. M. Jaeger, "Kinetically driven self assembly of highly ordered nanoparticle monolayers," *Nature Materials*, vol. 5, pp. 265-270, 2006.
[99] A. L. Efros and A. V. Rodina, "Band-edge absorption and luminescence of nonspherical nanometer-size crystals," *Physical Review B*, vol. 47, pp. 10005-10007, 1993.
[100] C. D. Dushkin, G. S. Lazarov, S. N. Kotsev, H. Yoshimura, and K. Nagayama, "Effect of growth conditions on the structure of two-dimensional latex crystals: experiment," *Colloid & Polymer Science*, vol. 277, pp. 914-930, 1999.
[101] F. Bresme and M. Oettel, "Nanoparticles at fluid interfaces," *Journal of Physics: Condensed Matter*, vol. 19, p. 413101, 2007.
[102] P. A. Kralchevsky and K. Nagayama, "Capillary interactions between particles bound to interfaces, liquid films and biomembranes," *Advances in Colloid and Interface Science*, vol. 85, pp. 145-192, 2000.
[103] N. D. Denkov, O. D. Velev, P. A. Kralchevsky, I. B. Ivanov, H. Yoshimura, and K. Nagayama, "Two-dimensional crystallization," 1993.
[104] http://en.wikipedia.org/wiki/Transmission_electron_microscopy.
[105] http://en.wikipedia.org/wiki/Atomic_force_microscopy.
[106] X. Jian, D. Cui, B. A. Lewis, A. Y. Wang, X. Shengyong, and M. Gerhold, "Microcavity light-emitting devices based on colloidal semiconductor nanocrystal quantum dots," *Photonics Technology Letters, IEEE*, vol. 17, pp. 2008-2010, 2005.
[107] B. E. Warren, *X-ray Diffraction*: Dover Pubns, 1990.

[108] V. E. Henrich and P. A. Cox, *The surface science of metal oxides*: Cambridge University Press, 1996.
[109] Z. Jialong, Z. Jingying, J. Chaoyang, B. Jolanta, B. Thomas, and M. Alf, "Electroluminescence from isolated CdSe/ZnS quantum dots in multilayered light-emitting diodes," *Journal of Applied Physics*, vol. 96, pp. 3206-3210, 2004.
[110] G. M. Whitesides, E. Ostuni, S. Takayama, and X. Jiang, "Soft lithography in biology and biochemistry," *Annual Review of Biomedical Engineering* , vol. 3, pp. 335–373 2001.
[111] T. Dobbertin, E. Becker, T. Benstem, G. Ginev, D. Heithecker, H. H. Johannes, D. Metzdorf, H. Neuner, R. Parashkov, and W. Kowalsky, "OLED matrix displays: in-line process technology and fundamentals," *Thin Solid Films*, vol. 442, pp. 132-139, 2003.
[112] G. Gu and S. R. Forrest, "Design of flat-panel displays based on organic light-emitting devices," *IEEE Journal of Selected Topics in Quantum Electronics*, vol. 4, pp. 83-99, 1998.
[113] E. Menard, M. A. Meitl, Y. Sun, J. U. Park, D. J. L. Shir, Y. S. Nam, S. Jeon, and J. A. Rogers, "Micro-and nanopatterning techniques for organic electronic and optoelectronic systems," *Chem. Rev*, vol. 107, pp. 1117-1160, 2007.
[114] B. Kuswandi, J. Huskens, and W. Verboom, "Optical sensing systems for microfluidic devices: a review," *Analytica Chimica Acta*, vol. 601, pp. 141-155, 2007.
[115] L. J. Rothberg and A. J. Lovinger, "Status of and prospects for organic electroluminescence," *Journal of Materials Research*, vol. 11, p. 3174, 1996.
[116] M. Stewart, R. S. Howell, L. Pires, M. K. Hatalis, L. Technols, and P. A. Allentown, "Polysilicon TFT technology for active matrix OLED displays," *IEEE Transactions on Electron Devices*, vol. 48, pp. 845-851, 2001.
[117] F. Papadimitrakopoulos, X. M. Zhang, D. L. Thomsen, and K. A. Higginson, "A Chemical Failure Mechanism for Aluminum(III) 8-Hydroxyquinoline Light-Emitting Devices," *Chemistry of Materials*, vol. 8, pp. 1363-1365, 1996.
[118] D. G. Lidzey, M. A. Pate, M. S. Weaver, T. A. Fisher, and D. D. C. Bradley, "Photoprocessed and micropatterned conjugated polymer LEDs," *Synthetic Metals*, vol. 82, pp. 141-148, 1996.
[119] H. L. Yip, J. Zou, H. Ma, Y. Tian, N. M. Tucker, and K. Y. J. Alex, "Patterning of robust self-assembled n-type hexaazatrinaphthylene-based nanorods and nanowires by microcontact printing," *Journal of the American Chemical Society*, vol. 128, pp. 13042-13043, 2006.
[120] Z. H. Huang, G. J. Qi, X. T. Zeng, and W. M. Su, "A method for undercut formation of integrated shadow mask used in passive matrix displays," *Thin Solid Films*, vol. 503, pp. 246-249, 2006.
[121] S. Noach, E. Z. Faraggi, G. Cohen, Y. Avny, R. Neumann, D. Davidov, and A. Lewis, "Microfabrication of an electroluminescent polymer light emitting diode pixel array," *Applied Physics Letters*, vol. 69, p. 3650, 1996.
[122] C. Kim and S. R. Forrest, "Fabrication of organic light-emitting devices by low-pressure cold welding," *Advanced Materials*, vol. 15, pp. 541-545, 2003.
[123] C. Kim, P. E. Burrows, and S. R. Forrest, "Micropatterning of organic electronic devices by cold-welding," *Science*, vol. 288, p. 831, 2000.

[124] K. Hoshino, T. Hasegawa, K. Matsumoto, and I. Shimoyama, "Organic light-emitting diode micro patterned with a silicon convex stamp," *Sensors and Actuators A: Physical*, vol. 128, pp. 339-343, 2006.
[125] J. Yu and V. Bulovi, "Micropatterning metal electrode of organic light emitting devices using rapid polydimethylsiloxane lift-off," *Applied Physics Letters*, vol. 91, p. 043102, 2007.
[126] D. A. Pardo, G. E. Jabbour, and N. Peyghambarian, "Application of screen printing in the fabrication of organic light-emitting devices," *Advanced Materials*, vol. 12, pp. 1249-1252, 2000.
[127] B. Jayesh and Y. Yang, "Polymer electroluminescent devices processed by inkjet printing: I. Polymer light-emitting logo," *Applied Physics Letters*, vol. 72, pp. 2660-2662, 1998.
[128] T. Granlund, T. Nyberg, L. S. Roman, M. Svensson, and O. Inganäs, "Patterning of Polymer Light-Emitting Diodes with Soft Lithography," *Advanced Materials*, vol. 12, pp. 269-273, 2000.
[129] B. Weng Sing, K. In Tae, Q. Dong, X. Younan, and M. W. George, "Formation of Patterned Microstructures of Conducting Polymers by Soft Lithography, and Applications in Microelectronic Device Fabrication," *Advanced Materials*, vol. 11, pp. 1038-1041, 1999.
[130] P. J. Yoo, S. J. Choi, J. H. Kim, D. Suh, S. J. Baek, T. W. Kim, and H. H. Lee, "Unconventional patterning with a modulus-tunable mold: From imprinting to microcontact printing," *Chemistry of Materials*, vol. 16, pp. 5000-5005, 2004.
[131] K. Hoshino, K. Yamada, and I. Shimoyama, "A diffraction-limited, real-time, full-colour display," *Journal of Micromechanics and Microengineering*, vol. 15, pp. 2194-2197, 2005.
[132] M. W. Davidson, "Numerical Aperture and Image Resolution" in *http://www.microscopyu.com/tutorials/java/imageformation/airyna/index.html*.
[133] E. Hecht, *Optics (2nd ed.),* Addison-Wesley, New York, 1987.
[134] E. Oesterschulze, "Recent developments of probes for scanning probe microscopy," *Advances in Imaging and Electron Physics*, vol. 118, pp. 129-206, 2001.
[135] R. C. Dunn, "Near-field scanning optical microscopy," *Chemical Reviews*, vol. 99, pp. 2891-2928, 1999.
[136] B. E. K. Alpan, "Apertureless SNOM: A New Tool for Nano-Optics," *Institut de Physique des Nanostructures*, Bilkent University, 2004.
[137] J. Hashizume, S. Shinada, and F. Koyama, "Near-field optical probing using a microaperture GaInAs/GaAs surface emitting laser," *Japanese Journal of Applied Physics Letters*, vol. 41, pp. 700-702, 2002.
[138] E. Betzig, A. Lewis, A. Harootunian, M. Isaacson, and E. Kratschmer, "Near field scanning optical microscopy (NSOM): development and biophysical applications," *Biophysical Journal*, vol. 49, pp. 269-279, 1986.
[139] K. Karra and R. D. Grober, "Piezo-electric tuning fork tip--sample distance control for near field optical microscopes," *Ultramicroscopy*, vol. 61, pp. 197-205, 1995.

[140] R. Cailleau, M. Olivé, and Q. V. J. Cruciger, "Long-term human breast carcinoma cell lines of metastatic origin: preliminary characterization," *In Vitro Cellular & Developmental Biology-Plant*, vol. 14, pp. 911-915, 1978.
[141] J. E. Price, "Metastasis from human breast cancer cell lines," *Breast Cancer Research and Treatment*, vol. 39, pp. 93-102, 1996.
[142] J. E. Price, A. Polyzos, R. Dan Zhang, and L. M. Daniels, "Tumorigenicity and metastasis of human breast carcinoma cell lines in nude mice," *Cancer Research*, vol. 50, p. 717, 1990.
[143] J. E. Price and R. D. Zhang, "Studies of human breast cancer metastasis using nude mice," *Cancer and Metastasis Reviews*, vol. 8, pp. 285-297, 1990.
[144] K. Nesaretnam, N. Guthrie, A. F. Chambers, and K. K. Carroll, "Effect of tocotrienols on the growth of a human breast cancer cell line in culture," *Lipids*, vol. 30, pp. 1139-1143, 1995.
[145] J. V. Dacie, *The Haemolytic Anaemias*: Churchill Livingstone Edinburgh, 1992.

Vita

Ashwini Gopal was born in Madras, India, on September 24, 1983, the daughter of Mr. K. Gopalakrishnan and Mrs. Chandra Gopalakrishnan. She studied at Padma Seshadri Bala Bhavan Senior Secondary School (CBSE) in K.K. Nagar, Chennai, India. In August 2001, she was admitted at the Sathyabama University at Chennai, India, where she received her undergraduate bachelor's degree in Electrical and Electronics Engineering. She enrolled in the Electrical and Computer Engineering graduate program at the University of Texas at Austin in August 2005. Ashwini Gopal earned her Master of Science degree in Electrical and Computer Engineering from the University of Texas at Austin in May 2007. Her Masters thesis research, supervised by Dr. Xiaojing Zhang focused on creating a nano-opto-mechanical system for measurement of neuronal membrane properties. Since then, she has specialized in optical and fluidic micro-electro-mechanical systems for multispectral detection under the guidance of Dr. Xiaojing Zhang and Dr. Kazunori Hoshino.

Permanent address: A8 Bharath Apartments,
Old 16, New 54, Raman Street,
T.Nagar, Chennai 600017
Tamil Nadu, India

This dissertation was typed by the author.